CHALMERS

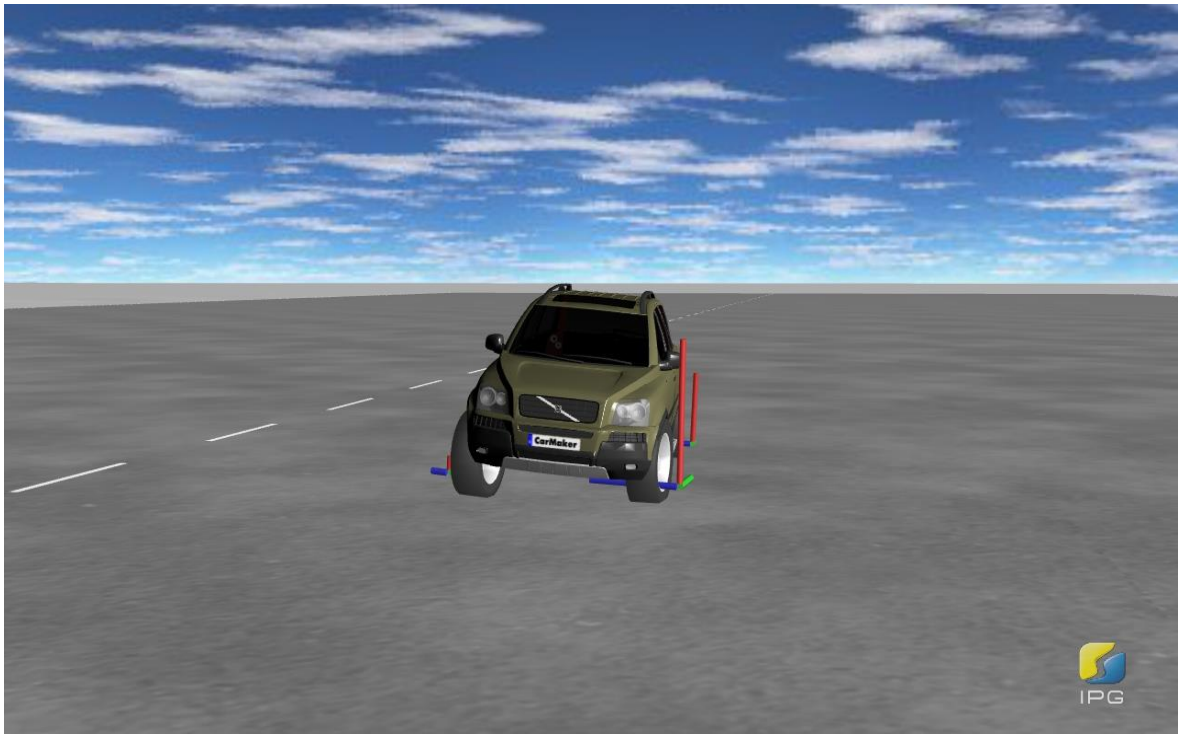

Brake Control Module Tuning using Computer Aided Engineering

A study in cooperation with Volvo Car Corporation

Master's Thesis in Automotive Engineering

SIDDHANT GUPTA

Department of Applied Mechanics
Division of Vehicle Engineering and Autonomous Systems
Vehicle Dynamics Group
CHALMERS UNIVERSITY OF TECHNOLOGY
Göteborg, Sweden 2015
Master's thesis 2015:79

MASTER'S THESIS IN AUTOMOTIVE ENGINEERING

Brake Control Module Tuning using Computer Aided Engineering

A study in cooperation with Volvo Car Corporation

SIDDHANT GUPTA

Department of Applied Mechanics
Division of Vehicle Engineering and Autonomous Systems
Vehicle Dynamics Group
CHALMERS UNIVERSITY OF TECHNOLOGY
Göteborg, Sweden 2015

Brake Control Module Tuning using Computer Aided Engineering
A study in cooperation with Volvo Car Corporation

SIDDHANT GUPTA

Master's Thesis 2015:79
ISSN 1652-8557
Department of Applied Mechanics
Division of Vehicle Engineering and Autonomous Systems
Vehicle Dynamics Group
Chalmers University of Technology
SE-412 96 Göteborg
Sweden
Telephone: + 46 (0)31-772 1000

Cover:
Volvo XC90 simulated in IPG CarMaker with Sine with Dwell Manoeuvre

Department of Applied Mechanics
Göteborg, Sweden 2015

Brake Control Module Tuning using Computer Aided Engineering

A study in cooperation with Volvo Car Corporation

Master's Thesis in Automotive Engineering
SIDDHANT GUPTA
Department of Applied Mechanics
Division of Vehicle Engineering and Autonomous Systems
Vehicle Dynamics Group
Chalmers University of Technology

ABSTRACT

Brake Control Module (BCM) tuning in terms of the Antilock Braking system (ABS) and the Dynamic Stability Traction Control (DSTC) is normally a time consuming and costly procedure since it involves comprehensive physical testing on the prototype vehicles in early phases of the vehicle development. To reduce prototype vehicles and make the procedure time efficient, it is envisioned that BCM tuning will be achieved using Computer Aided Engineering (CAE) in all future V54X cars at Volvo Car Corporation.

The thesis work aims to facilitate method development for Virtual Brake Software Release which constitutes BCM tuning using CAE tools in a closed loop control environment using Global Optimization tools.

The CAE environment demands a high correlation between the simulated model (plant) and the actual vehicle. For the preparation of this plant model, tire parameter optimization using global optimization tools is performed using data from physical tests carried out on the test track to achieve good correlation between virtual and physical tests. These maneuvers are reproduced on IPG CarMaker to optimize the tire parameters in the pure slip region.

Subsequently, the identification of a reference model was carried out using a 2 DOF model to tune with respect to the plant. The latter part of the thesis discusses various simplified DSTC strategies and a framework to perform the Brake Control Module tuning. It is realized that CAE tuning in terms of Brake Control Module is possible with an appropriate vehicle model in the CAE environment. As a future scope, sophisticated BCM model could be tuned using CAE tool; however, the constraints set up and weighting factors in the optimization would determine the final tuned values.

Keywords:

Brake Control Module, Computer Aided Engineering, Magic Formula, Costly Global Optimization,

Ahead of Austrian Grand Prix 2014 held after 11 years:

"I remember something that's quite funny: in the old days it was always said that the local cows stopped producing milk for a week, because of the noise from the F1 cars. Now that the cars make less noise, let's hope it's only a few days…" - Jean Alesi, Pirelli consultant.

Contents

Preface

This thesis work has been conducted as a partial fulfillment for the Master of Science Degree in Automotive Engineering at the Chalmers University of Technology, Gothenburg, Sweden in cooperation with Volvo Car Corporation. The thesis work has been carried out at the CAE Active Safety Department in Volvo Car Corporation, Gothenburg during the period January, 2014 – June, 2014 with a focus on promoting the development of Volvo cars employing CAE tools.

I would like to acknowledge and thank my supervisor at Volvo Car Corporation, Diomidis Katzourakis for his continuous support and valuable guidance which has been the key for this study to be carried out. The uncertainties involved in the study were high and without his moral support and technical advises, it would not have been possible. Special acknowledgement and thanks to my supervisor at the Chalmers University of Technology, Mathias Lidberg for sharing his knowledge and expertise at regular intervals of the project and making sure the project ran smoothly. Georgios Minos, Manager of CAE Active Safety, Volvo Car Corporation has been very supportive and encouraging with all the resources and administrative work. I would also like to extend my gratitude towards Max Boerboom, Volvo Car Corporation for his constant encouragement and expert guidance throughout my thesis work. I would also like to credit my colleagues Alexandros Leledakis, Marcus Ljungberg and Stavros Angelis at VCC for constant consulting and assisting in carrying out the thesis work efficiently.

Göteborg, September 2015

Siddhant Gupta

Nomenclature

Abbreviations

ABS	Antilock Braking System
BCM	Brake Control Module
CAE	Computer Aided Engineering
CAN	Controller Area Network
CoG	Centre of Gravity
ESC	Electronic Stability Control
K&C	Kinematics and Compliance
RMS	Root Mean Square
STM	Single Track Model
SWA	Steering Wheel Angle
Vxxx	Station Wagon

Tire parameters

B	Stiffness factor
C	Shape factor
D	Peak value
E	Curvature factor
F_x	Longitudinal wheel force
F_y	Lateral wheel force
F_z	Vertical wheel force
I_{xx}	Moment of inertia of sprung mass around x-axis
I_{yy}	Moment of inertia of sprung mass around y-axis
I_{zz}	Moment of inertia of vehicle around z-axis
L	Wheelbase
S_{Hy}	Horizontal shift
S_{Vy}	Vertical shift

Vehicle body constants

a	Longitudinal distance from CoG to axles
a_x	Longitudinal acceleration at CoG
b	Lateral distance from CoG to wheel centre
g	Gravitational constant
h	CoG height
l_f	Distance from CoG to front axle
l_r	Distance from CoG to rear axle
m	Vehicle mass
w	Track width

Vehicle dynamics variables

α	Slip angles
δ	Steer angle at wheels
φ	Body roll angle
θ	Pitch angle
ψ	Yaw angle
Φ	Phase angle
a_y	Lateral acceleration at CoG
a_z	Vertical acceleration at CoG
r	Yaw rate
v_x	Longitudinal velocity
v_y	Lateral velocity

List of Figures and Tables

1 INTRODUCTION

In the last twenty years, the use of Computer Aided Engineering (CAE), has taken a leap in the automotive industry and its development. Reliance on computer simulation and CAE tools has been the core to develop the design and assess a product performance before the physical prototypes are produced. Continuous development in the field of software engineering and technological advancements in the field of computer science has made this collaboration of automotive testing with CAE and simulation possible.

This master thesis project is carried out in cooperation with Volvo Car Corporation in the Active Safety CAE Department. The report describes the methodology for parameter optimization and framework for brake control module tuning in the CAE environment using global optimization tools.

1.1 Background

Developments in computer-aided design and engineering have focused on dense developments in the product design phase, and the development time has been known to reduce by around 40% for a complete vehicle (Keenan, 1995).

In the case of Vehicle Dynamics CAE, objective targets are necessary if the CAE process is applied effectively for the vehicle dynamics development. These objective targets need to be cascaded from complete vehicle to the component level to assist the tuning in the CAE environment. For an excellent correlation, it is also essential to resolve the design conflicts and balance the objective targets in the CAE environment.

Significant advances in the field of automotive technology and the focus towards automotive safety in the past decade has made it possible for most of the vehicles to be equipped with Anti-Lock Braking Systems (ABS) and Traction Control Systems (TCS) where the aim is to maximize the contact between tires and the road during heavy braking and acceleration. The latest development Electronic Stability Programme (ESP) focuses on preventing skidding by yaw stability control (Tjønnas & Johanse, 2006).

To include the vehicle ESP as a tunable unit in the vehicle CAE environment, a detailed vehicle model with realistic suspension and kinematics properties is essential. The tire also plays a vital role in this case, and a thorough knowledge of its properties is necessary for accurate modeling and tuning. The tires are tested-measured, and the corresponding data on their properties can be applied to semi-empirical tire models. The tire data available from these measurements have to be integrated in the vehicle CAE environment to analyze the properties of dynamic behavior of the vehicle.

As part of reducing the risk of rollover accidents and severe injuries due to these accidents, NHTSA has established safety standards for vehicle testing with ESC implemented. Research carried out at NHTSA suggests that the installation of ESC systems on the vehicle will reduce the single vehicle crashes of passenger cars by 34% and single vehicle crashes of SUVs by 59%. (NHTSA, 2006). As per the standard rules for the ESC systems to be implemented in the vehicle, the algorithm is required to brake the wheels individually in order to control the braking torques on all the wheels. It should be able to determine the vehicle yaw rate and side slip in real time and limit oversteer and understeer effectively.

1.2 Scope

The broader scope of the thesis is Virtual Brake Software Release which constitutes the development of framework to tune the BCM using CAE tools. Based on this scope, the thesis work aims at investigating the feasibility of tuning and optimizing the vehicle parameters in the CAE environment.

A vehicle dynamics model has been parameterized as a prototype M1 (mule) Volvo Car for its suspension, kinematics and compliance characteristics available in the CAE environment.

The thesis focused on various areas as briefed below:

- Analyzing the vehicle model in the simulation environment using CAE tools
- Verification and optimization of tire parameters in the CAE environment
- Comparing and optimizing the understeer characteristics of a 2 DOF vehicle model against the reference vehicle in CAE environment
- Validate the global optimization algorithms and their functionality with the simulation environment in tandem based on the previous point mentioned
- Build a mock-up BCM in the CAE environment and evaluate whether it's possible to tune its parameters for individual wheels

1.3 Research Questions

The master thesis work carried out should answer the following research questions:

- How to comprehensively analyze the vehicle behavior on a simulation platform?
- How to extract the best tire parameters suitable to carry out the CAE verification processes?
- How to identify a 2DOF vehicle dynamics reference model with respect to a plant model in CAE environment?
- How to carry out the evaluation and tuning of BCM in the CAE Environment?

1.4 VIRTUAL BRAKE SOFTWARE RELEASE

Figure 1 shows the schematic model of a closed loop control system where the desired output is achieved by controlling the error based on the reference. The plant in the closed loop control that is acted upon by the control effort depends on the feedback or optimization process. In section 5.3 this closed loop control will be used with various control strategies.

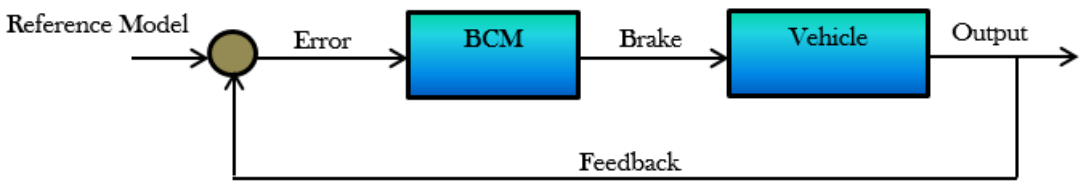

Figure 1 Schematic of Closed Loop Control

Work Procedure:

The methodology to execute the research statement and purpose of thesis work had to be supported with various tools and processes that were required to be tested for their functionality. Preceding BCM tuning, it was essential to tune the plant (CarMaker model) to the physical vehicle used for real tests which is outlined in step 0. Identification of an appropriate reference model was done by using a 2 DOF vehicle dynamics model, developed in Simulink and tuned to the CarMaker model [step 2]. A brief introduction on the development of framework to tune the BCM is given in step 3.

Step 1: Preparation of the Vehicle Model

The vehicle model in CarMaker represents the actual vehicle V526 M1.

Kinematics and Compliance: The simulation environment in IPG Carmaker® consists of the suspension, kinematics and compliance characteristics of the V526 M1 vehicle used as a test vehicle.

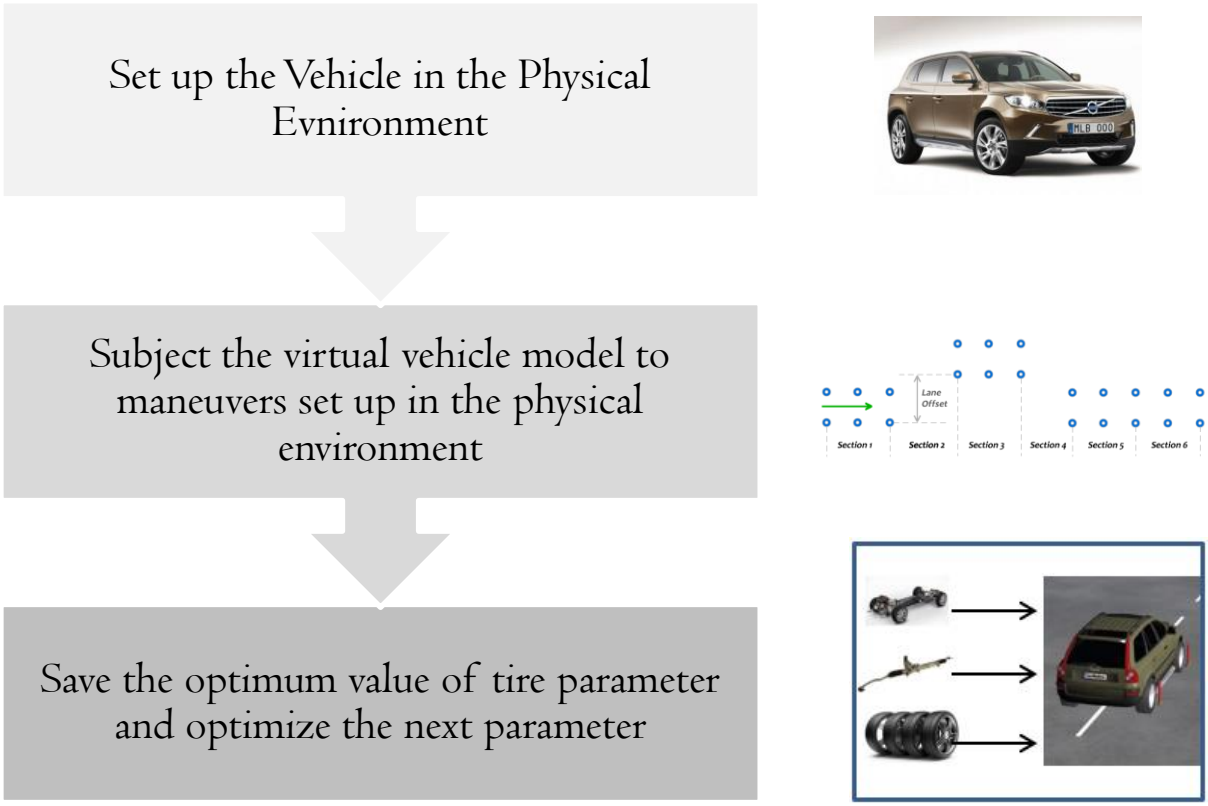

Figure 2 CAE Verification Loop

These Kinematics and Compliance characteristics are exported from data extracted from tests performed on a K&C rig. This ensures that the modeling of the vehicle in the simulation environment has high correlation with that of the test vehicle used for carrying out the maneuvers.

Steering System: High correlation of CarMaker model with that of real V526 M1 is necessary for carrying out the process of BCM tuning and optimization. This is in turn dependent on the parameterization of the vehicle model in CarMaker to suit the parameters of V526 M1. The steering system and its compliance are also taken into

account by the steering subsystem used in the M1 vehicle which is modeled as a separate block in Carmaker for Simulink.

Tires: Apart from the Suspension and Steering, Kinematics and Compliance, Powertrain and Vehicle Body characteristics, the other critical area to be modeled are the tires. The quality and reliability of vehicle dynamics simulations are highly dependent on the tire models used in IPG CarMaker. Hence, for optimization and tuning of the BCM optimization of tire models is essential to ensure that the simulation results are reliable. The measurements for the tires used on the test vehicle are received from the supplier for a specific tire (Michelin Latitude 275/45 R20). The tire file is by default in the ADAMS PAC 2002 format. However, this can be converted into IPG format for its use within IPG Carmaker® and used as a ".tir" file format.

Hence, the CAE verification process involves the tuning and optimization of tire parameters as a preceding task to the tuning of BCM [Section 2]. The CAE verification loop as seen in Figure 2 is followed; the vehicle model in CAE is tuned to the physical model by optimizing the tire parameters.

For identifying the tire parameters to be tuned, a thorough sensitivity analysis was carried out as explained in section 3.4. The detailed optimization on the identified tire parameters with a description of test maneuvers is given in section 3.5 with results.

Step 2: Identification of the 2DOF reference model

To facilitate better understanding of lateral vehicle dynamics and to generate a reference model which can be tuned against the CAE model in IPG CarMaker, a 2DOF vehicle model (Figure 3) was created in Simulink (APPENDIX A – 2DOF Simulink Model) based on the principles describes in Section 3.2.

With the 2DOF model built in Simulink, a global optimization process (Figure 4) was applied to optimize the cornering stiffness of the 2DOF vehicle model with respect to the CAE model available in CarMaker.

Adaptive Single Track maneuver (ASTM) catalogue was used to subject the CAE model and the 2DOF model to the same maneuvers. The cornering stiffness of the tires was altered in the optimization loop to minimize the error between the characteristics of the 2DOF model and the tuned CarMaker model.

The optimization process and its results are explained in section 4.

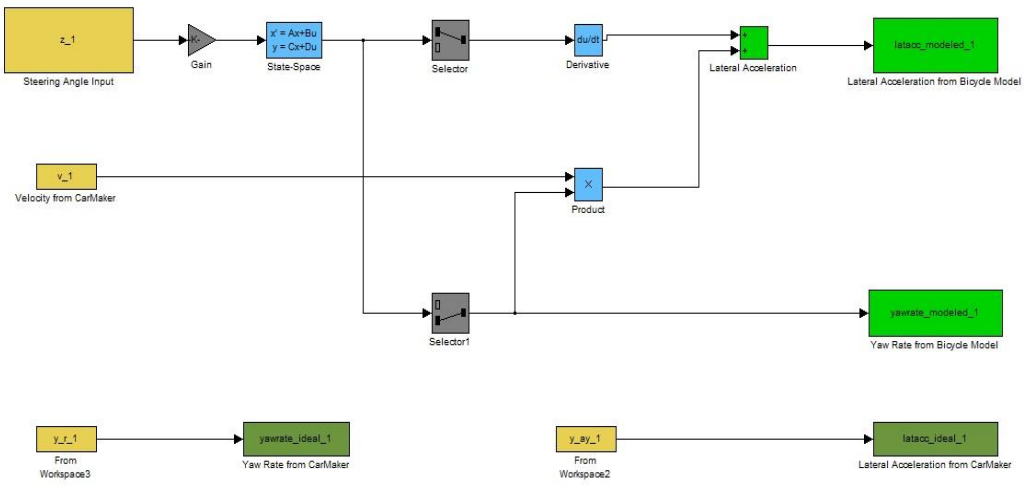

Figure 3 2DOF bicycle model in Simulink

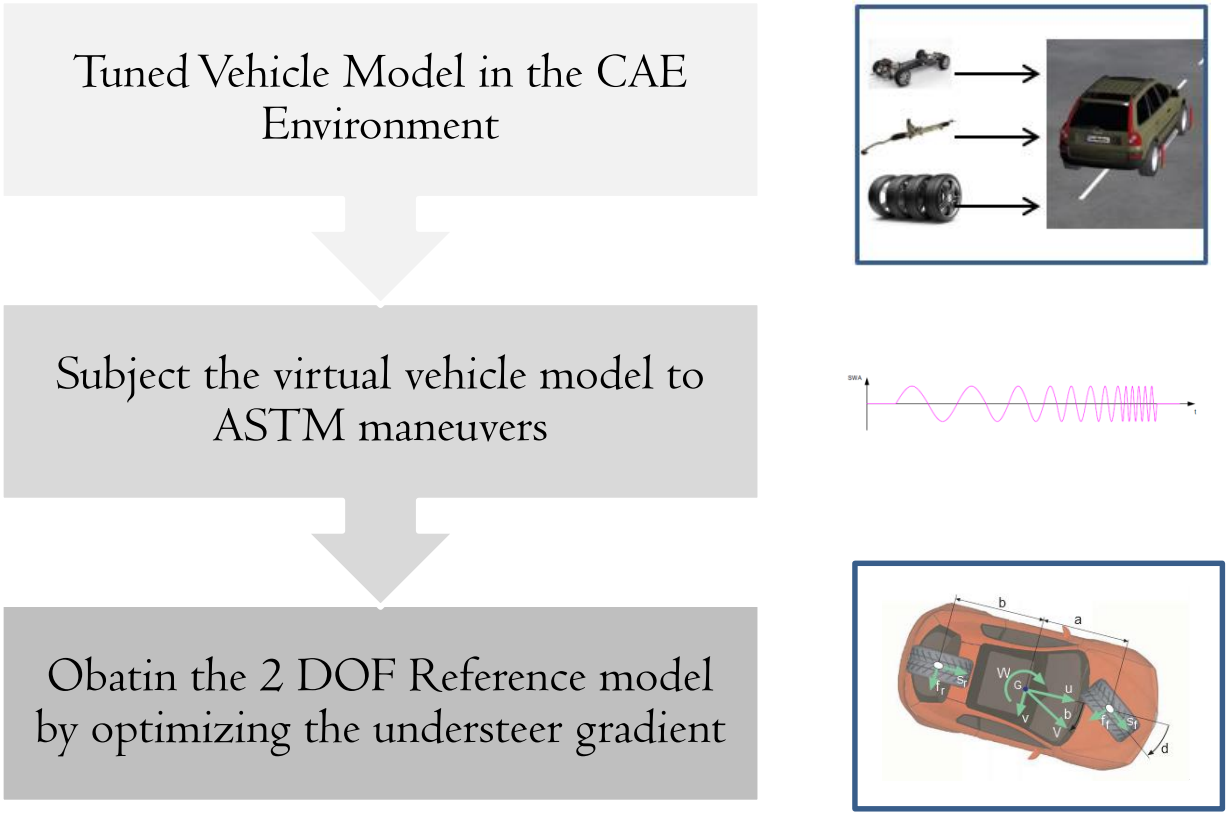

Figure 4 Optimization loop for Tuning of 2DOF vehicle model

Step 3: BCM tuning employing CAE

Electronic Stability Program (ESP) aids in stabilizing the vehicle movement. Anti-Lock Braking Systems (ABS) was the first active safety system introduced to prevent skidding of the vehicle and provide driver with more control which was a breakthrough in the safety sector of the Automotive Industry. ESP systems were introduced later which are meant to enhance the ABS with additional control systems. The ESP can be designed with different control algorithms and these control systems carry various abbreviations depending on the vehicle manufacturer and the prime focus of a specific control system. For e.g. Dynamic stability traction control (DSTC) wherein the traction applied at the wheels is also controlled in real time based on the maneuver, is developed by Volvo Car Corporation. DSTC along with yaw rate and sideslip control from the ESP forms the Brake Control Module (BCM) for Volvo Cars. With the use of CAN bus systems in the vehicle architecture, it has become easier to integrate more systems along with the ABS and ESC to control the vehicle movement.

BCM works by determining the intended path for the vehicle and by calculating the deviation from the actual path the vehicle is subjected to. With the aid of sensors for steering wheel angle, lateral acceleration and yaw rate, it tries to stabilize the vehicle depending on the maneuver. These situations may vary in the form of vehicle being understeer or over steered based on weather conditions, road conditions or driver error. With the desired vehicle path, the BCM intervenes by applying brakes on the appropriate wheels individually and hence stabilizing the vehicle.

The CAE Model preparation and reference model identification was subsequently followed by the initialization of the optimization process of BCM. Though the BCM was not optimized due to time and resource limitations, a framework for its tuning was developed (Figure 5) and the fundamentals behind the optimization process and the CAE validation for the same are explained in later sections.

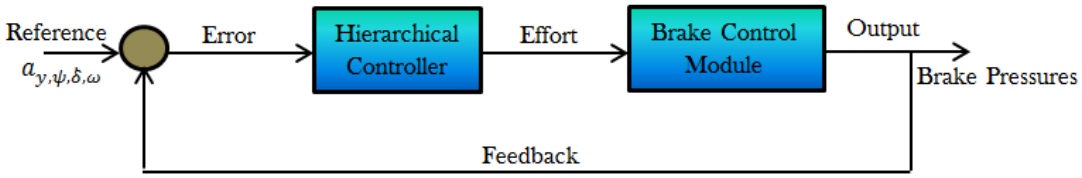

Figure 5 Closed Loop Control for Brake Control Module Tuning

1.5 Acquaintance with tools

Tandem working of tools for the purpose of global optimization was necessary for the thesis work to be carried out. The acquaintance with the tools was necessary in order to identify the areas of tool functionality that might be critical during the optimization process. Along with MatLab and Simulink, other tools used for the thesis work were the simulation platform IPG Carmaker® and the Global Optimization tool TomLab. The degree of functionality of IPG Carmaker® in tandem with TomLab was identified to support the optimization routines followed in the thesis work.

1.5.1 IPG CarMaker®

IPG Carmaker® provides the user with a virtual vehicle environment where the vehicle is modeled with a set of equations of motions, kinematics and compliance characteristics, etc. The behavior of the vehicle modeled in this virtual environment is envisioned to be as close as possible to the real counterpart. The correlation between the virtual model and a real car depends on how well the vehicle is parameterized in IPG Carmaker®. This parameterization can be done in the area of tires, powertrain, chassis, vehicle co-ordinates, etc.

IPG Carmaker® also provides the facility to integrate a well-defined model of a virtual road which can simulate a real world course for the purpose of testing. With the specification of a maneuver subjected to this virtual model, extensive testing can be carried out on the vehicle due to high flexibility of the interface of IPG Carmaker®.

CarMaker for Simulink is an integrated platform of IPG Carmaker® vehicle dynamics platform where the highly optimized and robust features of CarMaker are added and interfaced in a Simulink environment by the implementation of S-functions. This provides a high flexibility to add Simulink blocks if needed without any loss of functionality. Thus, the coupling of MathWorks environment with CarMaker ensures that the resulting simulation environment possess a good degree of performance and stability.

1.5.2 Global Optimization Tool: TomLab

TomLab serves as a tool for solving optimization problems in a MatLab environment for basis of research, teaching and solutions to practical problems. It provides a modeling and optimal control environment in MatLab and has grown to be a robust a reliable tool for the solution of applied optimization problems.

The advantage of TomLab over other numerical and optimization solvers lies in the area of standardization of problem formulation, preventing the rewriting of problem formulation in different languages and the interface flexibility of using various solvers on a predefined optimization problem.

The solution of a problem in the TomLab environment is carried out in two steps:

- In the first step, the problem is defined and is stored in a MatLab structure
- In the second step, the solver is executed with a problem structure which is a single argument.

The solver output resulting in a standard result structure can be used in accordance with a different solver to reduce computational time.

The TomLab/CGO environment provides the user with options to solve costly global optimization problems which include the solvers *rbfSolve*, *ego* and *arbfMIP*. These solvers solve the problem by using the approaches of both global and local solvers and hence the presence of a local solver is necessary. The solvers can also be used in tandem with each other since they use different strategies for building the response surface and interpolation.

1.6 Report Structure

This report outline follows the flow chronologically as carried out in the actual thesis work.

Section 2 provides the background on principles of Local Optimization and Global Optimization which form the core of the thesis.

Section 2 discusses the modeling and tuning of the CAE Model with the literature review in section 3.1 to section 3.3 providing the theoretical background for the necessary validation and study carried out in the thesis work. The root concept of mechanics of force generation in the tires is discussed. Section 3.2 deals with the fundamentals of lateral vehicle dynamics used for the modeling of the 2 DOF Reference Model. Section 3.4 and 3.5 explain the sensitivity analysis carried out for the tire parameter tuning and optimization process carried out on the tire parameters in the CAE environment by comparing the vehicle characteristics to the real test data.

Section 4 describes the identification process of the 2DOF reference model. It details the tuning of the reference model with respect to the plant model.

Section 5 explains the background of Brake Control Module formulation in the CAE environment and the possibility to tune the respective parameters with a more detailed model of BCM. This is followed by a discussion section (section 6) on the results obtained.

2 OPTIMIZATION

Optimization in general has been receiving considerable attention since the past two decades. Especially in the Automotive and the Semi-Conductor Industry, the emphasis is strong on designing and developing products using math/computer models. Designing of optimization algorithms, that deal with the expensive functions for e.g. a crash simulation, can be challenging and time consuming. Most of the applications constitute of nonlinear and non-convex functions resulting in local minima. The task of global optimization is to find the global minima for an objective function which results in several local minima. The standard optimization techniques tend to get stuck in the regions that are locally optimal even before the global optimum is reached and hence the need of using global optimization solvers arises. In the cases where the derivatives of functions are hard to obtain, global optimization techniques can be used since the derivative information to carry out the optimization process is not required in these algorithms. Nils-Hassan Quttineh presents a comprehensive literature on models and methods for costly global optimization and military decision support systems (Quttineh, 2012). Since this particular task focuses on the use of CGO solvers, a brief literature review on Radial Bias Algorithm and Design and Analysis of Computer Experiments is done. From the point of view of surrogate modeling, types of the merit function available and Experimental Design approaches are discussed.

2.1 Local Optimization

Local Optimization solvers were used as an initial study to understand the process of optimization and to clarify the difference between regions of local and global minima and maxima.
For a better understanding of optimization process, local optimization solvers were used in *MatLAB* which resulted in local minimum values. *fminsearch* finds the minimum of a scalar function of several variables, starting at an initial estimate. This is referred to as unconstrained nonlinear optimization
x = *fminsearch* (fun, x_o) starts at the point x_o and returns a value x that is a local minimizer of the function described in fun. X_o can be a scalar, vector, or matrix, fun is a function handle.

2.2 Costly Global Optimization

This section will focus in brief the literature study on Costly Global Optimization (CGO). Different surrogate models in the form of Radial Bias Function and the Efficient Global Optimization are discussed along with the types of merit functions the algorithms used to judge the evaluation of costly function.

The principles of these surrogate models based on the defined Experimental Design are used in tandem with the Global Optimization solvers throughout the thesis work.

The understanding of the functioning of global optimization solvers in tandem was essential to perform the tuning and optimization tasks carried out in Section 3and Section 4.

The problem is considered to be costly if it is time consuming in resulting a solution for the function value. It is presented with the restrictions in the form of upper and lower bounds which can be linear, nonlinear or both. The general form of this can be represented as follows:

$$minf(x)$$

$$-\infty \leq x_L \leq x \leq x_U \leq \infty$$

$$b_L \leq A_x \leq b_U$$

$$c_L \leq c_x \leq c_U$$

Where
$f(x) \in R$ *and* x_L, x, $x_U \in R^d$. Matrix $A \in R^{m1xd}$, b_L, $b_U \in R^{m1}$; defines the m_1 linear constraints and c_L, $c_x, c_U \in R^{m_2}$ defines the m_2 linear constraints (Björkman & Holmström, 2000).

These functions are treated as a black box where the input is the function itself and the outputs are the function values. The special need for CGO solvers arises out of the absence of derivatives and the lack of functioning of standard optimization solvers on the black box functions. Thus, the methodology to evaluate the black box functions is by using a surrogate model i.e. a response surface which approximates the expensive function. The surrogate models work on the principle that new sample points are created at subsequent iteration where the original function should be evaluated. This is done by optimizing a less costly function commonly known as the *merit function*.

2.2.1 Surrogate modeling and response surfaces

In his paper (Jones, 2001) describes the existing approaches of using response surfaces for global optimization methods. The response surfaces are gaining popularity since the formulation of the surrogate models to solve global optimization problems consume less time to run time-consuming simulations. By the choice of an experimental design which basically governs the initial set of points to run the simulation on, a response surface is plotted to the resulting input-output data and surrogates are obtained which can be used to carry out the optimization process.

2.2.2 Experimental Design

Since the formulation of these surrogate models depends on the selection of the initial points, choosing an experimental design, i.e. the initial set of sample points to build the first interpolation surface, is influential. The procedure of choosing these set of initial points is also called Design of Experiments or ExD. Various strategies can be used to choose the initial sample points by an ExD approach to fill the sample space. In a Corner Point Strategy, the points are sampled on the constraints provided by the user in the solver. A better chance of generating interior points occurs when the boundary points along with the midpoints are sampled. However, to have the good performance from the solver, the mid-point of the function should result in a lowest function value. To avoid generating a minimum on the boundary in the case of the midpoint not resulting

in a lowest function value, a half bounded box can be created around the mid-point to locate the appropriate minimum for the lowest function value.
The *Latin Hypercube Design* is one of the efficient strategies for ExD since it guarantees sampling of points over a suitable sample space by spreading them out in a random manner, and none of the points attain an equal value in any dimension and hence making it a non-collapsible feature.
In *TomLab*, *Direct Algorithm* can be implemented with the command of glcDirect where the user can define its own number of sampling points that are done on the basis of rectangle segmentation. This is however used only to get a good set of initial points and for a costly problem it has limitations on its efficiency.

2.2.3 Radial Bias Function

The algorithm for RBF as explained in (Björkman & Holmström, 2000) works on the principle of Radial Bias Interpolation. In this case the subsequent point for the objective function to be evaluated is chosen by the measure of the bumpiness of a radial function, for example σ. A target value is chosen as the global minimum of the function *f*. For each y not belonging to $x_{1,\ldots,} x_n$ there exists a radial basis function s_y that satisfies the following interpolation conditions.

$$s_y(x_i) = f(x_i),\ i = 1,\ldots,n,$$
$$s_y(y) = f_n^*$$

The next point where the function should be evaluated is calculated as the value of *y* in the feasible region on the condition where it minimizes σ (s_y).

2.2.4 Efficient Global Optimization

The EGO model is based on the DACE framework i.e. Design and Analysis of Computer Experiments. DACE models a function and fits a response surface based on the selection of random variables distributed with mean μ and variance σ^2. The methodology of building the response surface in this case is based on modeling the objective and the constraint function with stochastic processes. This method is good at modeling the nonlinear and multimodal functions since the fitment of stochastic process to the data calibrates the model which informs how the function behaves and the subsequent point to evaluate the function on is chosen by computing the function value which is most consistent (Schonlau, Jones, & Welch, 1998). In the area of Global Optimization, the stochastic approach is known as Bayesian Global Optimization. Hence, the DACE is about estimating the correlation parameters of how the function behaves which makes predictions based on interpolations and extrapolations from the fitted data.

2.2.5 Functioning of solvers in TomLab

The environment of TomLab works on the principle of designing the optimization problem once and being able to use various solvers suitable for the designed optimization problem. This needs a well-designed system to be modeled in TomLab. The scope is vast and broad because of layers of interface routines, global variables, string evaluations and structure arrays (Holmström, 1999). The solver *rbfSolve* works on the principle of Radial Bias Algorithm which is enhanced to handle linear equality and inequality constraints and nonlinear equality and inequality constraints as well as mixed integer problems (Göran, Holmström, & Edwall, 2008). On the initial sampled points, a response surface is fitted and the algorithm balances between minimizing the function and adding new points to the sampled set. The solver *ego* works on the principle of Efficient Global Optimization but it treats the linear and nonlinear constraints separately. Essentially, *rbfSolve* and *ego* differ on few aspects. While the former works well with the corner point strategy and up to 2000 functional evaluations the latter is more suited with Latin Hypercube Design recommended up to 150 functional evaluations.

3 PREPARATION OF THE VEHICLE MODEL

The literature review (Sections 3.1-3.3) will deal with the fundamental research done on global optimization of lateral dynamics during the thesis. Background study was also done regarding the tires and their behavior and standard test maneuvers (section 3.5.1)

In section 3.1-2, theoretical background of tire and vehicle is documented. Study of lateral vehicle dynamics fundamentals was integral part of the thesis work (section 3.2). A 2DOF vehicle model was developed as a reference model based on the concepts explained in this section. Semi Empirical tire modeling used in the CAE environment is also studied (section 3.3).

3.1 Tire and Vehicle Dynamics

Tire road interaction is an important phenomenon in generating the forces between the tires and road which governs the motion of the vehicle. Being the mechanical linkage between the road and the vehicle, the tires provide the necessary longitudinal and lateral forces required for a change in velocity and direction of the vehicle.

The tires deform when the normal weight is applied by the vehicle. The flattened area occurring due to contact with the road is called the *contact patch* where all the forces act. These tire forces are a non-linear function of slip angles. The simplest tire models can be characterized by representing the tire forces as a function of cornering stiffness C_α and coefficient of friction μ (see Figure 6) (Dugoff, Fancher , & Segel).

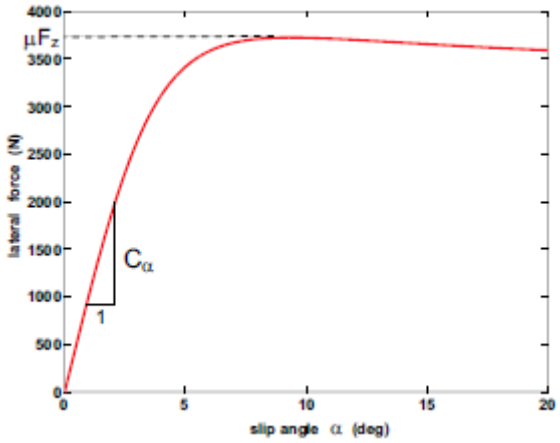

Figure 6 Generic Tire Curve

The slope of the curve of lateral force vs. slip angle is an important parameter in determining the behavior and handling of the vehicle in the linear region. As the slip angle increases, the friction forces exceed the limit, and the tire rubber begins to slide. When the tire is in the sliding region the maximum lateral force generated will be less than the peak force generated with the tire being in the linear or transient region. This is because the maximum lateral force the tire generates occurs at maximum tire grip. The nonlinear characteristics of the tire side force at higher accelerations have a major dependency on the load. Also, the tire characteristics might be offset from the origin which occurs due to the *tire pull phenomena* (Pacejka, 2002).

3.1.1 Mechanics of Force and Moment Generation

The tire forces are applied over the whole contact patch. The normal and the shear stresses acting on the contact patch result in the forces on the tire. Each tread element passing through the contact patch undergoes a shear mechanism which exerts shear stress. This shear stress integrated over the entire area results in tractive and/or lateral forces which are developed in the tire (Gillespie, 1992). The tire-road coupling due to friction is caused by two major phenomena, *adhesion* and *hysteresis*.

Consider Figure 7 and Figure 8 showing the force component due to adhesion and the hysteresis phenomena in rubber (Blundell & Harty, 2004).

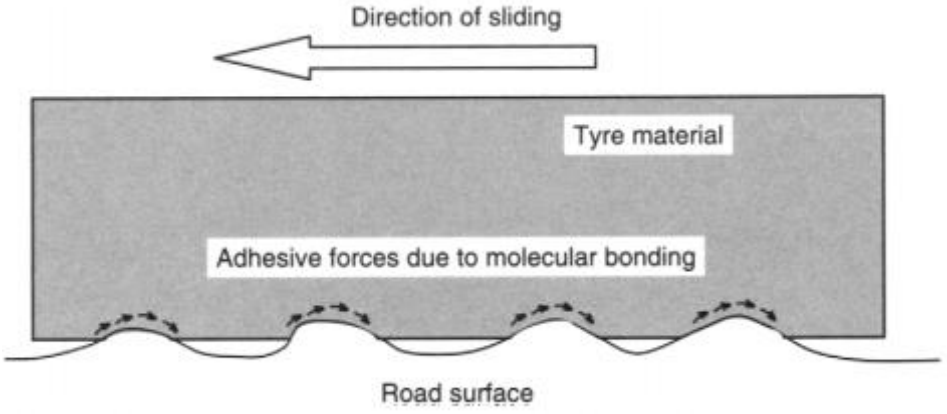

Figure 7 Frictional force component due to adhesion

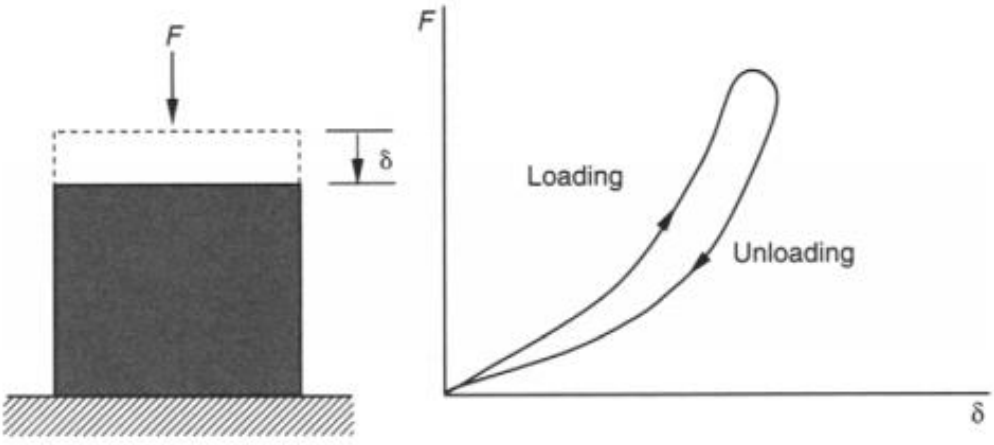

Figure 8 Hysteresis in rubber

The adhesion occurs because of the molecular bonding between the tire and the road surface which results in the adhesion force. The tire is viscoelastic and hence the properties of loading and unloading are different. The force during loading is higher than unloading and hence energy loss occurs when the tire slides over an aggregate on the road.

Pressure Distribution in the Contact Patch

During tire rolling, the pressure distribution in the contact patch is not symmetric. It tends to be higher in the front region of the contact patch. Figure 9 shows a more realistic representation of the parabolic pressure distribution (Pacejka, 2002).

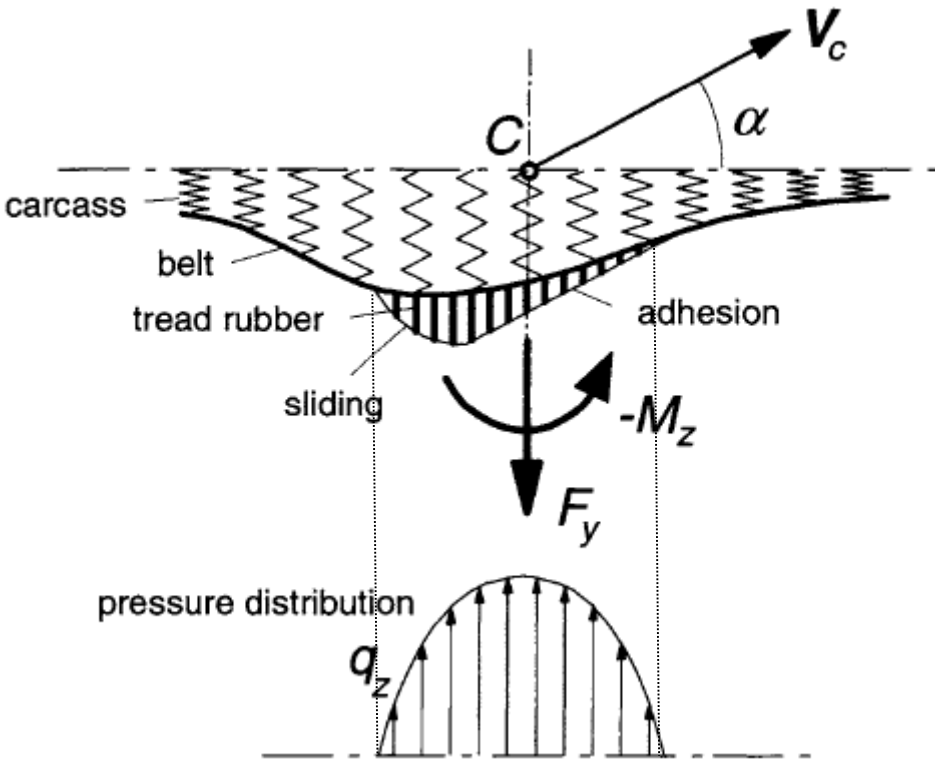

Figure 9 Tire model with flexible carcass at steady state rolling with slip angle α

Tire Brush Model

The tire brush model is a physical representation describing the generation of forces and moment due to the phenomena of adhesion and sliding. It was a well-known method for modeling the tire forces before the empirical models gained popularity for research purposes.

Consider Figure 10 showing the tire brush model (Pacejka, 2002). The model consists of elastic bristles which touch the road plane and are capable of deflecting in the direction parallel to the road plane.

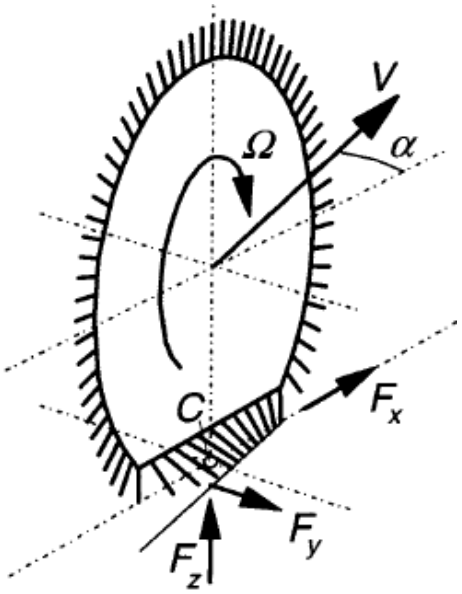

Figure 10 The tire brush model

These bristles can be assumed as treads. As the tire rolls freely without any side slip, there is no horizontal deflection in the tread elements. Due to the velocity vector *V* as shown in Figure 10, side slip angle α exists. Hence, the deflection of tread elements occurs, and their movement starts from the leading edge (right side of the picture) to the trailing edge. Figure 11 shows the tire brush model in pure slip region.

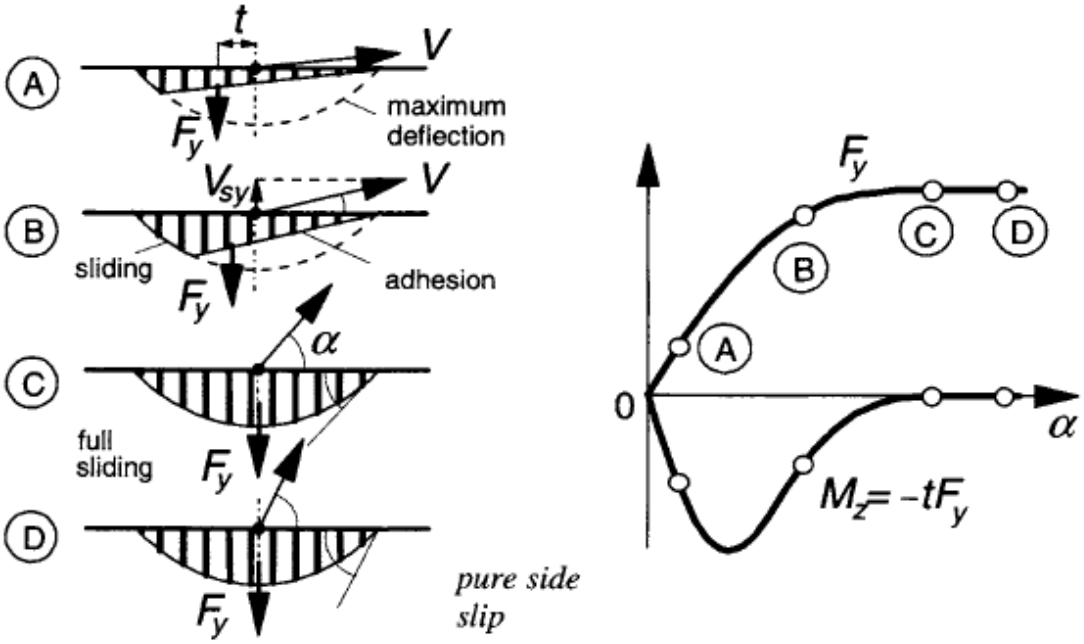

Figure 11 Tire brush model under pure side slip

The slip increases from small to large values because the deflections in the tread element move further from the contact patch. Also, the deflection has a linear variation and the tips form a straight line which is parallel to the velocity vector *V*. The maximum deflection that can be achieved is dictated by the coefficient of friction μ and stiffness of the tread element.

The pressure distribution in this case is assumed to take the shape of a parabola. At higher slip angles, the side force generated increases up to a certain region linearly. This side force acts at a point behind the tire contact center (point A) and the distance of this point from the tire contact center is called *pneumatic trail* termed as *t*. The aligning torque in the tire forces arises due to this pneumatic trail when multiplied with the side force.

The trail gets smaller and diminished as the slip angle increases (point B and C). The amount of adhesion with the road surface also decreases, and the tire enters the sliding region. When the wheel velocity vector is no longer parallel to the tangent of parabola, full sliding occurs (point D). At this point, the shape of pressure distribution is symmetric, and the side force generated attains the maximum value (Pacejka, 2002).

This mechanism of aligning torque generation is quite influential in the study of *steering feel* as it causes the centering effect. The aligning moment curve is also linear for the small slip angles and the gradient of this curve at zero slip angles is termed as the *aligning moment stiffness* for a given tire load.

3.2 Lateral Vehicle Dynamics

The prime goal of the thesis was brake control module tuning in the CAE environment. BCM, which involves the use of anti-lock braking systems maintaining the yaw stability of the vehicle, prevents the vehicle from skidding or drifting out unintentionally. In such cases, study of lateral vehicle dynamics becomes an integral part.

3.2.1 2-DOF Vehicle Model

Figure 12 shows the 2-DOF vehicle model for lateral vehicle dynamics also known as the bicycle model (Rajamani, Vehicle Dynamics and Control, 2006). The two degrees of freedom in this case are the vehicle's lateral position *y* and the yaw angle ψ which is measured with respect to the global *X* axis.

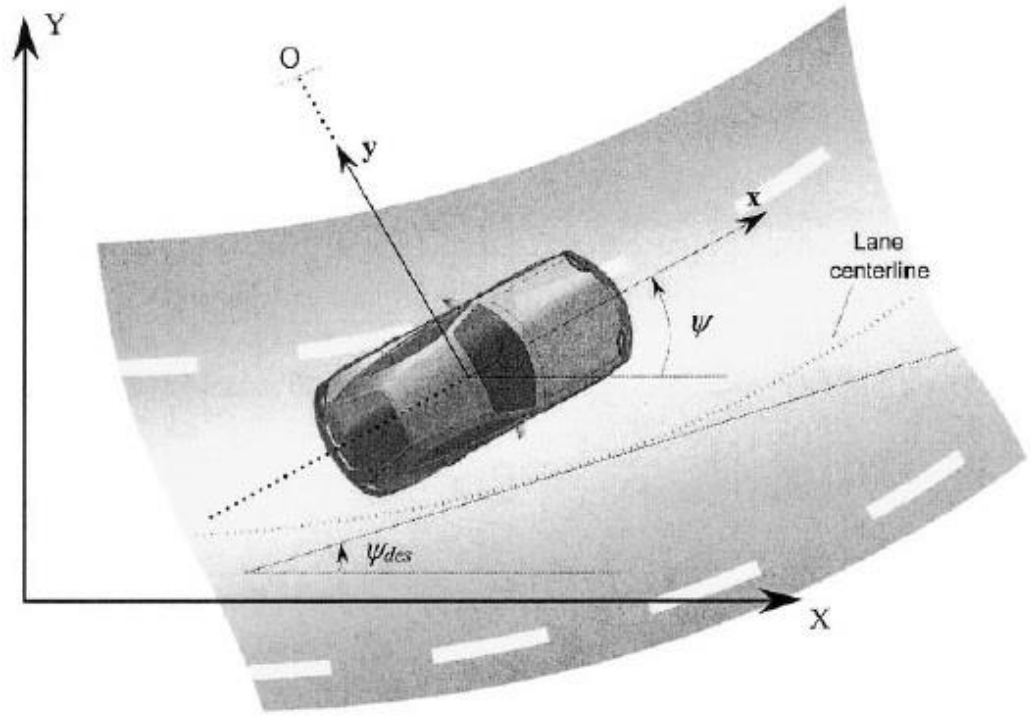

Figure 12 Bicycle model Lateral Vehicle Dynamics

By applying Newton's second law,

$$ma_y = F_{yf} + F_{yr}$$

Where F_{yf} and F_{yr} are the lateral tyre forces acting on the front and rear wheels respectively.

Also,

$$a_y = \dot{V}y + V_x\dot{\psi}$$

Where $\ddot{y}$ is the acceleration in the Y axis and $V_x\dot{\psi}$indicates the centripetal acceleration. Thus,

$$m(\ddot{y} + V_x\dot{\psi}) = F_{yf} + F_{yr}$$

The moment balance around the z axis leads to the following equation for the yaw dynamics. In this case $\dot{\psi}$ is the yaw rate and $\ddot{\psi}$ is the rate of change of yaw rate with l_f and l_r being the distances of the front tire and rear tire from the center of gravity of the vehicle.

$$I_z\ddot{\psi} = l_f F_{yf} - l_r F_{yr}$$

Now the slip angles for the front tire (α_f) and rear tire (α_r) can be written as,

$$\alpha_f = \delta - \theta_{vf}$$

$$\alpha_r = -\theta_{vr}$$

Where θ_{vf} and θ_{vr} are the angles made by the velocity vector with the heading direction of the tire. Thus, the lateral force on the front and rear wheel can be written as,

$$F_{yf} = 2\,C_{\alpha f}(\,\delta - \theta_{vf})$$

$$F_{yr} = 2\,C_{\alpha r}(-\theta_{vr})$$

Where $C_{\alpha f}$ and $C_{\alpha r}$ are the cornering stiffness of the front and rear tires respectively. Now,

$$\tan(\theta_{vf}) = (V_y + l_f\dot{\psi})/V_x$$

$$\tan(\theta_{vr}) = (V_y - l_r\dot{\psi})/V_x$$

Using small angle approximations,

$$\theta_{vf} = (V_y + l_f\dot{\psi})/V_x$$

$$\theta_{vr} = (V_y - l_r\dot{\psi})/V_x$$

The following state space form can be hence derived

$$\begin{bmatrix} V_y \\ \dot{\psi} \end{bmatrix} = \begin{bmatrix} \frac{-2\,C_{\alpha f} + 2\,C_{\alpha r}}{m\,V_x} & -V_x - \frac{2\,l_f\,C_{\alpha f} - 2\,l_r\,C_{\alpha r}}{m\,V_x} \\ -\frac{2\,l_f\,C\alpha f - 2\,l_r\,C\alpha r}{I_z\,V_x} & -\frac{2\,l_f{}^2\,C_{\alpha f} + 2\,l_r{}^2\,C_{\alpha r}}{I_z\,V_x} \end{bmatrix} + \begin{bmatrix} 2\frac{C_{\alpha f}}{m} \\ 2\,l_f\frac{C\alpha f}{I_z} \end{bmatrix}\delta$$

Note that the tire cornering stiffness values are multiplied by a factor of 2 in this case to indicate the total stiffness of the axle.

At reasonable speeds of vehicle turning and cornering, lateral forces and slip angles are developed in each wheel subjecting the vehicle to accelerate in the lateral direction.

3.2.2 Cornering Force and Slip Angle

During cornering, the forces acting on the tires deform it causing the resultant velocity vector and its body to deviate; this is the lateral tire slip. This slip angle is the difference between the heading angle of the wheel and the direction of travel. It is denoted by α. Figure 13 shows the relationship between lateral force and slip angle of the tire (The Racing and High Performance Tire , 2004). Lateral force is generated when the tire is deformed which results it to develop a slip angle.

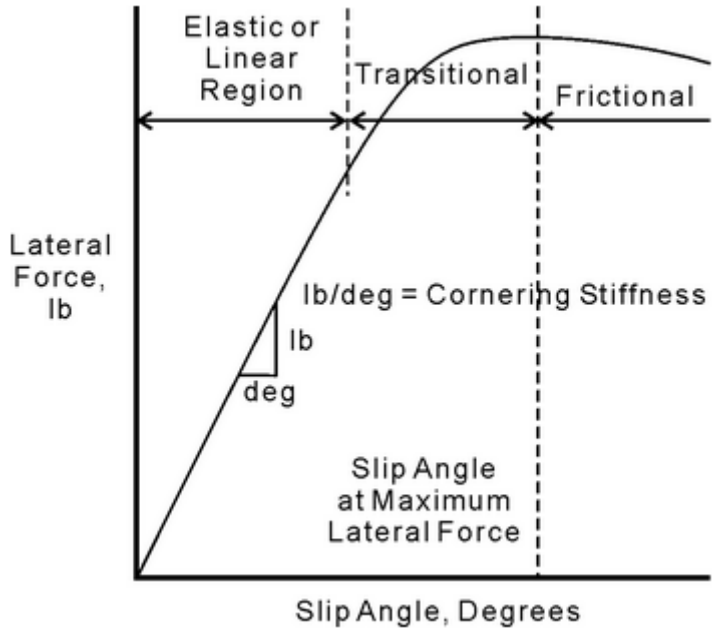

Figure 13 Lateral Force vs. Slip Angle

The slope of the linear region of variation of lateral force with slip angle determines the *cornering stiffness* of the tire. This slope might vary with the difference in tire design. The stiffness in this region depends on the stiffness in treads and sidewalls (The Racing and High Performance Tire , 2004).

The lateral force also called the cornering force is denoted by F_y

The relationship between the lateral force and the slip angle in the linear region is:

$$F_y = C_\alpha \alpha$$

Where C_α is the proportionality constant termed as cornering stiffness of the tire.

3.2.3 Effective Understeer Gradient

According to the geometry of the bicycle model, to complete a turn the steering angle is given by:

$$\delta = \frac{L}{R} + \left(\frac{W_f}{C_{\alpha f}} - \frac{W_r}{C_{\alpha r}}\right)\frac{V^2}{gR}$$

The above equation can also be written as:

$$\delta = \frac{L}{R} + K\, a_y$$

Where K is the *understeer gradient*

The understeer gradient in the above equation is an important parameter influencing the turning response of the vehicle. The term $\left(\frac{W_f}{C_{\alpha f}} - \frac{W_r}{C_{\alpha r}}\right)$ represents the understeer nature of the vehicle with the relative cornering compliance on front tires being larger than the rear. Three scenarios normally exist for a vehicle with specific values of understeer gradient.

i. Neutral Steer (K=0):

This is the ideal scenario when the lateral acceleration at CoG is compensated by increase in slip angle at both front wheels requiring no change in steering angle with increase of speed on a constant radius turn. K will be zero and hence the steer angle required will be $\frac{L}{R}$.

ii. Understeer (K>0):

The steering angle on a constant radius turn has to be increased with an increase in vehicle speed proportional to K. In this case, the front wheels are subjected to more slip than the rear wheels and hence more steering effort is required to keep the vehicle on its path.

iii. Oversteer (K>0):

In this scenario, the rear wheels are subjected to a higher slip. They tend to drift outward and hence the steer angle has to decrease to compensate for the vehicle path on a constant radius turn. As the speed increases on a constant radius, steering angle decreases.

The physical significance being that, under the effect of lateral force, the ratio expresses the number of degrees of slip angle per axle for every "g." It is also called *cornering compliance* (Gillespie, 1992).

There are additional factors influencing the cornering properties of the vehicle under the influence of lateral acceleration. Tire cornering stiffness determining the understeer affects the cornering force. Additionally, suspension and steering systems also have an influence on the cornering force. The two relevant effects arising out of this phenomenon are described.

Lateral Force Compliance Steer

Due to the bushings used in the suspension linkages, a high possibility of steering effect occurring due to lateral compliance in the suspension geometry exists. The compliance is assumed to be acted as a rotation on the yaw center. The effect of compliance steer depends on the geometry of the steering. If the rear axle is driven, and the yaw center is forward (in front of CoG), it causes an over steering effect, and if the yaw center is backward (behind CoG), it causes an understeering effect. Vice versa, on the front axle driven vehicle, a rearward yaw center causes an over steering effect, and a forward yaw center causes understeer effect.

Aligning Torque

The aligning torque contributes as an understeering effect as it acts counteracting the steering effort and the turn. Aligning torque arises from the fact that the lateral forces acting on the tire act at a point behind the tire center and the distance of this point from the tire center is called the *pneumatic trail*. The phenomena of pneumatic trail and its influence due to the aligning moment are explained in detail in section 3.1.1.

The understeer due to this effect is usually not that high and is in the order of 0.5. (Gillespie, 1992).

3.3 Semi-Empirical Tire Models

Semi-empirical tire models are developed on measured tire data instead of physical models. The term is called semi-empirical because the model is developed on measured data but it contains structures that have roots in the concepts explained in the previous sections. The tire model which is widely used is based on the work by Pacejka and is referred to as the *Magic Formula*.

Majority of the vehicle dynamic simulation studies carried out today are based on the tire models developed by curve fitting of experimental data involving empirical adjustments. Magic Formula (MF) tire models constructed on the basis of principles presented in section 3.1 are considered to be the state-of-the-art models for modeling the tire-road interaction forces for studies involving vehicle dynamics on simulation platforms.

In their research paper, (Bakker, Nyborg, & Pacejka, Tyre Modelling for Use in Vehicle Dynamics Studies, 1987), a method of describing and understanding the tire behavior through measured data is described. The representation of tire data extracted was suggested to be carried out using a formula fulfilling the following criteria:

- The side/lateral forces be represented as a function of slip angle
- The braking force be represented as a function of longitudinal slip
- The self-aligning torque be represented as a function of slip angle

In another joint effort between Volvo Car Corporation, Sweden and the Delft University of Technology, The Netherlands, (Bakker, Pacejka, & Lidner, A New Tire Model with an Application in Vehicle Dynamics Studies, 1989), the earlier method was revised which resulted in describing all characteristics of side force, brake force and aligning moment with greater accuracy.

Model Description

Hans B. Pacejka in (Pacejka, 2002) describes the general form of the formula that describes the tire characteristics for the given values of vertical load and camber angle as follows:

$$y = D \sin [C \arctan \{B x - E (B x - \arctan (B x))\}]$$

with

$$Y(X) = y(x) + S_V$$

$$x = X + S_H$$

Where Y is output variable F_x, F_y, or possibly M_z ; X is input variable tanα or κ

And B is stiffness factor, C is shape factor, D is the peak value, E is curvature factor, S_H horizontal shift and S_v vertical shift

For a set of given values of B, C, D and E, the curve gathers an asymmetric shape around the origin. The two shifts S_H and S_V are the shifts of the curve from the origin in the X and Y direction.

The Magic Formula creates characteristics curves which are very similar to that of the lateral force, aligning moment and longitudinal force. These curves are plotted against slip angle α or longitudinal slip κ. The effect of load F_Z and camber angle γ is also included when producing these curves.

Figure 14 shows the characteristic plot produced from the Magic Formula with certain parameter values. D indicates the peak value of the curve. The C factor controls the limits of the sine function in the Magic Formula and hence dictates the shape. The B factor determines the slope at the origin and is called the *stiffness factor*, whereas the product of factors B, C and D gives the *cornering stiffness* of the tire. These factors are later described in detail in the area of pure slip and aligning moment in section 3.4.2.

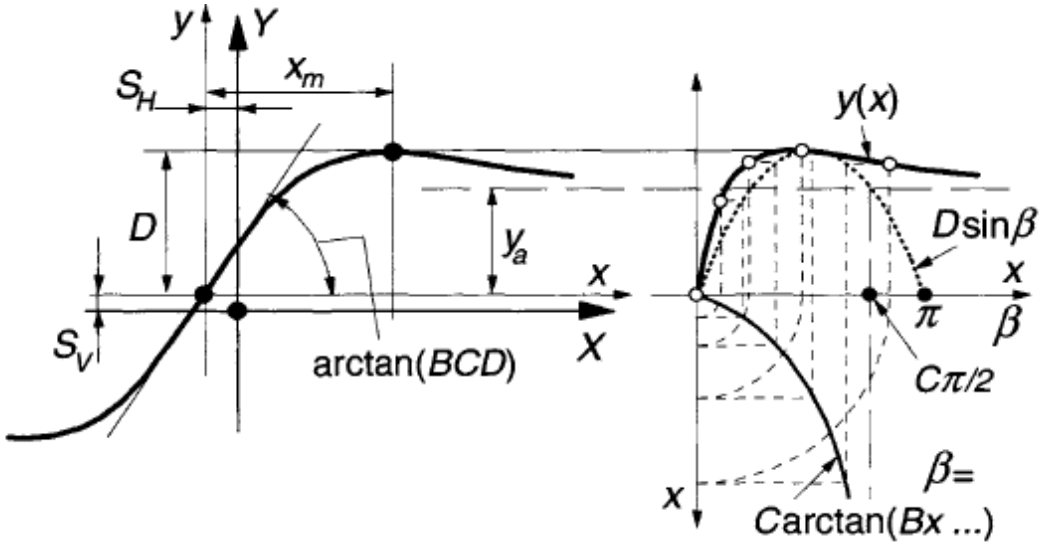

Figure 14 Characteristic curve produced from Magic Formula (Pacejka, 2002)

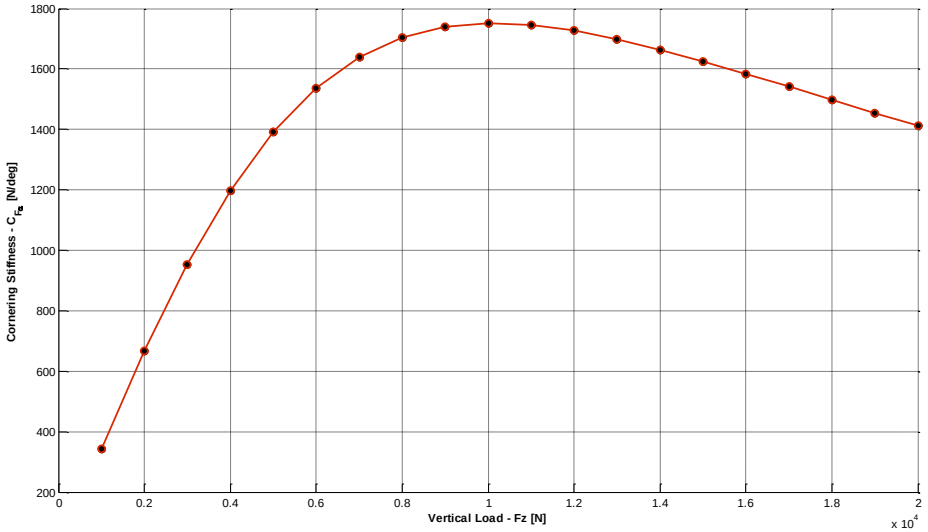

Figure 15 Cornering Stiffness vs. Vertical Load

Figure 15 shows the dependency of cornering stiffness with vertical load. The blue marker indicates the maximum value of cornering stiffness at zero camber angles. Figure 16 shows the dependency of lateral force on camber angle. For a cambered wheel, the cornering stiffness i.e. the slope of the lateral force curve decreases with an increase in camber angle.

The nondimensional parameters which include the effect of absolute values, variation with load and variation with camber are included for longitudinal force, lateral force and aligning moment in both pure and combined region. These parameter values when

calculated based on fitting tire measurement data are compiled as a tire file which is representative of the tire measured.

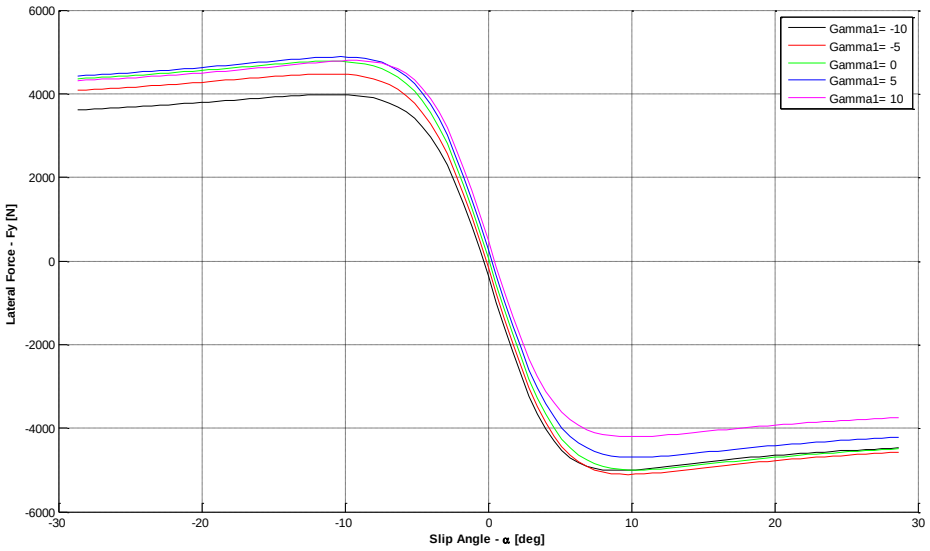

Figure 16 Dependency of Cornering Stiffness on Camber Angle

Below, parameters and equations are listed for lateral force, aligning moment and some transient parameters which are included in a tire file.

Formulas for Lateral Force in pure Side Slip

$F_y = F_{y0}(\alpha,\gamma,Fz)$

$F_{yo} = D_y \sin[C_y \arctan\{B_y \alpha_y - E_y(B_y \alpha_y - \arctan(B_y \alpha_y))\}] + S_{Vy}$

$\alpha_y = \alpha + S_{Hy}$

$\gamma_y = \gamma \cdot \lambda_{\gamma y}$

$C_y = p_{Cy1} \cdot \lambda_{Cy}$

$D_y = \mu_y \cdot F_z \cdot \zeta_2$

$\mu_y = (p_{Dy1} + p_{Dy2}\, df_z) \cdot (1 - p_{Dy3}\, \gamma^2_y) \cdot \lambda_{\mu y}$

$E_y = (p_{Ey1} + p_{Ey2}\, df_z) \cdot \{1 - (p_{Ey3} + p_{Ey4}\, \gamma_y)\, sgn(\alpha_y)\} \cdot \lambda_{Ey}$ with $E_y \leq$

The cornering stiffness can be expressed as:

$K_y = P_{Ky1} \cdot F_{z0} \cdot \sin[2\arctan\{\frac{F_z}{P_{Ky2} F_0 \lambda_{Fz0}}\}] \cdot \lambda_{Fz0} \cdot \lambda_{Ky}$

$K = K_{y0} \cdot (1 - p_{Ky3}|\lambda_y|) \cdot \zeta_3$

$B_y = K_y / (C_y D_y)$

$S_{Hy} = (p_{Hy1} + p_{Hy2}\, df_z) \cdot \lambda_{Hy} + p_{Hy3}\, \lambda_y \cdot \zeta_0 + \zeta_4 - 1$

$S_{Vy} = F_Z \cdot \{(p_{Vy1} + p_{Vy2}\, df_z) \cdot \lambda_{Vy} + (p_{Vy3} + p_{Vy4}\, df_z) \cdot \gamma_y\} \cdot \lambda_{\mu y} \cdot \zeta_4$

Lateral Force coefficients in pure Side Slip

Following table shows the parameters for lateral force coefficients in pure Side Slip which are used in the Adams Tire Property file for CAE purposes.

Table 1 Lateral Force coefficients in pure Side Slip

Name	Name used in the tire property file	Explanation
P_{Cy1}	PCY1	Shape factor Cfy for lateral forces
P_{Dy1}	PDY1	Lateral friction Muy
P_{Dy2}	PDY2	Variation of friction Muy with load
P_{Dy3}	PDY3	Variation of friction Muy with squared inclination
P_{Ey1}	PEY1	Lateral curvature Efy at Fznom
P_{Ey2}	PEY2	Variation of curvature Efy with load
P_{Ey3}	PEY3	Inclination dependency of curvature Efy
P_{Ey4}	PEY4	Variation of curvature Efy with inclination
P_{Ky1}	PKY1	Maximum value of stiffness Kfy/Fznom
P_{Ky2}	PKY2	Load at which Kfy reaches maximum value
P_{Ky3}	PKY3	Variation of Kfy/Fznom with inclination
P_{Hy1}	PHY1	Horizontal shift Shy at Fznom
P_{Hy2}	PHY2	Variation of shift Shy with load
P_{Hy3}	PHY3	Variation of shift Shy with inclination
P_{Vy1}	PVY1	Vertical shift in Svy/Fz at Fznom
P_{Vy2}	PVY2	Variation of shift Svy/Fz with load
P_{Vy3}	PVY3	Variation of shift Svy/Fz with inclination
P_{Vy4}	PVY4	Variation of shift Svy/Fz with inclination and load

Among the above parameters, the chosen parameters to be tuned after the sensitivity analysis were:

- PCY1
- PDY1
- PKY1

The steady state characteristics were influenced by above mentioned parameters. Influence due to variation of load, inclination or both were not investigated to simplify the optimization process.

Aligning Torque coefficients in pure Side Slip

Following table shows the two parameters for Aligning Torque coefficients in pure Side Slip which are used in the Adams Tire Property file for CAE tuning. The formulas pertaining to the aligning moment in pure side slip and other parameters in the tire property file can be found in APPENDIX B.

Table 2 Aligning Torque coefficients in pure Side Slip for Optimization

Name	Name used in the tire property file	Explanation
Q_{bz1}	QBZ1	Trail slope factor for trail Bpt at Fznom
Q_{dz1}	QDZ1	Peak trail Dpt = Dpt*(Fz/Fznom*R0)

Steering compliance can be present due to the lateral compliance in the suspension. And it usually acts as a rotation about the yaw center. The aligning moment generated from the tires on a vehicle acts as the resisting force to the steering and hence contributes to the understeering characteristics of the vehicle. As explained in 3.1.1, the lateral forces are developed behind the tire center at a distance p which is the pneumatic trail. Hence in this study, both the factors that directly influence the pneumatic trail; i.e. the peak trail and the slope factor are investigated.

Transient parameters

Relaxation behavior in the tire accounts for the fact that the lateral forces in the tire do not build up instantaneously, and the steady state levels are only attained once the tire travels a certain distance.

A brief analysis on the transient parameters was also done in this study. In the PAC 2002 format, the low-frequency behavior of the tire is taken into consideration using the stretched spring model explained in section.

Coefficients for transient response

Table 3 Transient parameters in the tire file for CAE Study

Name	Name used in the tire property file	Explanation
P_{Tx1}	PTX1	Longitudinal relaxation length at Fznom
P_{Ty1}	PTY1	Peak value of relaxation length for lateral direction

In this study for transient maneuvers, only two parameters PTX1 and PTY1 were varied to study the influence. No optimization was carried out on the parameters due to limitations in defining the transient maneuver in IPG and time constraints.

3.3.1 PAC 2002 tire model

The MF tire model can be used for CAE analysis subject to the following conditions:

- Cases when the road obstacle wavelengths are larger than that of the tire radius with frequency up to 8 Hz
- Applicable to car, truck and aircraft tires with camber angles with respect to the road not exceeding 15 degrees

Due to these properties embedded in the tire model, the PAC 2002 MF tire model can be used effectively in the following vehicle driving scenarios:

- Steady State Cornering
- Single or double lane change
- Braking or power off in a turn
- Split – mu braking effects
- ABS braking

The PAC 2002 tire file is developed on the principles of a semi-empirical tire model.

In the following study, some parameters in the tire property file will be examined based on particular steady state and transient maneuvers. The parameters chosen to be studied are based on the sensitivity analysis carried out in section 3.4. These maneuvers are carried out in the real test environment on V526 M1 model, and the same maneuvers are simulated in IPG Carmaker®.

The test maneuvers carried out on the test vehicle are subjected in IPG Carmaker® by using the same vehicle speed and the steering wheel angle as recorded from the test data. This ensures that the test maneuver is simulated without any discrepancy between the real data and simulated data.

Subsequently, the simulated data and real data are compared, and the tire properties are optimized which is explained in section 3.5.3**Error! Reference source not found.**. An xample of tire file in the PAC 2002 format also used within IPG is shown in APPENDIX D – Example of PAC2002 Tire Property File

3.4 Sensitivity analysis

To understand which tire parameters to tune and optimize, a sensitivity analysis was carried out on the influence of different tire parameters. The influence of parameters contained in the Adams Property File is complicated to comprehend and analyze under a dynamic simulation. Thus, an initial study was done based on static models to realize the trend of parameters affecting the behavior of the tire. Later, the tire parameters selected to be tuned (section 3.4.2) were modified in the optimization loop by subjecting the tire file to the selected maneuvers. This optimization process is explained in section 3.5.2.

3.4.1 Comparison of tire files

Two tires files (Tire A and Tire B) were studied with different parameter values which were measured on the test bench. Figure 14 to Figure 16 show the characteristics of particular curves for both the tire files. Tire A (black) and Tire B (red) is compared on the basis of pure lateral force (Figure 17) and pure aligning moment (Figure 18). The same markers in the figures indicate that the tire characteristics are plotted with same normal load.

Considerable difference was seen in the tire curves. In the case of pure lateral force (Figure 17) the Tire B attains a higher value of lateral force at same normal loads. The influential factor is the D factor in the tire file (**PDY1**) which was different in both tire files. Also, at high normal loads, the slope of the curve, and hence the cornering stiffness was different for both tires influenced by factor **PKY1**. Similar trend was observed in the case of pure aligning moment. The shape factor **PCY1** was approximately same in both tire files and therefore the shape around the peak value also remained the same. Variations will not be noticeable if PCY1 lies between 1 and 1.5 in different tire files.

The peak value of the aligning moment was higher for Tire A for various normal loads. This was accounted due to the factor **QDZ1**. **QBZ1**, which dictates the slope of aligning moment was similar in both tire files, hence not much difference is seen in the slope of aligning moment.

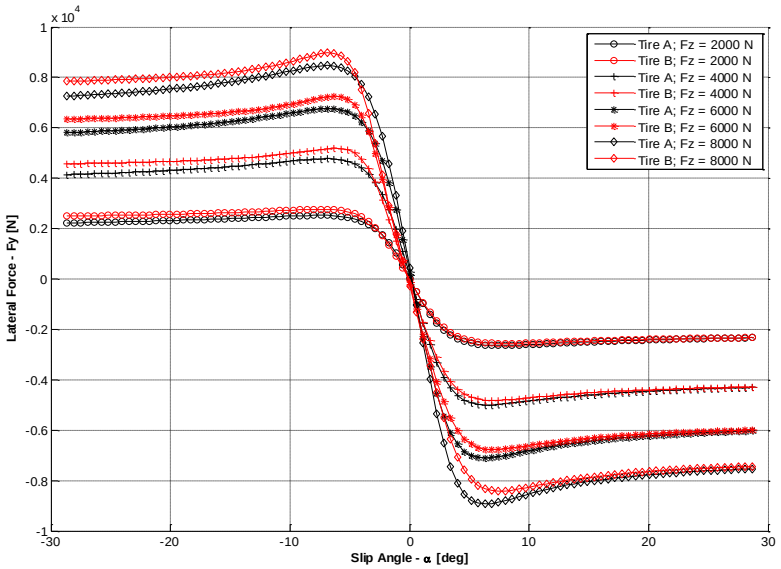

Figure 17 Lateral force comparison for two tire files

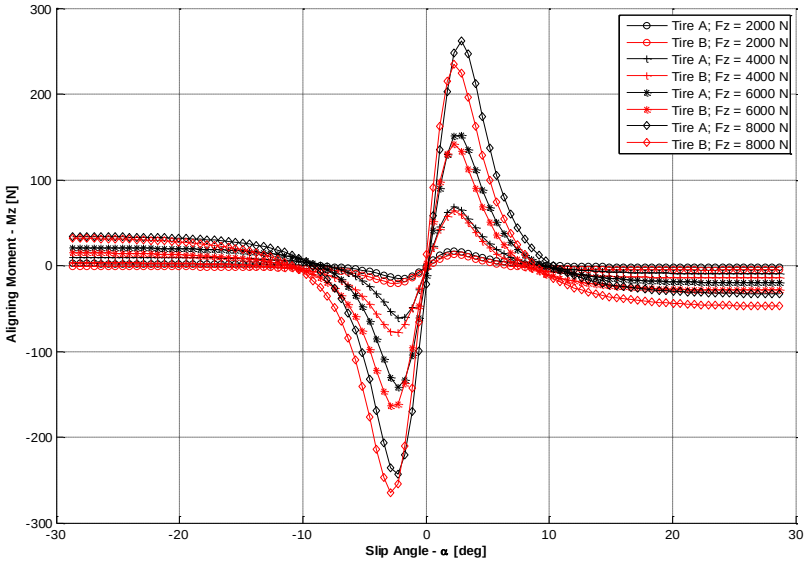

Figure 18 Aligning moment comparison for two tire files

3.4.2 Parameters chosen for optimization and their influence

This section provides the reasoning on the tire parameters chosen to be optimized in the Adams Property File and the influence of these factors on force characteristics.

After an analysis of static characteristics derived out of different tire files, a parameter influence study was done on the tire file corresponding to the tires used on V526. In this study, the parameters to be optimized had to be selected.

The study deals with the tire optimization in the area of lateral force (pure side slip) and aligning moment (pure side slip). Effect of transient parameters is also studied briefly.

The sequence, methodology and validation of optimization of the tire parameters are explained below. The subsequent section contains the corresponding results.

3.4.3 Parameter influence for lateral force in pure slip

Consider Figure 19 shown for Lateral Force vs. Slip Angle produced with the Magic Formula

$y = D \sin [C \arctan \{B x - E (B x - \arctan (B x))\}]$

Similar curves can be produced for F_y and M_z with inputs tanα or κ.

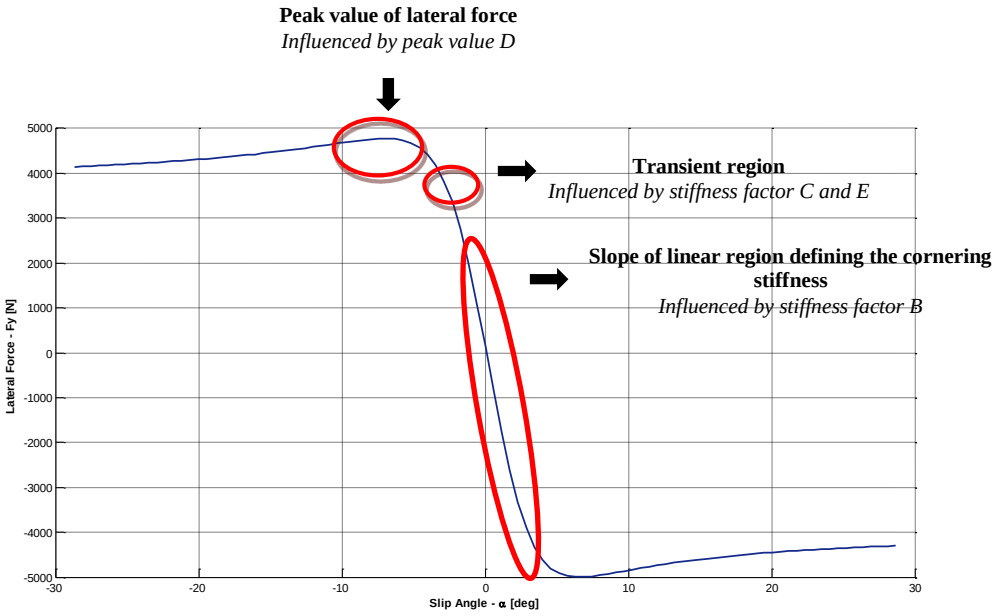

Figure 19 Lateral Force vs. Slip Angle curve at a given nominal load

The slope of the linear region defines the cornering stiffness. The factor B determines the slope at this origin and is termed as the stiffness factor. As the slip angle increases, the tire reaches the peak lateral force which is determined by peak value D in the tire file. Also, the transition to this nonlinear region is affected by two factors, C and E. C determines the drop of lateral force with the increasing slip angles and E determines the curvature of the curve around the peak value. In other words, factors C and E together control the horizontal position of the peak along with the sharpness of its curvature.

The B Factor is influenced by PKY1 in the tire property file as seen in Figure 20. The slope of the linear region varies as the parameter value is changed, however the peak value of lateral force remains the same.

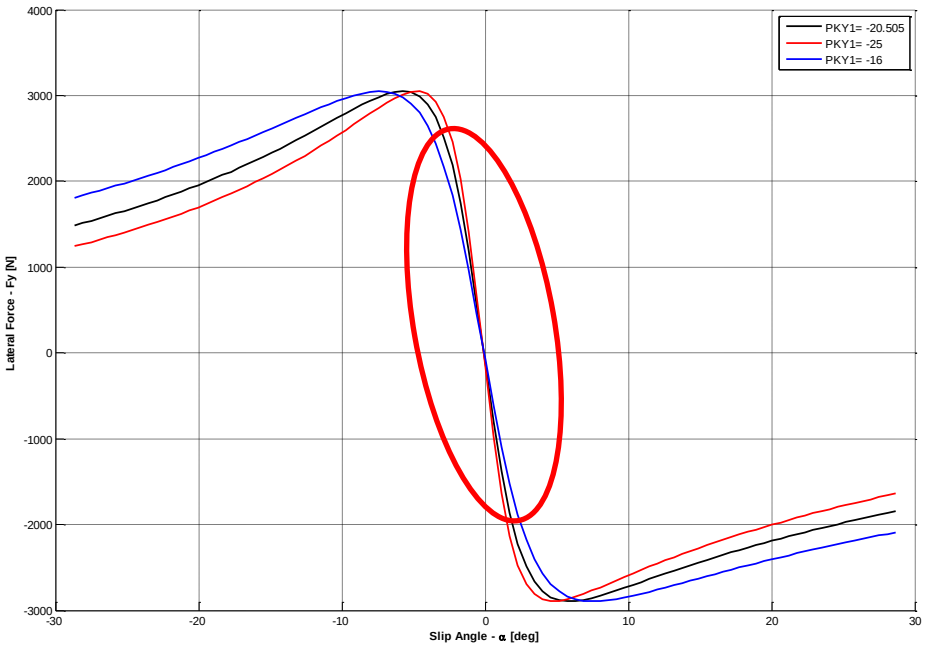

Figure 21 shows the influence of C factor on the lateral force curve with the change in PCY1 parameter. C is termed as the shape factor and determines the range of the sine function appearing in the Magic Formula equation. PCY1 should be greater than 1 in order for the lateral force to attain a suitable value; if it is too high (for e.g. the value being 2.1 as seen in Figure 21 (black)), force inversion takes place that causes severe force drop at high slip angles.

Figure 20 Influence of stiffness factor on cornering stiffness of a tire

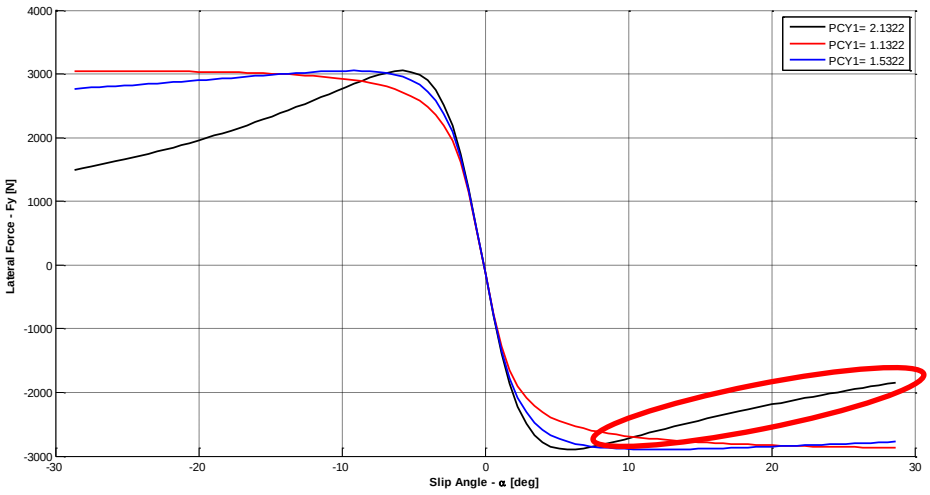

Figure 21 Influence of shape factor on lateral force curve

The D factor dictates the peak value of the lateral force. By varying the parameters PDY1 in the Adams Property File, the influence of the peak value of lateral force that the tire can achieve can be influenced as seen in Figure 22.

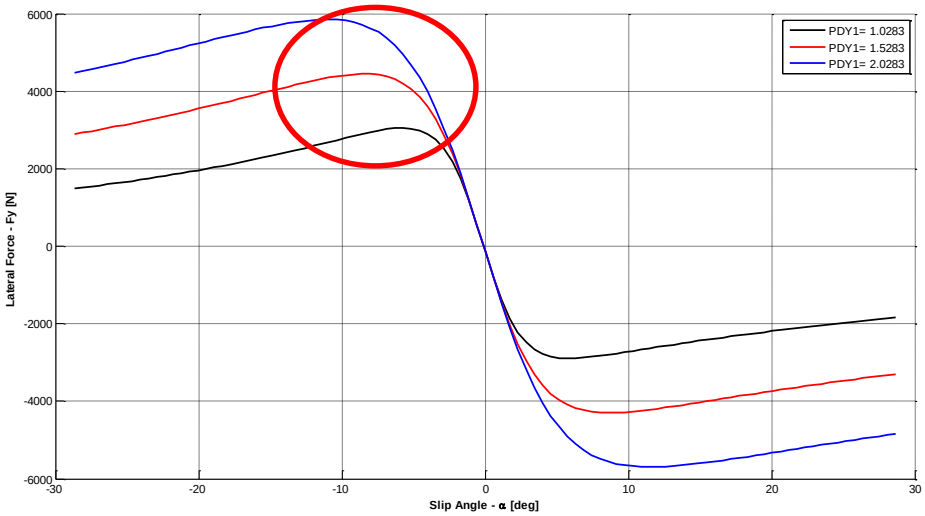

Figure 22 Influence of peak value factor PDY1 on lateral force curve

3.4.4 Parameter influence for aligning moment in pure slip

Figure 23 shows the aligning moment behaviour with respect to lateral force curve for a particular tire file at a given normal load. It has a linear region up to certain value of slip angle which is influenced by Trail Slope Factor B, similar to stiffness factor B in the case of lateral force curve. After the peak aligning moment is reached, there is a sudden fall in the trend of aligning moment and then it decays. Peak Trail Factor D determines the peak value of aligning moment.

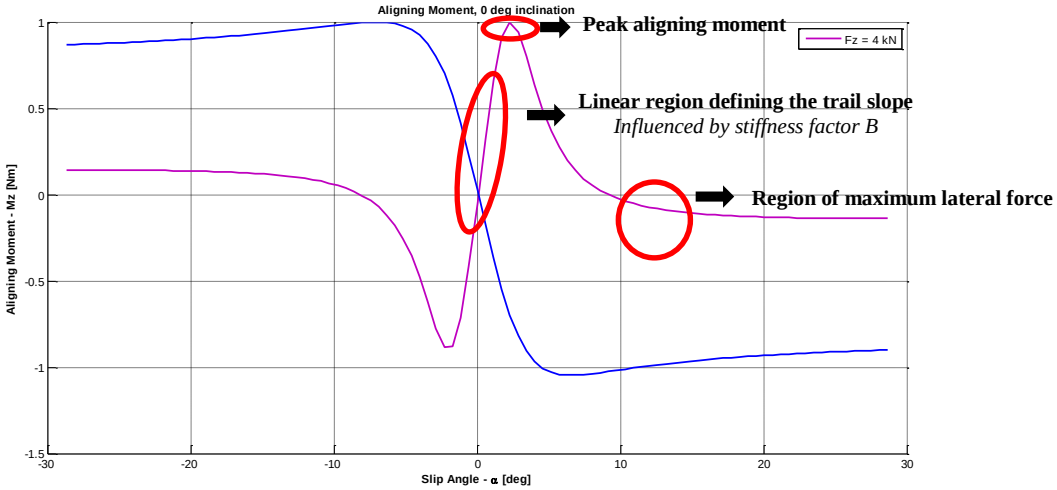

Figure 23 Aligning moment and tire lateral force

Maximum value of aligning moment is attained at certain slip angle (Figure 24 and Figure 25) with the presence of high pneumatic trail.

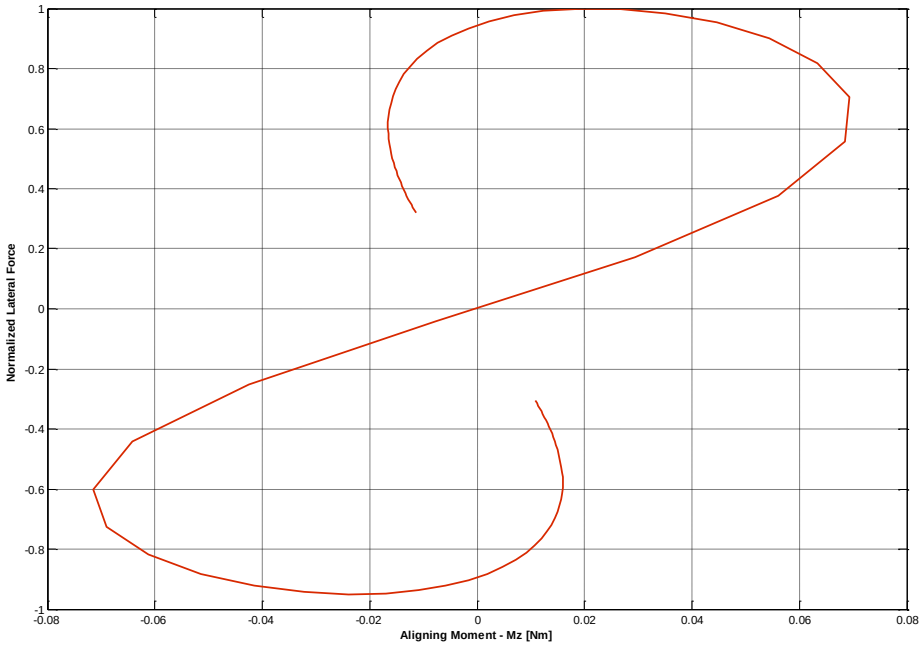

Figure 24 Lateral Force vs. Aligning Moment for a specific tire file

The pneumatic trail decays with the increase in slip angles as the lateral force increases. Thus, in the region of high lateral forces, the aligning moment is comparatively low which might be only contributed due to residual torque. Figure 25 and Figure 26 show the influence of factors QBZ1 and QDZI on aligning moment with respect to slip angle.

Residual moment is not considered in this study. The peak aligning moment usually occurs in the range of 4-5 degrees of slip angle and then starts to drop with higher slip angles. Hence, the peak aligning moment (D_T) is a critical parameter in this study that primarily influences the magnitude of M_z. The angle, i.e. the slope of M_z is dictated by shape factor (B_T).

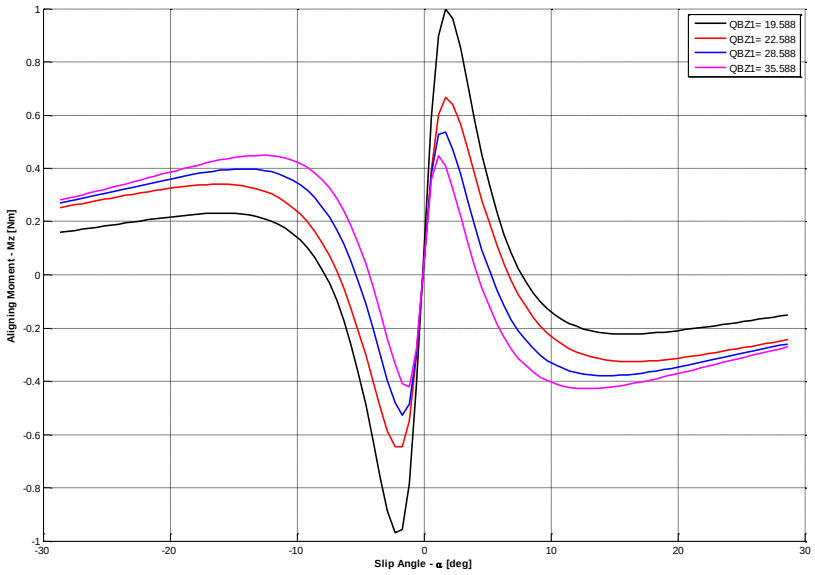

Figure 25 Influence of Trail Slope factor QBZ1 on the aligning moment curve

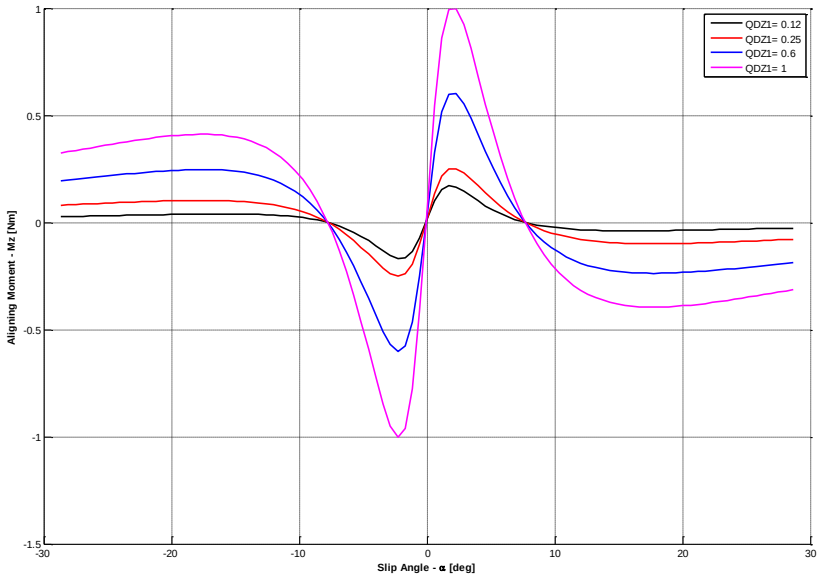

Figure 26 Influence of Trail Slope factor QDZ1 on the aligning moment curve

3.5 CAE Model Verification and Tuning

The test maneuvers carried out on the physical vehicle subjected to controlled inputs of steering and vehicle speed should be suitable for the validation of CAE model and other vehicle attributes. This is necessary to determine the measures and characteristics of the vehicle under steady state conditions.

3.5.1 Test Maneuvers

The light vehicle handling and the electronic stability control research program was created by the NHTSA in 2004. In 2006, it was announced by NHTSA that ESC should be installed as standard equipment on all light vehicle models being produced from 2012 onwards.

In 2005, NHTSA examined the effectiveness of ESC installed on the vehicles using twelve maneuvers divided into three groups (Forkenbrock G. J., 2005). Five test vehicles were used and the tests were performed under the nominal loading conditions. NTHSA considered that any test which depicts a good value of ESC effectiveness should be able to subject the vehicle under high level of severity, should be repeatable and reproducible to extract multiple data with the same input. It should consider high responsiveness, lateral stability and compliance of the vehicle. The NHTSA Fishhook and the J-turn maneuver are the most severe tests from NHTSA and provide the capability of quantifying on road, un-tripped rollover propensity. In 2006, NHTSA proposed the Sine with Dwell test as the standard test for ESC systems installed on the vehicles. To confirm that the vehicle can successfully mitigate over steer, the vehicle should not spin out in neither left nor right hand Sine with Dwell maneuver. Specifically, a single sine input is performed on the vehicle with a gap of 500 ms between the completion of third quarter of sine input of 0.7 Hz and before the fourth quarter is initiated (Forkenbrock & Boyd, 2007).

The standard test maneuvers for various vehicle testing depend on the metrics proposed to be measured. These maneuvers can be grouped on the basis of automated steering; driver based steering and open or closed loop steering maneuvers. The open or closed loop maneuvers are conducted with a robot steering input to maintain the uniformity among different tests.

Test Maneuvers selected for the study

Steady State Cornering

This test is carried out by keeping the path radius constant with an increase in the vehicle speed. The procedure is executed in clockwise and anti-clockwise direction with the lateral acceleration up to 8 m/s^2. The test focuses on the understeering characteristics of the vehicle. With the simultaneous increase in steering angle and vehicle speed, the lateral acceleration builds up providing a good correlation between the steering angle and lateral acceleration. The behavior is linear up to 3 m/s^2 followed by excessive understeer until the limits of adhesion. The steady state circular test is also considered as a standard test to validate the tire models based on the tire-related measurands logged in the controlled environment.

Figure 27 and Figure 28 show the real data extracted from the test (red) carried out on the test vehicle and filtered (blue) for the optimization of tire parameters.

On center

This test is done to evaluate the vehicle response to small steering wheel angle input. The On Centre test takes into account the effect of steering torque and hence is an important maneuver to evaluate the vehicle behavior based on a certain model of steering system. It is carried out at a maximum acceleration of 4 m/s^2 at 75 kmph and 120 kmph with a maximum steering wheel angle input of 0.3 radians.

Figure 29 shows the real data extracted from the test (red) carried out on the test vehicle and filtered (blue) for the optimization process.

Sine with dwell

Sine with Dwell is a standard test carried out by organizations like The National Highway Traffic Safety Administration (NHTSA) and the Euro NCAP on all the cars to check the performance of the ESC system. The test procedure is carried out by subjecting the vehicle up to a certain desired speed and then executing the steering angle as shown in Figure 30. The maneuver is based on a single cycle sinusoidal steering input with the maximum amplitudes being identical in the first and second half of the maneuver. The test is supposed to excite the oversteer response of the vehicle.

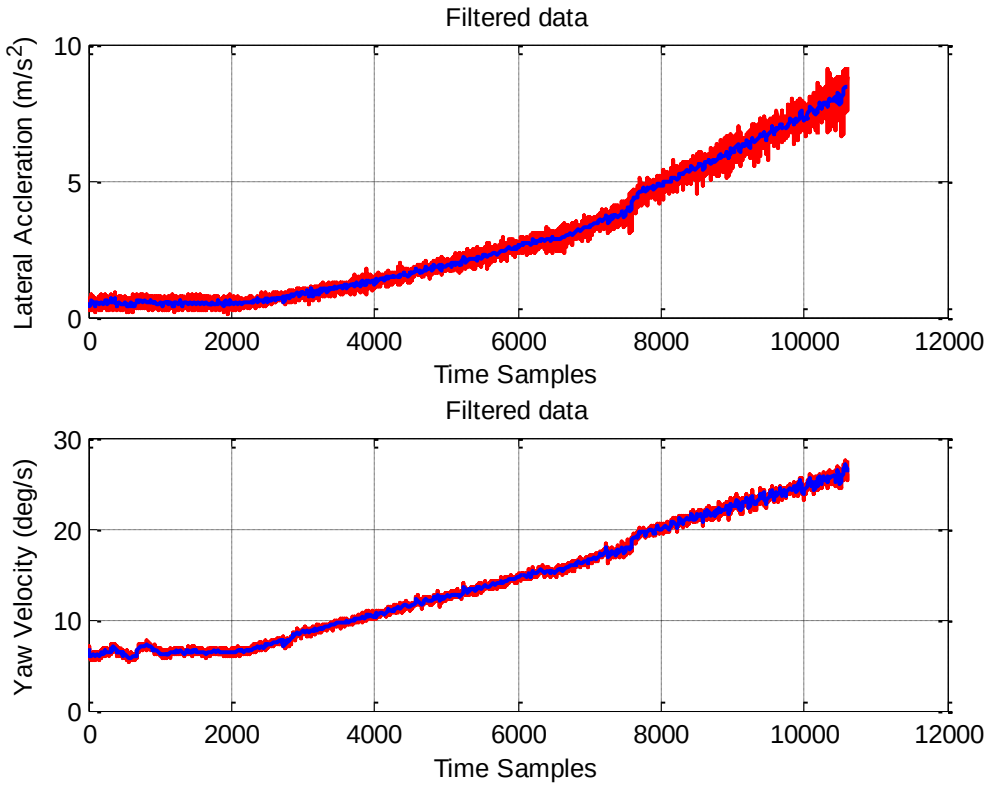

Figure 27 Steady State Cornering Left Turn

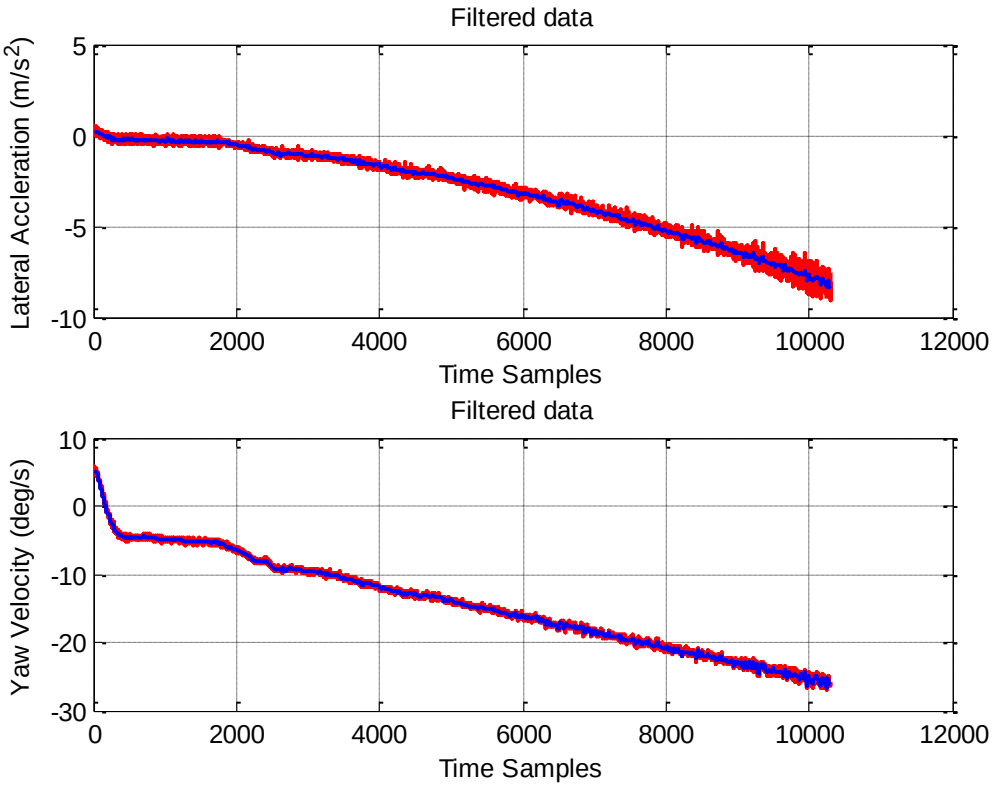

Figure 28 Steady State Cornering Right Turn

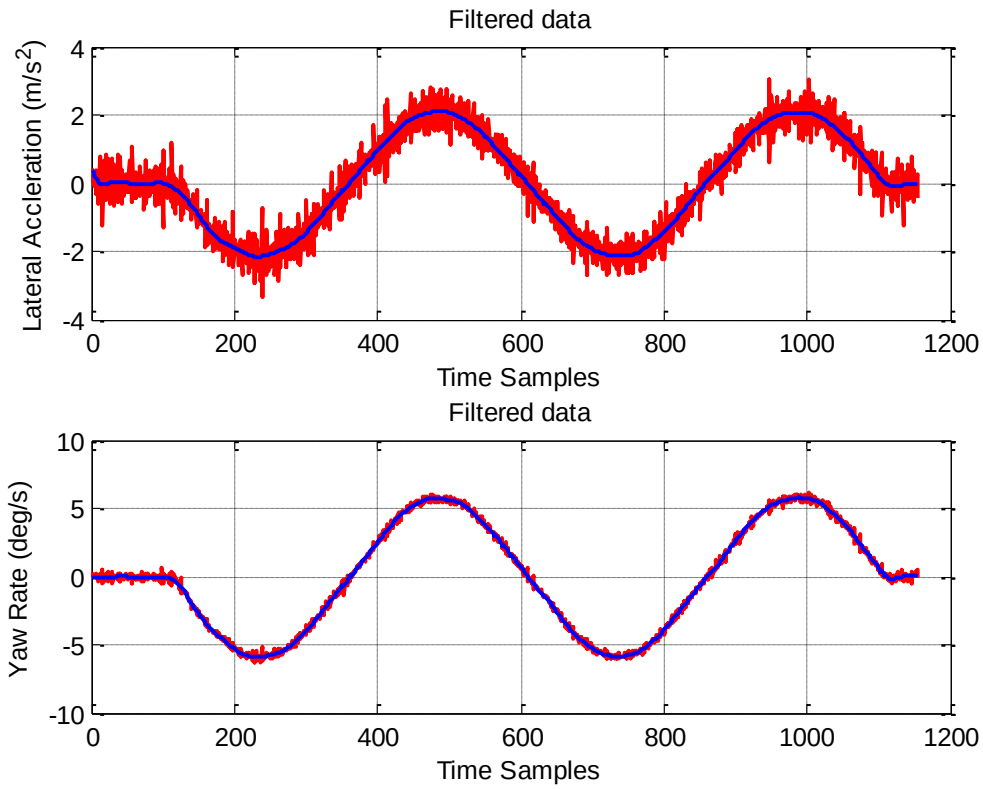

Figure 29 On Centre Test

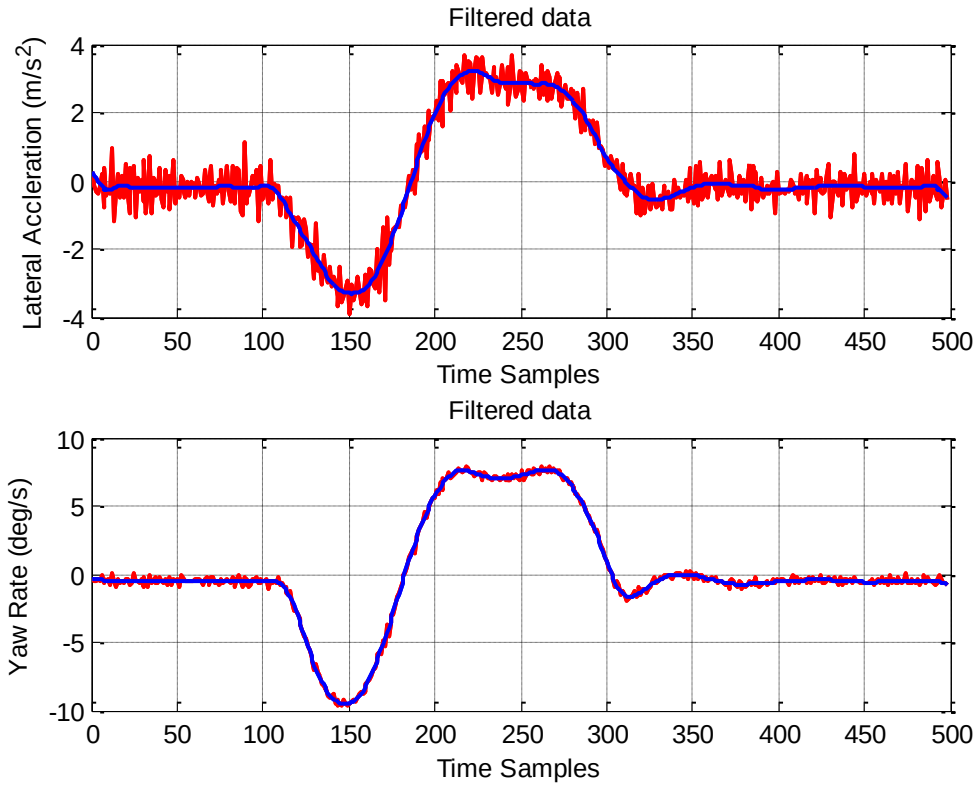

Figure 30 Sine with Dwell, Right to Left

3.5.2 Tuning of Tire Parameters

The process carried out to optimize and tune the tire parameters based on real test data extracted from the maneuvers is explained in this section. The flowchart of optimization sequence and selection of weighting parameters and error function is mentioned in 3.5.2.1. Section 3.5.2.1 details the optimization process with supported concepts: each optimization step is followed by corresponding results in order to facilitate better understanding of the optimization process.

3.5.2.1 Optimization Sequence and Process Flowchart

Figure 31 shows a flowchart of the optimization process for tuning the tire parameters.

The extracted data for the steering wheel angle and the vehicle velocity from the actual test data is compiled into ASCII formatted text files which are used as an input in the driver model of IPG CarMaker. Default tire file in the IPG format converted from Adams 2002 format is used in the simulation platform. In the optimization loop, simulation is performed for a specific maneuver, and the characteristics for yaw rate and lateral acceleration are compared with real test data to generate the error. The specific tire parameter is then changed in the optimization loop based on the solver algorithm to minimize the lateral acceleration and yaw rate error. The output of the global optimization solver and hence the optimum value of the tire parameter is the value that gives the least error.

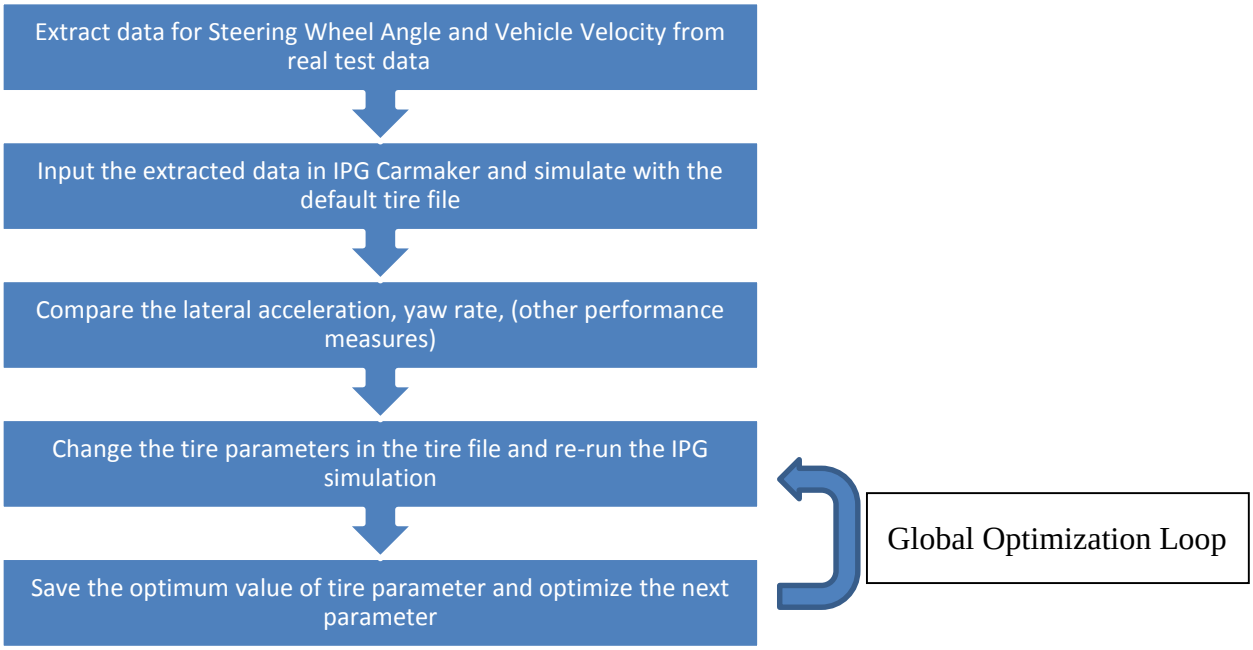

Figure 31 Flowchart for Optimization Process

3.5.2.2 Weighting parameters and Error Function

The error function is developed based on the error between the simulated and real values of lateral acceleration and yaw rate.

$$f_n = \sqrt{\frac{(lateral\ acceleration_{real} - lateral\ acceleration_{simulated})^2}{n}}$$

$$g_n = \sqrt{\frac{(yaw\ rate_{real} - yaw\ rate_{simulated})^2}{n}}$$

$$error_{function} = w_1 . f_n + w_2 . g_n$$

Where f_n and g_n are the functions for lateral acceleration error and yaw rate error respectively with *real* being the values from real test data and *simulated* being the values from IPG Carmaker simulation carried out with respective maneuver. The total error function (*error function*) is a weighted approximation with w_1 and w_2 being the weighting functions on lateral acceleration and yaw rate respectively.

The weighting parameters were selected by normalization process carried out against using the weighting value for lateral acceleration as 1. The weighting values of yaw rate were then evaluated for different maneuvers as shown in Table 4

Table 4 Weighting parameters for the error function

Maneuver	Weighting Function on Lateral Acceleration	Weighting Function on Yaw Rate
Steady State Cornering	1	10
On Centre	1	8
Sine with Dwell	1	20

3.5.3 Optimization Process and Results

The steps carried out for the optimization of various tire parameters are explained below. Subsequent steps in the process of optimization inherit the data from preceding steps.

Step 1: Optimization of PKY1

PKY1 dictates the cornering stiffness of the tire i.e. the slope of the lateral force curve in the linear region. The real rest data from the steady state cornering left hand turn (constant radius) test was used in the linear region of slip angles.

The global optimization process yields an optimum value of PKY1 as -15.6.

Figure 32 and Figure 33 show the behavior of lateral acceleration and yaw rate for steady state cornering in the linear region, left and right turn respectively.

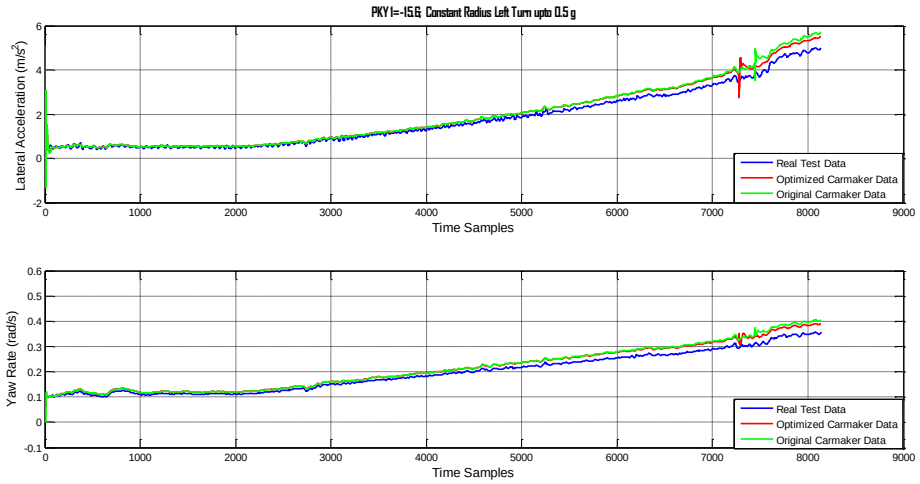

Figure 32 Optimum PKY1 for Steady State Cornering Left Turn in Linear Region

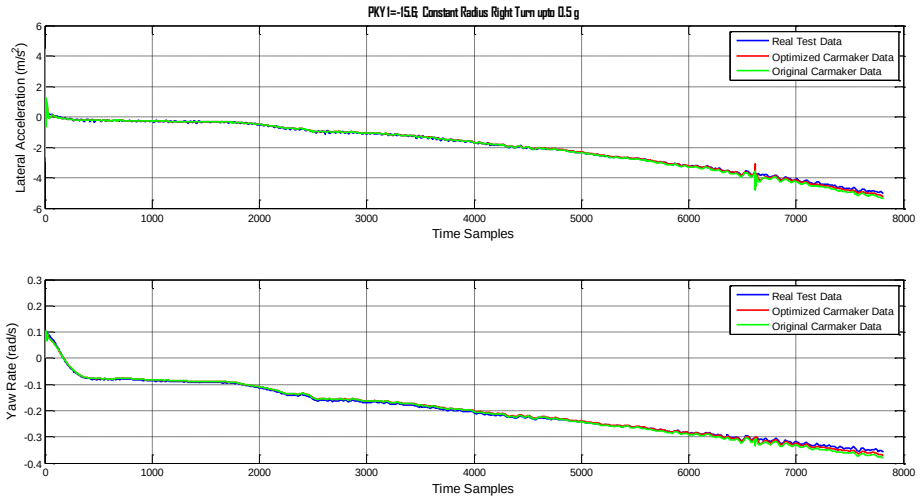

Figure 33 Optimum PKY1 for Steady State Cornering Right Turn in Linear Region

Step 2: Optimization of PDY1

The peak value factor of the tire file dictated by the peak value of the lateral force is influenced by PDY1. Data in the nonlinear region of the steady state cornering test was used for the optimization process. The peak value of lateral force in the tire file is higher than optimal. At higher slip angles, lateral acceleration and yaw rate characterized by higher deviation from the real test data (Figure 34 and Figure 35).

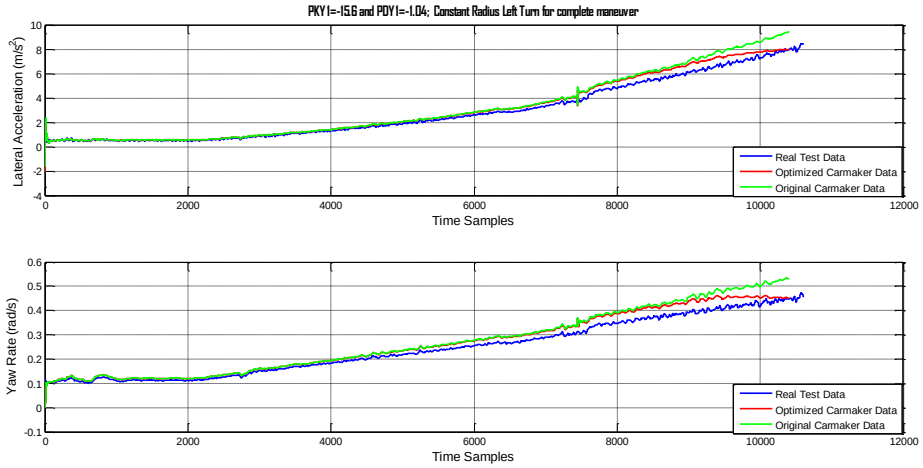

Figure 34 Optimum PDY1 for Steady State Cornering Left Turn in the complete maneuver range

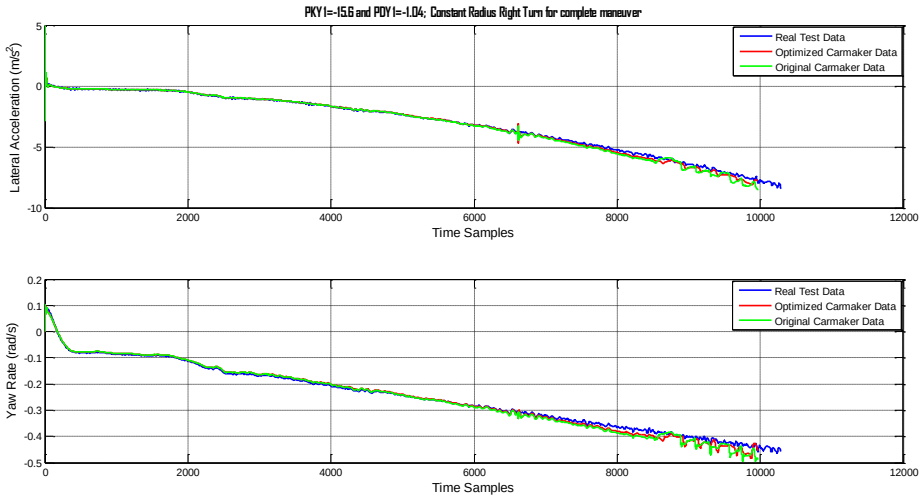

Figure 35 Optimum PDY1 for Steady State Cornering Right Turn in the complete maneuver range

Optimization of QBZ1 and QDZ1

QBZ1 dictates the trail slope factor at a given nominal load and QDZ1 influences the peak value of aligning moment. Both these tire parameters are interdependent as shown in Figure 25 and Figure 26.

Hence, the optimization of QBZ1 and QDZ1 is an iterative process.

- QBZ1 is optimized using the steady state cornering radius tests in the linear region (Figure 36 and Figure 37) since the sensitivity of aligning moment stiffness is higher in this region.
- Subsequently, the on center tests are subjected to the optimization loop (Figure 38) with the extracted value of QBZ1 from previous step since the on center tests are a good characteristic representation of the steering compliance.
- Followed by this the optimum value of QBZ1 is kept constant, and the constant radius tests are used in the full maneuver range to optimize QDZ1.

Step 3: Optimization of QBZ1

QBZ1 is optimized with a wide window of constraints using the steady state cornering radius tests in the linear region (Figure 36 and Figure 37).

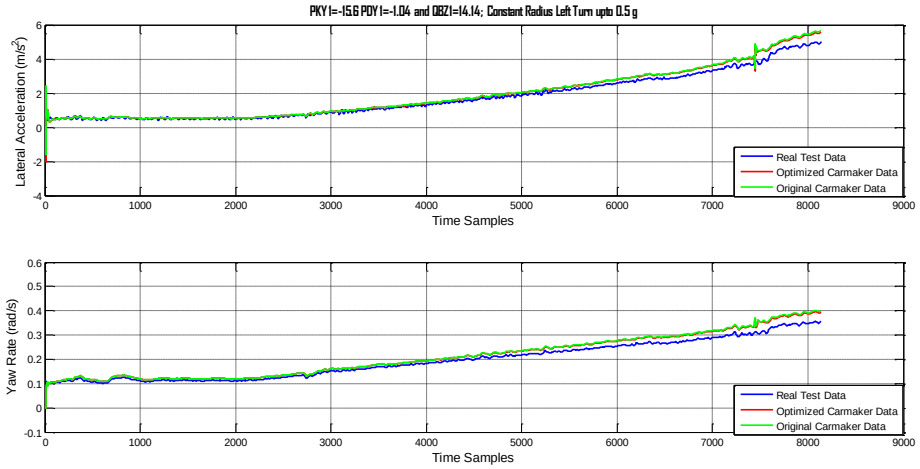

Figure 36 Optimum QBZ1 for Steady State Cornering Left Turn in the linear range

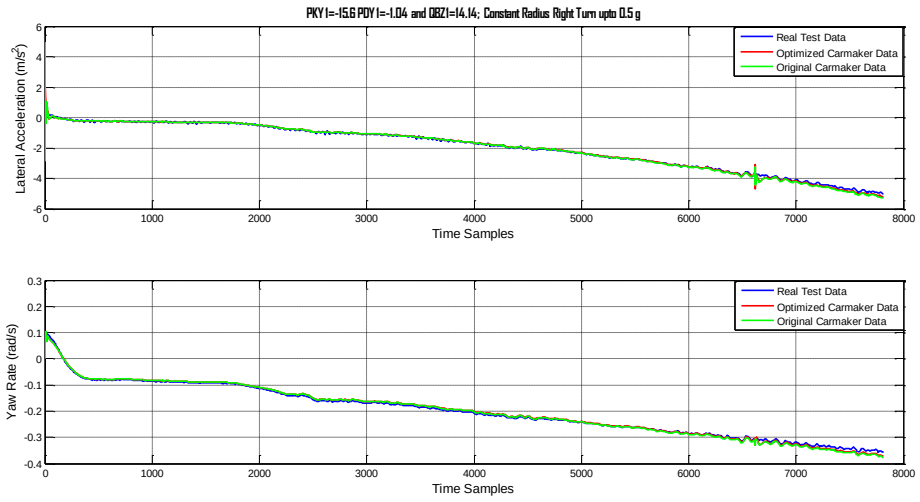

Figure 37 Optimum QBZ1 for Steady State Cornering Right Turn in the linear range

This resulted in a preliminary optimum value of QBZ1. Followed by that, the constraints for QBZ1 were narrowed for the optimization process with on center tests (Figure 38). This resulted in the final optimum value for QBZ1 which was used in step 4. It can be seen that with original tire file, the vehicle tends to achieve higher valued of lateral acceleration and yaw rate with same driver inputs. This can be attributed to higher values of PDY1 and QDZ1 in the default tire file.

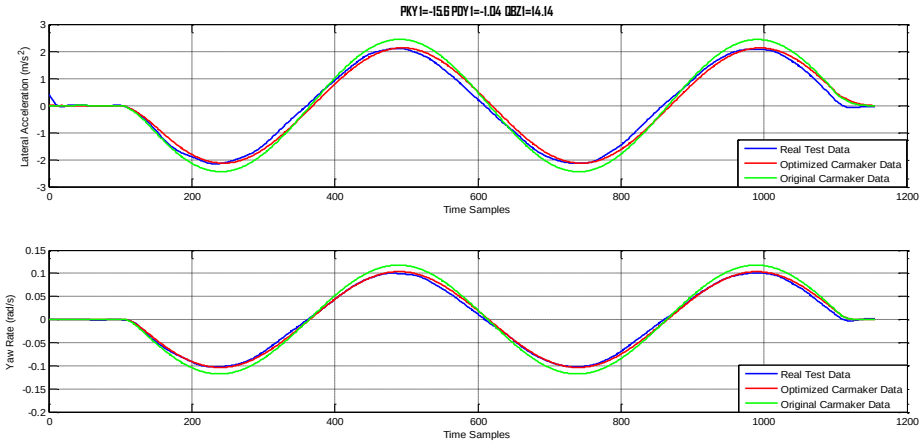

Figure 38 Optimum QBZ1 for On Centre Test

Step 4: Optimization of QDZ1

The peak value of aligning moment is dictated by QDZ1 and is optimized by steady state cornering test in the full maneuver range. Figure 39 and Figure 40 show the characteristic lateral acceleration and yaw rate for the optimum values of QDZ1. The optimum values of PKY1, PDY1 and QBZ1, were used in this case hence this result is with the optimized tire file.

These optimum values were tested against the maneuvers of on-center and sine with dwell to evaluate how much deviation the optimization results carried. This process was carried out with the steering model of ZFLS implemented in the loop. A comprehensive steering system ensured steering compliance was taken into account for the optimization verification. The results can be observed in Figures 39 – 41. Figure 41 shows the characteristics result for On Center test for optimum tire parameters.

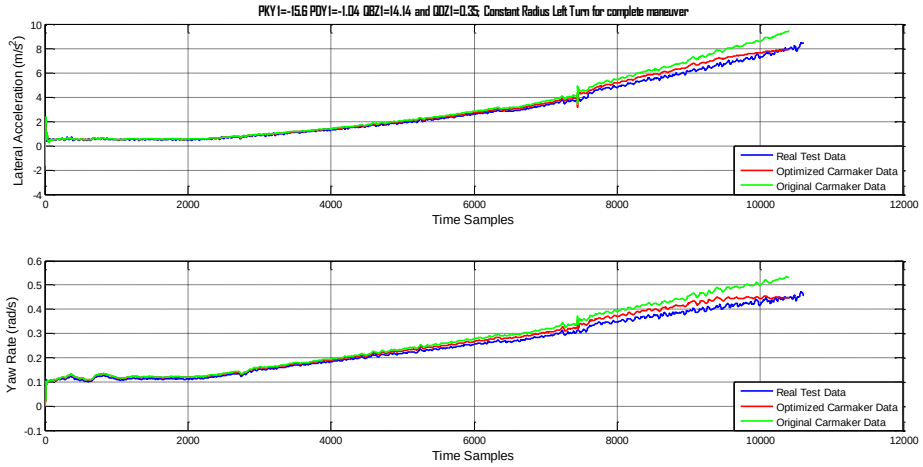

Figure 39 Optimum QDZ1 for Steady State Cornering Left Turn in the complete maneuver range

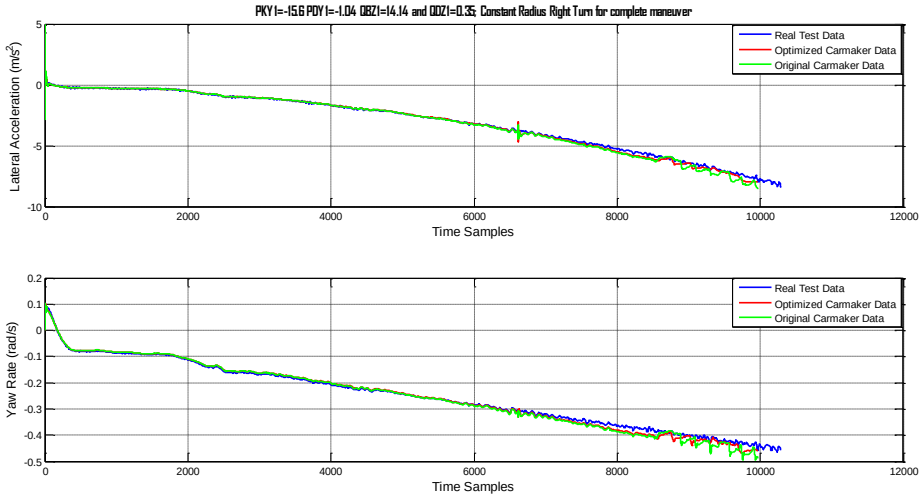

Figure 40 Optimum QDZ1 for Steady State Cornering Right Turn in the complete maneuver range

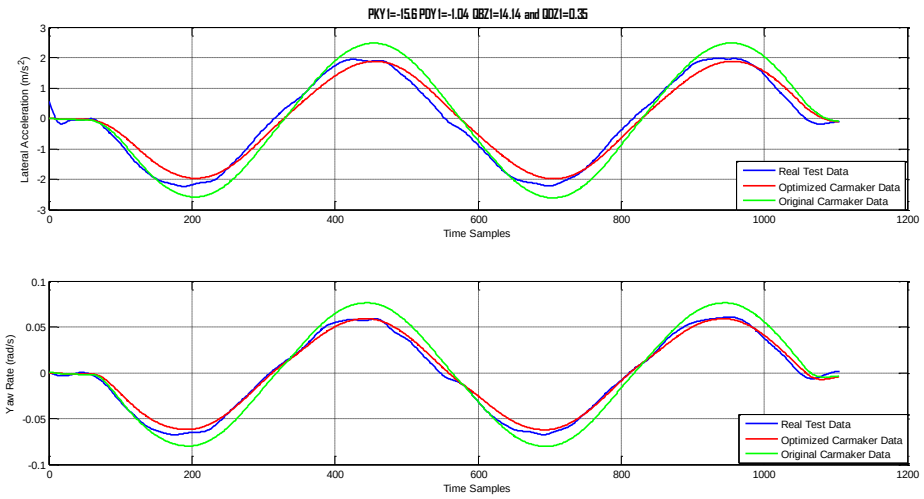

Figure 41 Optimum values of tire parameters in On Centre test with ZFLS in loop

Figure 42 and Figure 43 show the characteristics for Sine with Dwell maneuver performed with optimum tire characteristics.

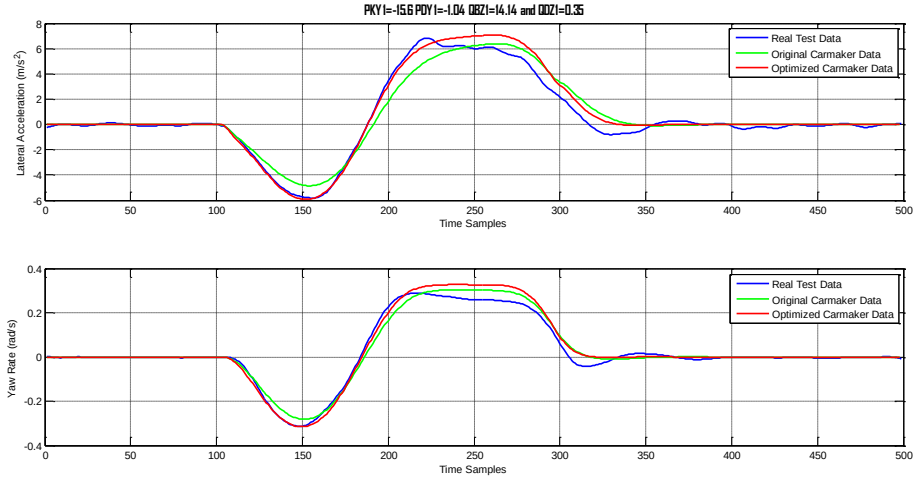

Figure 42 Optimum values of tire parameters in Sine with Dwell 05

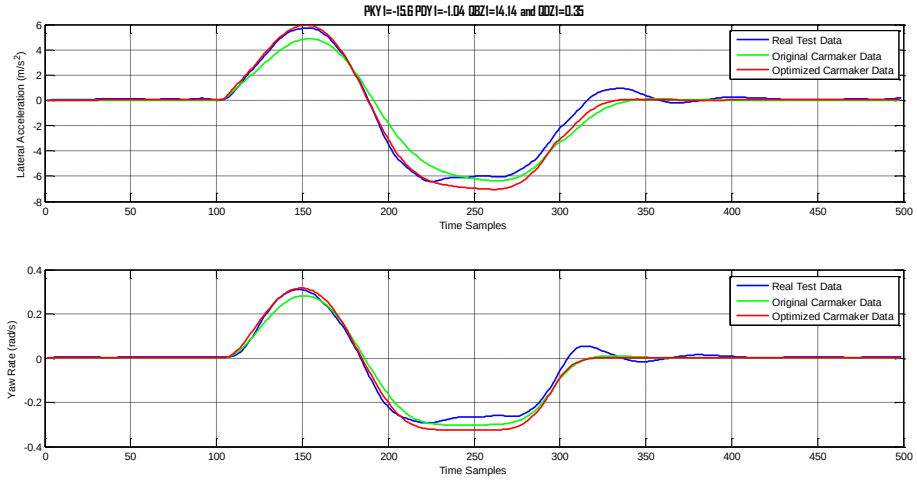

Figure 43 Optimum values of tire parameters in Sine with Dwell 06

Note:

Sine with Dwell 05 and Sine with Swell 06 were two maneuvers carried out with same steering wheel angle and vehicle speed (80 kmph), but left and right turn respectively. The on-center test was carried out at 120 kmph. For steady state cornering, the vehicle speeds were increased from 20 kmph to 80 kmph.

Step 5: Effect of Transients

To observe the effect of variation of transient parameters in the tire file, the study was done on High G Swept Steer where the steering wheel angle is increased gradually with constant vehicle speed (

Figure 45). High lateral accelerations up to 1 g are obtained. Figure 44 shows this phenomenon with variation in PTX1 parameter that is the relaxation length in the longitudinal region. It can be seen that as the value of the PTX1 is increased which translates to increasing the relaxation length, the build-up of lateral forces in the tire becomes slower.

However, tuning and optimizing the transient parameters in view of PTX1 and PTY1 requires a more comprehensive model for the tie in the transient region and a good braking model for the driver based on real test data. Sine with Dwell with high lateral acceleration and braking can be used to tune if a good co-relation between real test data and IPG CarMaker simulation is developed.

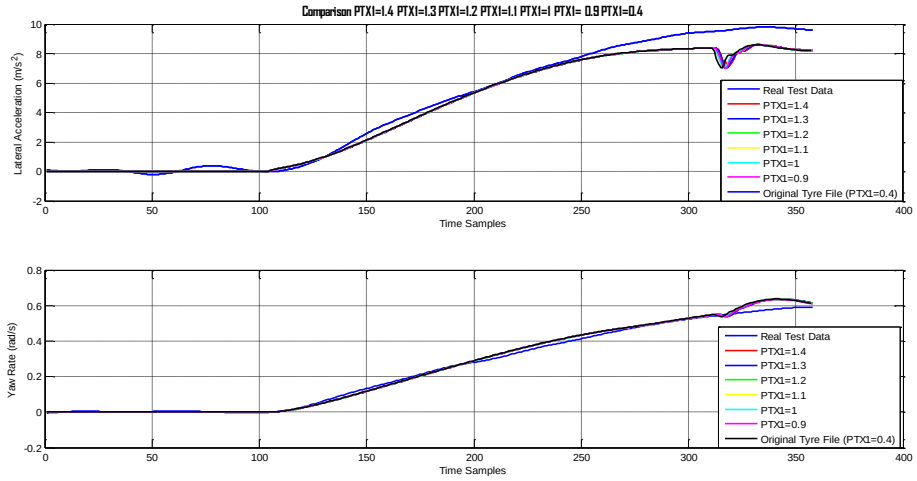

Figure 44 Influence of PTX1 on force buildup

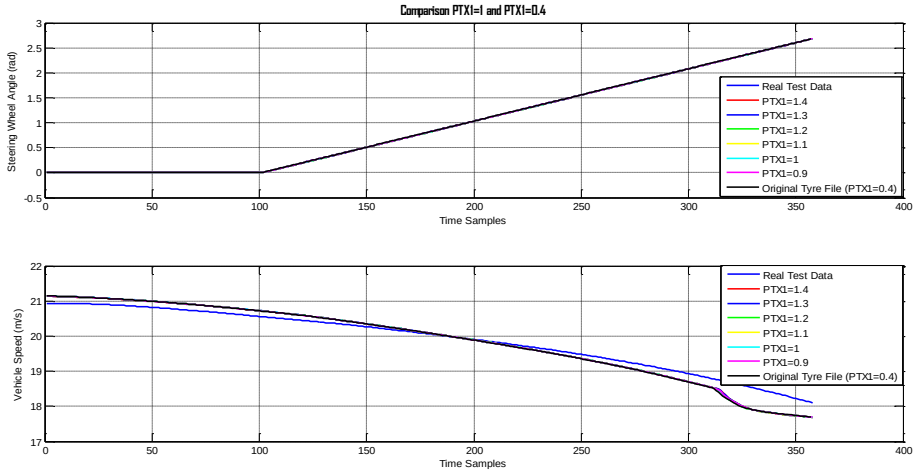

Figure 45 Steering Wheel Angle and Vehicle Speed for High Swept Steer

The steering wheel angle and vehicle speed used as an input in these simulations were extracted from the real test data and used in the driver model.

Figures 48-51 show the steering wheel angle and the vehicle speeds for various maneuvers used as an input in IPG CarMaker. The steering wheel angle and the vehicle speed are identical for the real test data, and that used in the simulation so maintain high co-relation with the results.

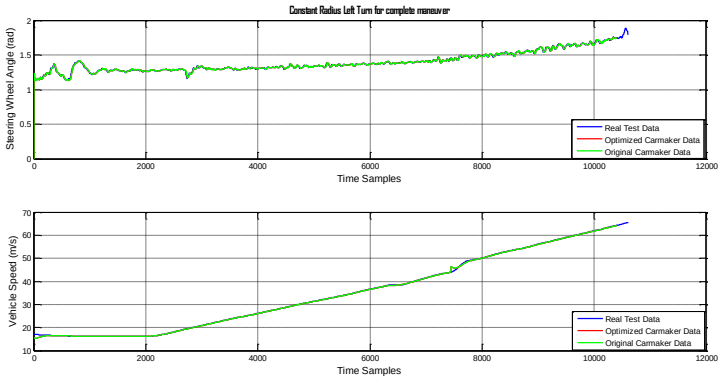

Figure 46 Steering Wheel Angle and Vehicle Speed for Constant Radius Left turn

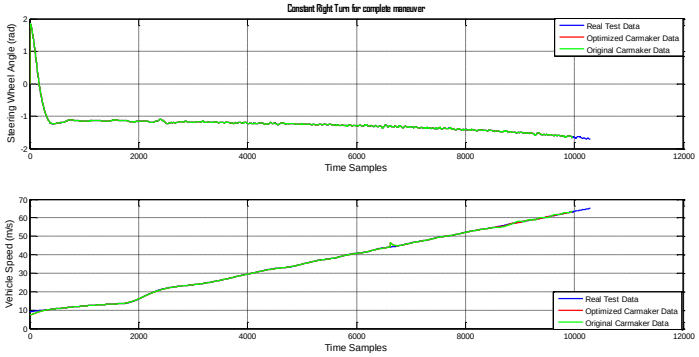

Figure 47 Steering Wheel Angle and Vehicle Speed for Constant Radius Right turn

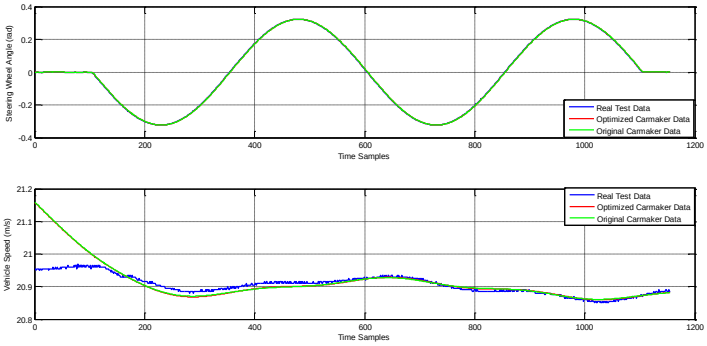

Figure 48 Steering Wheel Angle and Vehicle Speed for On Center test

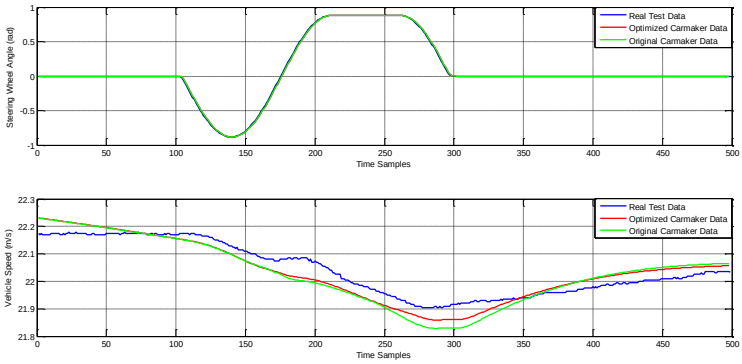

Figure 49 Steering Wheel Angle and Vehicle Speed for Sine with Dwell

Optimized tire parameter values

The table below lists the default and resulting optimum tire parameter values present in the tire file used in the optimization process.

Table 5 Final Result for optimized and Original Tire Parameter Values

	Optimized Value	Default Value
PKY1	-15.6	-20.506
PDY1	-1.04	-1.50
QBZ1	14.14	11.95
QDZ1	0.35	0.80

4 IDENTIFICATION OF THE 2 DOF REFERENCE MODEL

The identification process which involves cornering stiffness optimization is implemented by subjecting both the vehicle model in IPG Carmaker and the Bicycle Model in Simulink to the ASTM Maneuvers specified in the ASTM catalogue.

For the comparison of the results obtained from IPG CarMaker, a 2-DOF vehicle model was implemented in Simulink (section 0).

The equations were formulated in the form of transfer function, relating the steering input (δ) to the lateral velocity (v_y) and yaw rate (ψ) (section 3.2).

The ASTM maneuver catalogue provides four maneuvers at different speeds resulting in a total of 16 maneuvers.

- Frequency Sweep at 30, 60, 90, 120 and 150 kmph
- Step Steer at 30, 60, 90, 120 and 150 kmph
- Ramp Steer at 30, 60, 90, 120 and 150 kmph
- Clothoid at 12 kmph

The values obtained after simulation for yaw rate and lateral acceleration extracted in both cases are accounted for error Figure 50, and the optimum value of cornering stiffness for front and rear axle is determined by minimizing this error.

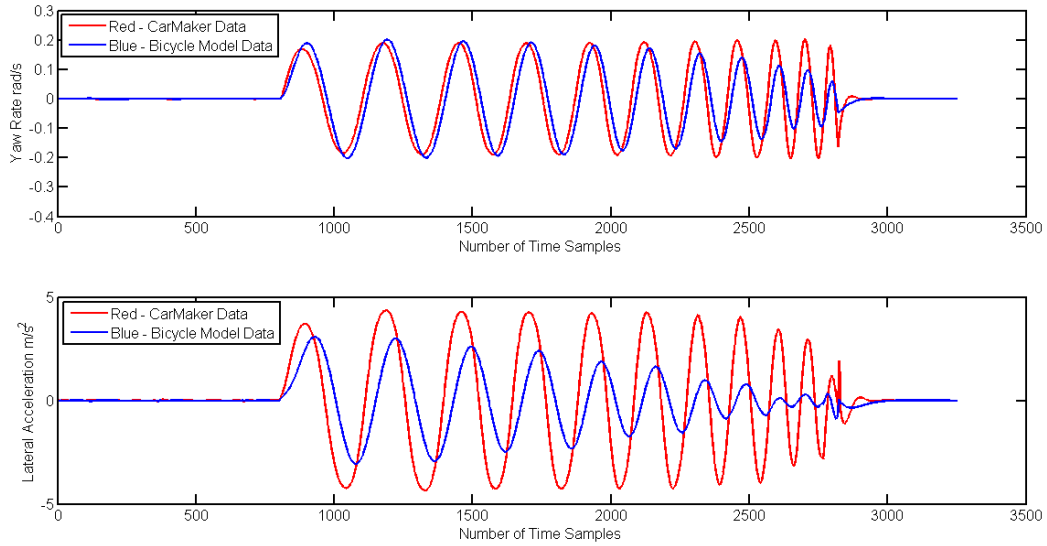

Figure 50 Data extracted for yaw rate and lateral acceleration for both models before optimization

Based on the value of cornering stiffness, the understeer gradient is calculated for the vehicle model.

These 16 maneuvers are implemented in an optimization loop in the TomLab environment for minimizing this error between the yaw rate and lateral acceleration obtained from the bicycle model and CarMaker model.

4.1 Formulation of Error Function

The reference values of yaw rate and lateral acceleration obtained from IPG Carmaker were compared with the values of yaw rate and lateral acceleration extracted from 2 DOF Bicycle Model developed in Simulink. This was done for all maneuvers at the specified speed according to the catalogue.

The error function developed was hence the function of yaw rate and lateral acceleration, minimizing which resulted in the optimum value of cornering stiffness for front and rear axle.

$$\text{Error} = w_1 * \textit{function}\,(\text{yawrate}_{\text{IPG}} - \text{yawrate}_{\text{BICYCLE MODEL}}) + w_2 * \textit{function}\,(\text{lateralacceleration}_{\text{IPG}} - \text{lateralacceleration}_{\text{BICYCLE MODEL}})$$

4.2 Selection of Weighing Matrices

The error function for each maneuver constituted of error values of yaw rate and acceleration in the rms form at specified speeds i.e. v_o = 30 kmph; v_o = 60 kmph; v_o = 90kmph; v_o = 120 kmph; v_o = 150 kmph. At each speed, the weighing values assigned to the error of yaw rate and lateral acceleration were different since the scaling between the values of yaw rate and lateral acceleration increased with an increase in speed. The total error for one maneuver was a function of the sum of the error developed due to individual speeds. Hence, suitable weighing values had to be chosen for yaw rate and lateral acceleration at each speed. The selection of weighing values also affected the way the Solver behaves while performing the functional evaluations and iterations.

4.3 Tuning of Understeer Gradient

There are some differences in the parameterization of Bicycle Model and IPG Carmaker Model. Moreover, the linear tire model does not capture the characteristics at high speeds since it does not account for the time to build the lateral acceleration in the tires. Due to these reasons the fit is not optimum for all maneuvers with one value of cornering stiffness. However, the value of understeer gradient achieved was reasonable along with the curve fitting. The CGO Solver works well in the case of global optimization for all maneuvers together; however, more detailed and comprehensive results can be extracted with the incorporation of a non-linear tire model.

> *Global Optimization with Warm Start:* The CGO solvers search for a local minimum and a global at the same time, and since the problem is subjected to advance interpolations and several sub optimizations at each iteration, the simulation process is time-consuming. By activating *WarmStart* function in TomLab, results from previous iterations can be loaded and used with the same solver or a different solver. TomLab also provides the option of defining the number of functional evaluations in an optimization problem from the user, and these evaluations can be increased with *WarmStart* being activated to decrease the simulation time.

The optimum values for cornering stiffness which resulted after the optimization process for Front Axle and Rear Axle were ***126385 Nm/rad and 150000 Nm/rad,*** respectively.

The figures below show the curve fitting for Ramp Steer at v_o = 30kmph, Step Steer at v_o = 60kmph, Frequency Sweep at v_o = 90kmph and Clothoid at v_o = 12kmph. These are plotted for both IPG Carmaker and Simulink vehicle model by choosing the optimum value of cornering stiffness obtained after the optimization process is carried

out. As mentioned before, only one value of cornering stiffness for front and rear axle is used for all the maneuvers and the curve fitting is evaluated. The value of Understeer Gradient is calculated as ***1.2963deg/g***.

The figures for curve fitting for other maneuvers can be referred to in APPENDIX B – Formulas and Tire Property File for Aligning Moment in Pure Slip and Transient Region

Formulas for Aligning Moment in pure Side Slip

$Mz' = Mz0\ (\alpha,\gamma,Fz)$

$Mzo = -t\ .\ Fy0 + Mzr$

Where t is the pneumatic trail

$t(\alpha t) = Dt \cos [Ct \arctan \{Bt\ \alpha t - Et\ (Bt\ \alpha t - \arctan (Bt\ \alpha t))\}].\cos(\alpha)$

$\alpha t = \alpha + SHt$

and the residual moment MZr:

$MZr(\alpha r) = Dr \cos [Cr \arctan (Br\ \alpha r)].\cos(\alpha)$

$\alpha r = \alpha + SHf$

$SHf = SHy + SVy / Ky$

The scaled inclination angle is:

$\gamma z = \gamma\ .\ \lambda\gamma z$

With coefficients

$Bt = (qBz1 + qBz2\ dfz + qBz3\ dfz2)\ .\ (1 + qBz4\ \gamma z + qDz5\ |\gamma z|).\ \lambda Ky / \lambda\mu y$

$Ct = qCz1$

$Dt = Fz\ .\ (qDz1 + qDz2\ dfz)\ .\ (1 + qDz3\ \gamma z + qDz4\ \gamma 2z)\ .\ \frac{R_0}{F_{z0}}\ .\ \lambda t\ .\ \zeta 5$

$Et = (qEz1 + qEz2\ dfz + qEz3\ dfz2)\ .\ \{1 + (\ qEz4 + qEz5\ \gamma z)\ .\ \frac{2}{\Pi}\ .\ \arctan(Bt.Ct.\alpha t)\}$ with $Et \leq 1$

$SHt = (qHz1 + qHz2\ dfz) + (qHz3 + qHz4\ dfz).\lambda z$

$Br = qBz9\ .\ \lambda Ky / \lambda\mu y + qBz10\ .\ By.Cy.\zeta 6$

$Cy = \zeta 7$

$Dr = Fz\ .\ [(qDz6 + qDz7\ dfz)\ .\ \lambda r + (\ qDz8 + qDz9\ dfz)\ .\ \gamma z\ ].\ R0\ .\ \lambda\mu y + \zeta 8 - 1$

An approximation for the aligning moment stiffness reads:

$Kz = -t\ .\ Ky$

$(\approx -\frac{\partial M_z}{\partial \alpha}\ \text{at}\ _{\alpha} = 0)$

Aligning ***Torque coefficients in pure Side Slip***

Following table shows the parameters for Aligning Torque coefficients in pure Side Slip which are used in the Adams Tire Property file for CAE purposes.

Table 6 Aligning Torque coefficients in pure Side Slip

Name	Name used in the tire property file	Explanation
Qbz1	QBZ1	Trail slope factor for trail Bpt at Fznom
Qbz2	QBZ2	Variation of slope Bpt with load
Qbz3	QBZ3	Variation of slope Bpt with load squared
Qbz4	QBZ4	Variation of slope Bpt with inclination
Qbz5	QBZ5	Variation of slope Bpt with absolute inclination
Qbz9	QBZ9	Slope factor Br of residual moment Mzr
Qbz10	QBZ10	Slope factor Br of residual moment Mzr
Qcz1	QCZ1	Shape factor Cpt for pneumatic trail
Qdz1	QDZ1	Peak trail Dpt = Dpt*(Fz/Fznom*R0)
Qdz2	QDZ2	Variation of peak Dpt with load
Qdz3	QDZ3	Variation of peak Dpt with inclination
Qdz4	QDZ4	Variation of peak Dpt with inclination squared
Qdz6	QDZ6	Peak residual moment Dmr = Dmr/(Fz*R0)
Qdz7	QDZ7	Variation of peak factor Dmr with load
Qdz8	QDZ8	Variation of peak factor Dmr with inclination
Qdz9	QDZ9	Variation of Dmr with inclination and load
Qez1	QEZ1	Trail curvature Ept at Fznom
Qez2	QEZ2	Variation of curvature Ept with load
Qez3	QEZ3	Variation of curvature Ept with load squared
Qez4	QEZ4	Variation of curvature Ept with sign of Alpha-t
Qez5	QEZ5	Variation of Ept with inclination and sign Alpha-t
Qhz1	QHZ1	Trail horizontal shift Sht at Fznom
Qhz2	QHZ2	Variation of shift Sht with load
Qhz3	QHZ3	Variation of shift Sht with inclination
Qhz4	QHZ4	Variation of shift Sht with inclination and load

Transient parameters

Relaxation behavior in the tire accounts for the fact that the lateral forces in the tire do not build up instantaneously, and the steady state levels are only attained once the tire travels a certain distance.

Both the longitudinal and the lateral relaxation lengths are defined as per the vertical load as:

$$\sigma\kappa = Fz \,.\, (pTx1 + pTx2\, dfz) .exp\,(\, pTX3\, dfz\,) \,.\, \frac{R_0}{F_{z0}} \,.\, \lambda\sigma\kappa$$

$$\sigma\alpha = PTy1 \;\; sin\,(2\, arctan \left\{\frac{F_z}{P_{Ty2} F_0 \lambda_{Fz0}}\right\}) (1 - pKy3|\gamma y|)\, Ro\, \lambda Fz0\, \lambda\sigma\alpha$$

Coefficients for transient response

Table 7 Transient parameters in the tire file

Name	Name used in the tire property file	Explanation
PTx1	PTX1	Longitudinal relaxation length at Fznom
PTx2	PTX2	Variation of longitudinal relaxation length with a load
PTx3	PTX3	Variation of longitudinal relaxation length with exponent of load
PTy1	PTY1	Peak value of relaxation length for lateral direction
PTy5	PTY2	Shape factor for lateral relaxation length
Qtz1	QTZ1	Gyroscopic moment constant
Mbelt	MBELT	Belt mass of the wheel

APPENDIX C – Optimization of Cornering Stiffness

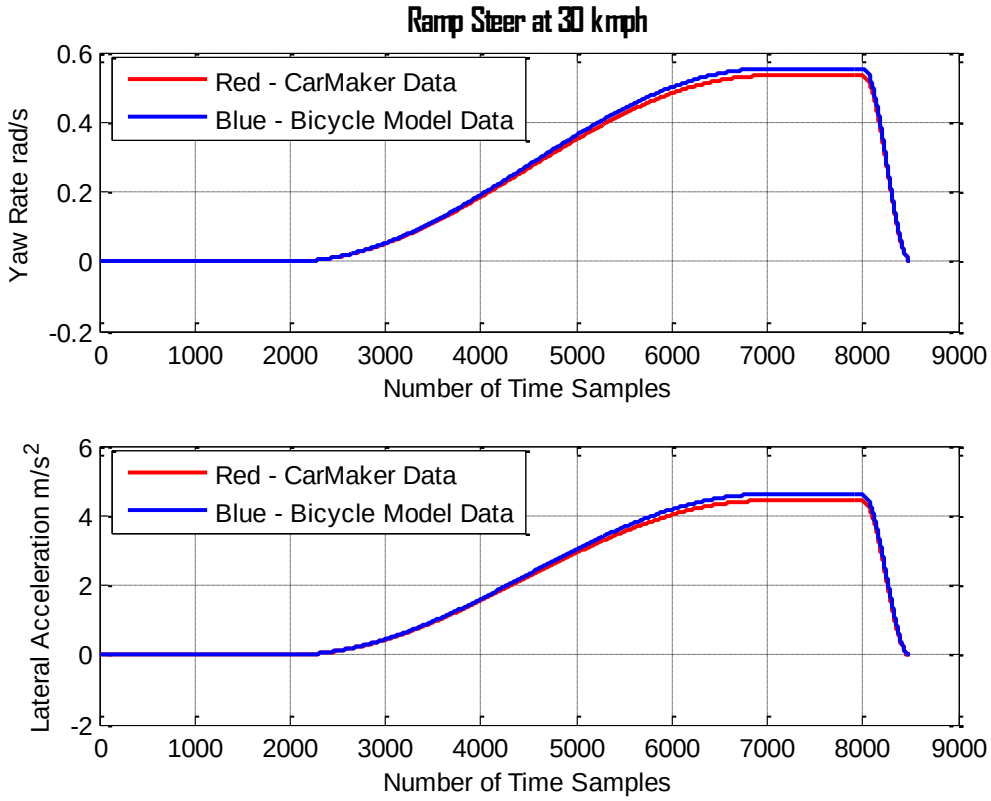

Figure 51 Ramp Steer at 30 km/h

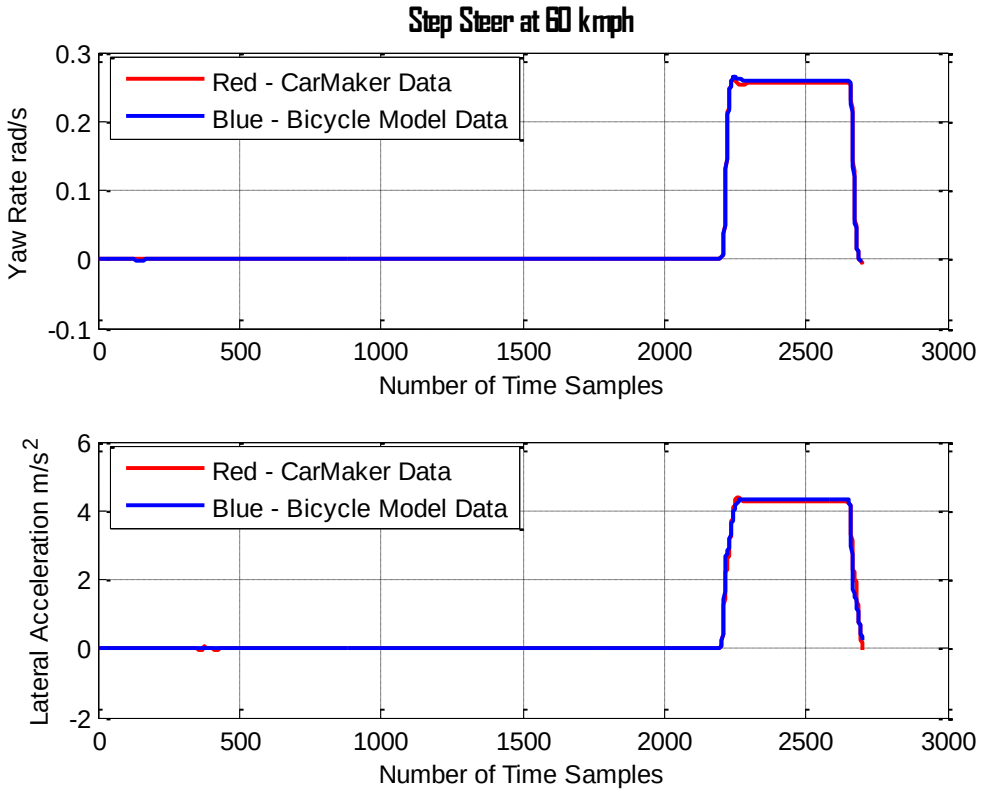

Figure 52 Step Steer at 60 km/h

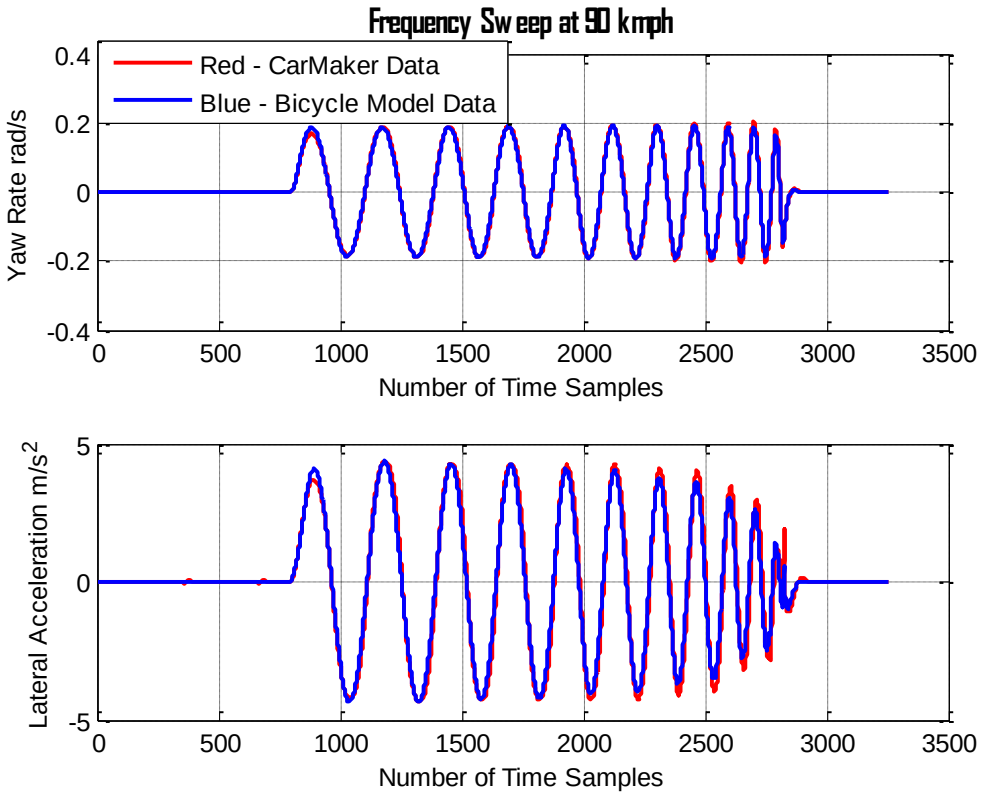

Figure 53 Frequency Sweep at 90 km/h

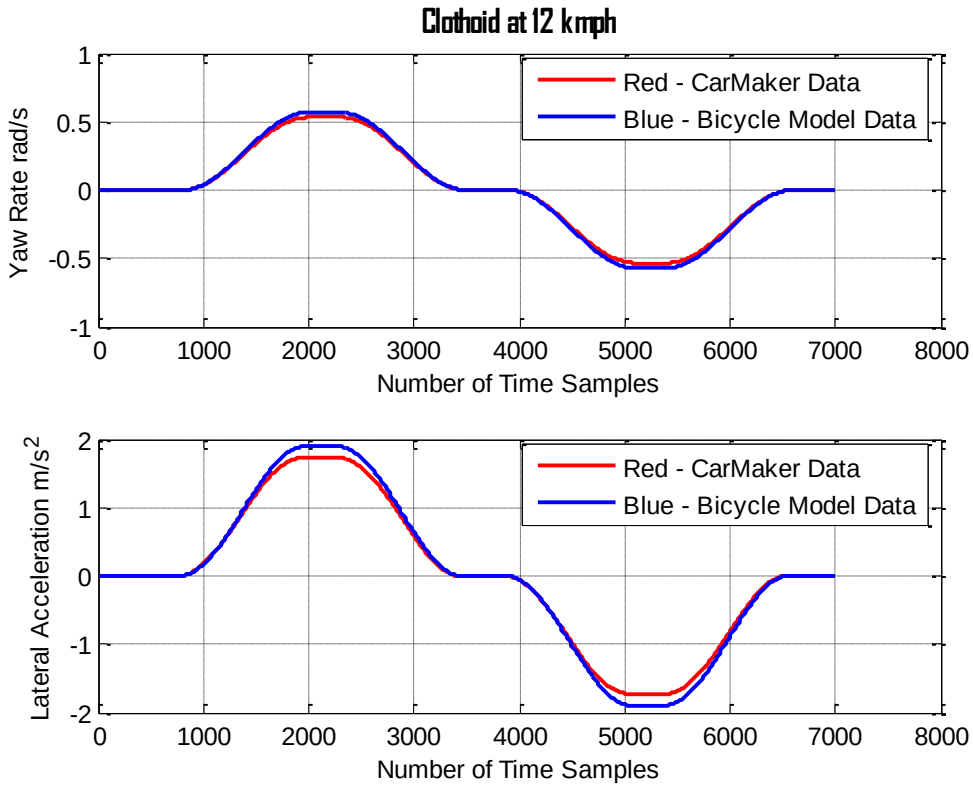

Figure 54 Clothoid at 12 km/h

5 BCM TUNING EMPLOYING CAE

The formulation of BCM in the CAE environment allows for the objective assessment of the vehicle behavior with dynamic simulations and hence assisting the physical testing phase. The BCM can be designed to operate on one or more defined goals based on the complexity of the functionality required.

5.1 Methodology for yaw moment control:

The wheel that requires the least braking force is chosen to brake when ESP intervenes in case of an evasive or aggressive maneuver. This guarantees that the control torque applied on the wheel is enough to stabilize the maneuver, and the wheel requires the least brake force which optimizes the comfort factor.

In certain scenarios, the stabilization cannot be achieved by applying control torque on just one wheel. In this case, then, the additional control torque required will be subjected to the wheel that requires second least brake force.

The behavior of the brake application also depends on the characteristics of understeer or over-steer and the sign of the control torque being applied. Practically, it is essential to determine whether it is useful to exploit the whole primary and secondary torque for each wheel. If the secondary control torque is produced, the wheel is braked into the sliding region. If the wheel is not necessary to be subjected to the secondary torque, a threshold is necessary which governs that the wheel is kept in the sliding region.

There can be a difference in the control algorithm in order to decide the objective from this particular method of ESP intervention. The control method can be applied to make sure that the vehicle should be stabilized as early as possible by a combination of vehicle trajectory and the brake pressure applied. The alternate way can be to evaluate if the vehicle is following the desired path inferred from the driver's steering angle, the optimal recovery from the understeer is then defined as the optimal control problem (Klomp, Lidberg, & Gordon, 2014)

5.2 Performance evaluation of ABS and ESP

Performance evaluation of the BCM in the virtual environment will depend on the parameters being tuned within the BCM. Pertaining to the areas mentioned below, BCM functionality will be affected depending on ABS and ESP parameters.

- Intelligent vehicle highway systems
- Vehicle stability and stability control
- Vehicle dynamics
- Accident reconstruction

ABS braking is affected by the speed of the vehicle at the beginning of braking maneuver; this is another area which can be assessed regarding ABS performance.

In terms of initial vehicle speed in braking maneuver:

ABS braking average deceleration is a function of vehicle speed. Higher vehicle speeds resulted in overall improved ABS braking under test conditions that included speeds up to 115 kmph. (MarshekKurt, JohnsonMark, CudermanJerry, 2002).

The ABS index of performance, ABSIP, the ratio of ABS braking to locked wheel braking varies as a function of speed and from the vehicle to vehicle.

5.3 BCM formulation in CarMaker for Simulink

Evaluating the BCM and its performance is a complex process and involves a lot of physical testing to tune the BCM parameters. A mock-up Brake Control Module was interfaced in CarMaker for Simulink for evaluating the possibility of tuning and optimizing the BCM parameters in the CAE environment.

5.3.1 Principles of formulation of BCM

The BCM in CarMaker for Simulink was designed based on the principles of upper controller and lower controller design as mentioned in (Rajamani, Electronic Stability Control, 2006). The control architecture is based on a hierarchical approach where the upper controller dictates the desired value of yaw torque and hence prioritizes the yaw stability. This is done by extracting data from the wheel speed sensors, lateral accelerometer, a steering angle sensor and the yaw rate sensor. The control law derived from the data gathered from these sensors computes the desired value of yaw torque. The lower controller on the other hand ensures that the desired yaw torque demanded by the upper controller is obtained from the brake system. This is done by controlling the braking pressures on all the four wheels by utilizing the rotational dynamics and hence obtaining the desired yaw torque.

5.3.2 Desired Yaw Rate

The desired yaw rate which the vehicle should attain is obtained from the steering angle in accordance with the understeer gradient (Rajamani, Electronic Stability Control, 2006). It is expressed as:

$$\dot{\Psi}_{des} = \dot{x}/R = \frac{\dot{x}}{l_f + l_r + \frac{m\,\dot{x}^2(l_r C_{\alpha r} - l_f C_{\alpha f})}{2 C_{\alpha r} C_{\alpha f}}} \cdot \delta$$

5.3.3 Desired Side Slip Angle

The steady state slip angle is also expressed in the terms of the steady state steering angle (Rajamani, Electronic Stability Control, 2006):

$$B_{des} = \frac{l_r - \frac{l_f\, m\, V^2}{2 C_{\alpha r}(l_f + l_r)}}{l_f + l_r + \frac{m\, V^2 (l_r C_{\alpha r} - l_f C_{\alpha f})}{2 C_{\alpha r} C_{\alpha f}(l_f + l_r)}}$$

5.3.4 Upper Controller

The objective of the upper controller is to determine the desired yaw rate and the desired side-slip of the vehicle. This is done by developing an error function based on the difference between the real-time yaw rate and sideslip and the desired yaw rate and sideslip of the vehicle.

The controller is based on the sliding mode control design methodology.

5.3.5 Lower Controller

The lower controller determines the brake pressure at each wheel of the vehicle based on the control torque determined by the upper controller. The net torque produced from all wheels should adhere to the control torque demanded from the upper controller in order to stabilize the vehicle.

The differential force in the longitudinal direction is calculated as:

$$\Delta F_{xf} = \frac{2 M_{\psi b}}{l_w}$$

The term $M_{\psi b}$ is the control torque which is determined by the upper controller and is given by:

$$M_{\psi b} = \left[\frac{l_f}{I_z}\left(F_{yfl} + F_{yfr}\right) cos\,\delta + \frac{l_r}{I_z}\left(F_{yrl} + F_{yrr}\right) - \eta s + \ddot{\psi}_{target} - \xi(\dot{\beta} - \dot{\beta}_{target})\right] / \left[\frac{\rho + \cos(\delta)}{I_z}\right]$$

As evident from the expression above, the control torque requires feedback from the slip angles, its derivative and lateral tire forces.

The weighing factor between the sideslip and yaw rate can be modified based on the sensitivity required for the respective parameter. The differential force calculated is then used to determine the braking pressures at each wheel using appropriate gain factor.

5.4 BCM in CarMaker environment

Using the above-mentioned control methodology, the mock up BCM was implemented in CarMaker environment to verify if it can be tuned for the various parameters and can be used for performance evaluation in different scenarios.

Figures 55-58 show the implementation of the mock up BCM in the CarMaker environment.

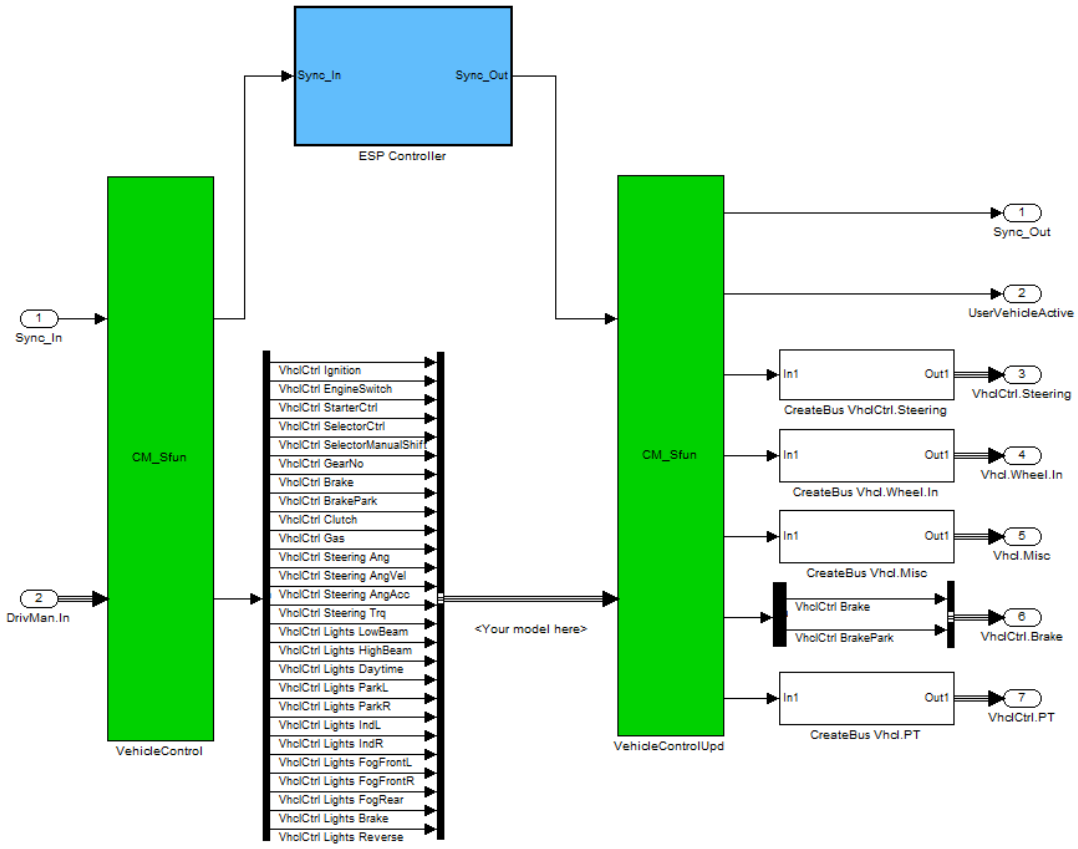

Figure 55 ESP controller in CarMaker environment

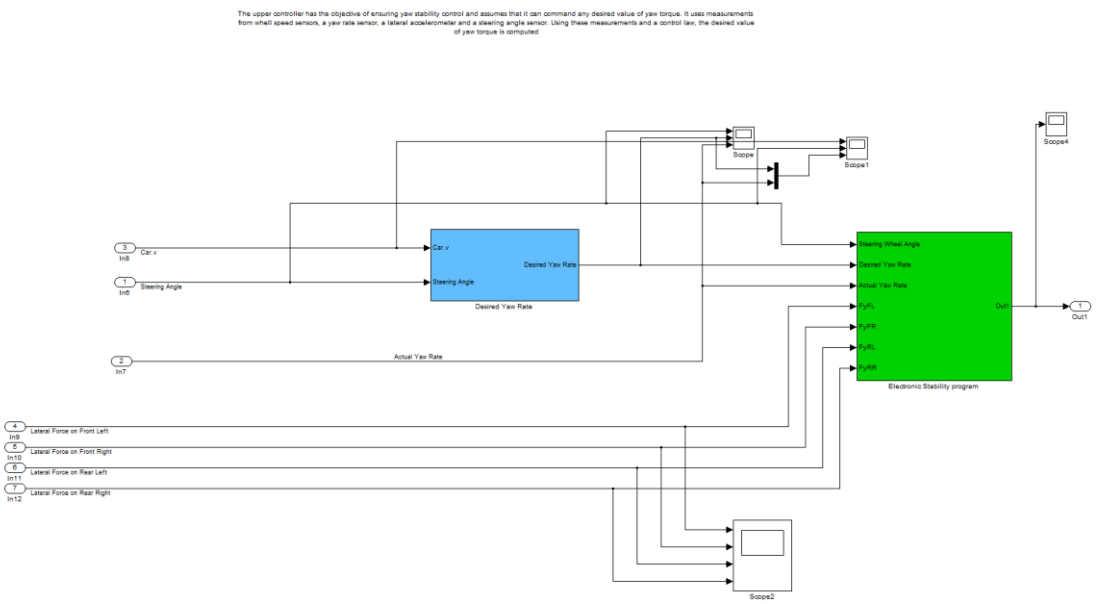

Figure 56 Desired Yaw Rate and ESP Sub-blocks

The ESP controller consists of sub-blocks that are used for the calculation of desired yaw rate and the control torque for determination of the differential force. This differential force is then fed into the anti-lock braking system where the braking pressures are calculated for each wheel. This interface does not have a reference of slip angle, but it can be implemented with a weighting factor against the desired yaw rate. The set-up of mock-up BCM integrates well with the CarMaker environment and by choosing different values of gains, braking pressures can be modified.

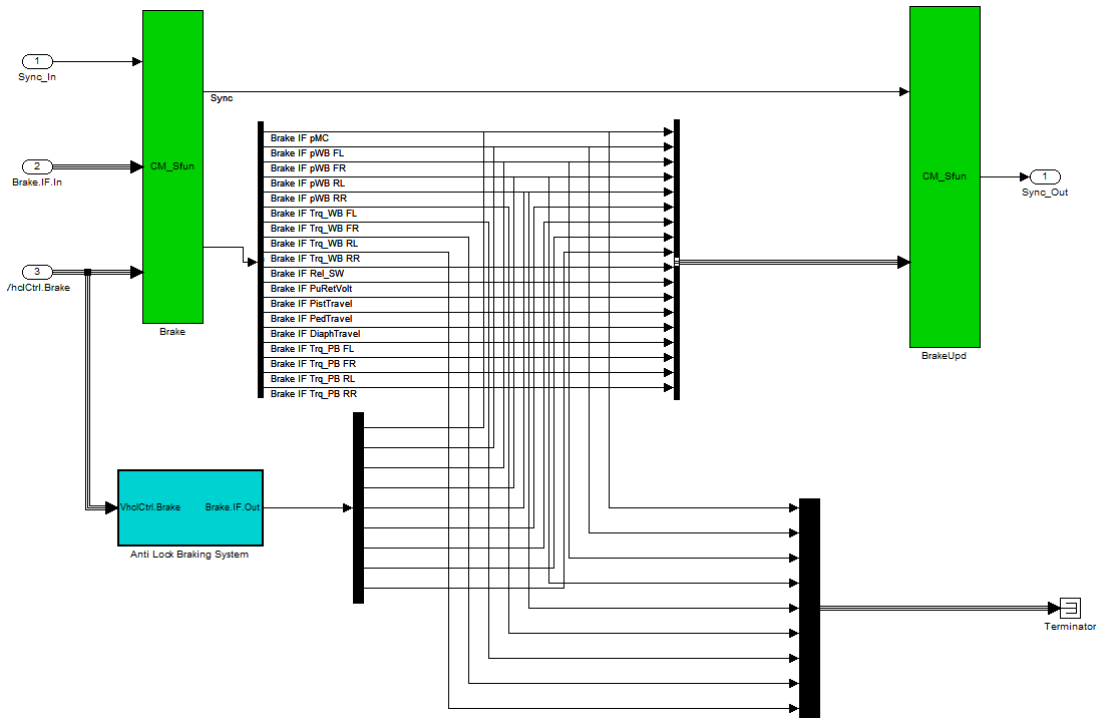

Figure 57 Anti-lock Braking System sub-block

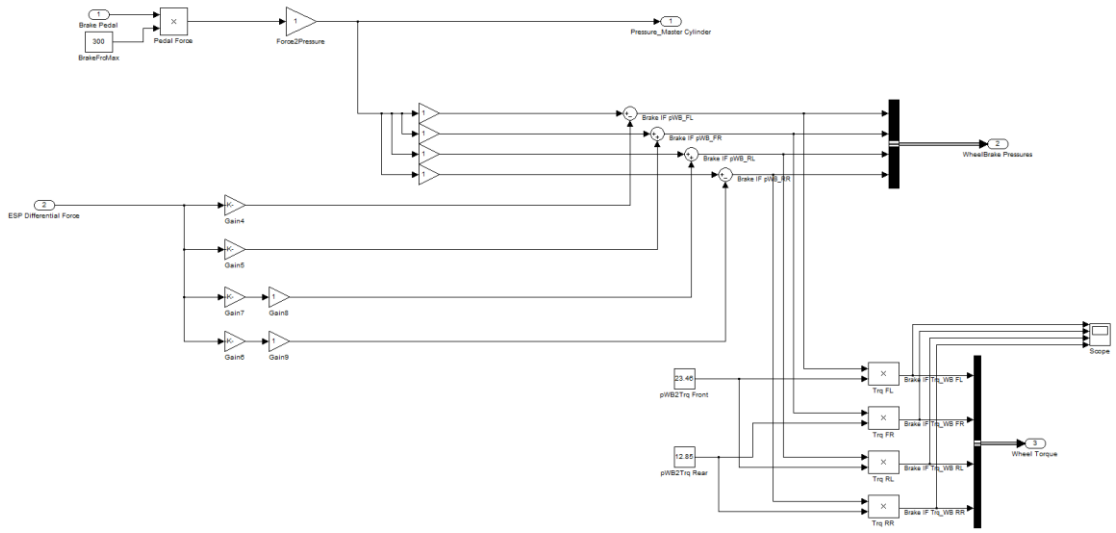

Figure 58 Brake pressures at each wheel

6 DISCUSSION

The tire parameter tuning and optimization process explained in section 3.5 was focused in the area of pure lateral slip. This was a convenient approach since the characteristics for the vehicle in terms of lateral acceleration, and yaw rate for various maneuvers was easily accessible. The tire files which were optimized were received from the supplier, and the optimization process developed served as a tool for confirming whether the parameter values received from the supplier are suitable for vehicle dynamic simulations performed in various CAE environments.

The cornering stiffness in the tire files was observed to be 30% higher than the value resulted from the optimization process. The optimization process carried out for the aligning moment parameters constituted some uncertainties because the variation of both aligning moment parameters, QBZ1 and QDZ1 had a mutual influence. Tuning the aligning moment with respect to torque on the torsion bar would have been an alternate approach but the co-relation between the simulated results and the real test data in this case was not ideal.

The PAC2002 tire format provides the functionality of tire mirroring. The label 'Tyre Side' in the tire file indicates which side on the vehicle the tire is mounted. If the tire measured on the left side and mounted on the right side on the vehicle, it can result in asymmetric behavior.

A similar optimization approach can be used for the transient and longitudinal parameters in the tire file. However, suitable maneuvers have to be chosen for this purpose and relevant characteristics from the practical tests have to be logged. Moreover, a comprehensive brake model has to be implemented for the driver in the CAE environment that can replicate the braking phenomena in the real test with appropriate braking pressure and torque.

In terms of the Brake Control Module tuning, the interface of BCM from Volvo Car Corporation's supplier was available in the CarMaker environment. Initial efforts were made to tune and optimize the parameters in the BCM. But, since the BCM interface from the supplier was quite comprehensive with more than 900 parameters in-built and with lack of knowledge on specific parameters to tune which control the BCM tuning, this effort was put to halt. At present this tuning is performed with physical testing; however, it is proposed that the method will be developed for its tuning in the CAE environment in future since it was established that tuning of these parameters is fundamentally possible.

The mock-up BCM formulated in the CarMaker environment did not function as well as the BCM from the supplier in a Sine with Dwell maneuver. This was expected because the controller did not adapt to suitable gains for brake pressures required. Even though the desired yaw rate was calculated to be within limits, the actual yaw rate of the vehicle couldn't be reached equal to the desired yaw rate. This caused the vehicle to spin out. However, more developments done on the developed interface in the future can result in desired functionality since it has a high degree of tuning and optimization possibility in the CarMaker environment.

7 CONCLUSION

The tire parameters considered in the optimization algorithm were restricted in the pure slip region. A detailed study was done on the tire characteristics with respect to parameters in the area of pure slip and their optimization was carried out with respect to data available from maneuvers carried out on the test track. This method ensured a way of evaluating whether the tire measurements from the supplier lie in the suitable range or not. This is necessary since tire modeling in the CAE environment should carry high correlation with the actual tires mounted on the vehicle. In the area of relaxation length and transient parameters, a more comprehensive tire model along with a good brake model in the CAE environment is necessary for optimization purposes.

The formulation of BCM in the CarMaker environment served as a tool for investigating the possibility of its functioning and tuning. Though the mock up BCM in terms of the hierarchical controller was embedded rightly in the CAE environment, its functionality was not obtained as desired. This was due to limitations on time and the gains couldn't be tuned appropriately to achieve the desired yaw torque and corresponding brake pressures.

However, a more comprehensive BCM software interface was available in the CarMaker environment from the supplier corresponding to the hardware fitted on the actual vehicle. This is proposed to be integrated in the CAE environment in the future with an appropriate vehicle model to virtually carry out its tuning in future V54X vehicles.

8 FUTURE SCOPE

The tire parameter optimization process carried out in the area of pure slip can be extended towards estimating the longitudinal parameters, combined slip parameters and transient parameters as well. Detailed study on how the parameters correlate with the maneuvers carried out on the actual test track has to be studied and with a concrete vehicle model in the CAE environment, this optimization and tuning process for a tire file can be possible.

The BCM model available from the supplier has more than 900 parameters inbuilt which can be tuned in various respects to modify the behavior of the BCM. This tuning is carried out physically on the test track which is a time consuming and expensive procedure. However, it is evident that with a suitable vehicle model this tuning can be carried out in the CAE environment. This would however, require good insight from the test engineers and real test data to formulate an optimization loop with appropriate constraints on the parameters to tune. BCM tuning, hence in future, should be possible to carry out in the CAE environment which will be a complex yet efficient procedure.

9 REFERENCES

Bakker, E., Nyborg, L., & Pacejka, H. B. (1987). *Tyre Modelling for Use in Vehicle Dynamics Studies.* Society of Automotive Engineers.

Bakker, E., Pacejka, H. B., & Lidner, L. (1989). *A New Tire Model with an Application in Vehicle Dynamics Studies.* SAE Technical Paper 890087.

Björkman, M., & Holmström, K. (2000). Global Optimization of Costly nonconvex functions using radial bias function . *Optmization and Engineering*, 373-397.

Blundell, M., & Harty, D. (2004). *The Multibody Systems Approach to Vehicle Dynamics.* Elsevier Butterworth-Heinemann.

Dugoff, H., Fancher , P. S., & Segel, L. (u.d.). *An analysis of tire traction properties and their influence on vehicle dynamics performance* . SAE Paper No. 700377.

Forkenbrock, G. J. (2005). *NHTSA'S LIGHT VEHICLE HANDLING AND ESC EFFECTIVENESS RESEARCH PROGRAM.* NHTSA,Paper Number 05-0221.

Forkenbrock, G. J., & Boyd, P. L. (2007). *Light Vehicle ESC Performance Test Development.* NHTSA Paper Number 07-0456.

Gillespie, T. D. (1992). *Fundamentals of Vehicle Dynamics.* SAE International.

Göran, A. O., Holmström, K., & Edwall, M. M. (November 2008). User's guide for TomLab / CGO.

Holmström, K. (1999). The Tomlab optimization environment in matlab. *Advanced Modeling and Optmization* .

Jacobson, B. (2012). *Vehicle Dynamics Compendium.* Göteborg: Chalmers University of Technology.

John, S., & Pedro, J. O. (2013). *Hybrid Feedback Linearization Slip Control for Anti-lock Braking System.* Acta Polytechnica Hungarica.

Jones, D. R. (2001). A taxonomy of global optimization methods based on response surfaces. *Journal of Global Optimization*, 345-383.

Kang, J., Kyongsu, Y., & Heo, H. (2012). *Control Allocation based optimal torque vectoring for 4wd electrical vehicle.* SAE 2012-01-0246.

Keenan, T. (Mar 1995). *Wards Auto.* Hämtat från wardsauto.com: http://wardsauto.com/news-amp-analysis/engineering-revolution-cadcae-advancements-changing-vehicle-development

Klomp, M., Lidberg, M., & Gordon, T. J. (2014). On Optimal Recovery from Terminal Understeer. *Proc ImechE Part D: J Automobile Engineering*, Vol.228(4) 412-425.

Marshek, K. M., Johnson, M., & Cuderman, J. (2002). *Performance of anti-lock Braking System Equipped Passenger Vehicles - Part II: Braking as a function of Initial Vehicle Speed in Braking Maneuver.* University if Texas at Austin: SAE International.

NHTSA. (2006). *Federal Motor Vehicle Safety Standards; Electronic Stability Control Systems.* National Highway Traffic Safety Administration.

Pacejka, H. B. (2002). *Tyre and Vehicle Dynamics.* Butterworth-Heinemann.

Quttineh, N.-H. (2012). *Models and Methods for Costly Global Optimization and Military Decision Support Systems.* Linköping: Linköping Studies in Science and Technology.

Rajamani, R. (2006). Electronic Stability Control. i R. Rajamani, *Vehicle Dynamics and Control* (ss. 221-255). Sringer.

Rajamani, R. (2006). *Vehicle Dynamics and Control.* Minnesota: Springer Science+Business Media.

Schonlau, M., Jones, D. R., & Welch, W. J. (1998). Efficient Global Optmization of expensive black-box functions. *Journal of Global Optmization* , 455-492.

Siampis, E., Massaro, M., & Velenis, E. (2013). *Electric Rear Axle Torque Vectoring for Combined Yaw Stability and Velocity Control near the Limit of Handling.* IEEE Conference on Decision and Control.

The Racing and High Performance Tire . (February 2004). *Sports Car International*.

Tjønnas, J., & Johanse, T. A. (2006). *Adaptive Optimizing Dynamic Control Allocation Algorithm for Yaw Stabilization of an Automotive Vehicle using Brakes.* Trondheim, Norway: Department of Engineering Cybernetics, Norwegian University of Science and Technology.

Velenis, E., Katzourakis, D., Frazzoli, E., Tsiotras, P., & Happee, R. (2011). Steady-statedriftingstabilizationofRWDvehicles. *Control Engineering Practice* , 1363-1376.

APPENDIX A – 2DOF Simulink Model

For the comparison of the results obtained from IPG CarMaker, a 2-DOF vehicle model was implemented in Simulink.

The equations were formulated in the form of transfer function, relating the steering input (δ) to the lateral velocity (y') and yaw rate (ψ').

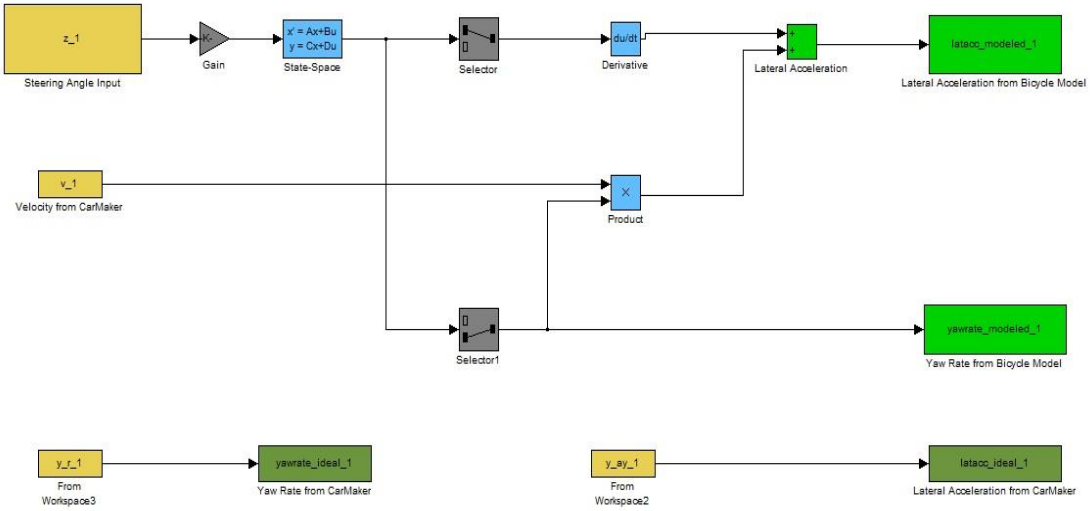

Figure 59 Bicycle Model in Simulink

In this case the state space block contains the equations for A, B, C and D matrices for the steering wheel angle used as input.

APPENDIX B – Formulas and Tire Property File for Aligning Moment in Pure Slip and Transient Region

Formulas for Aligning Moment in pure Side Slip

$M_z' = M_{z0}(\alpha,\gamma,Fz)$

$M_{zo} = -t \cdot F_{y0} + M_{zr}$

Where t is the pneumatic trail

$t(\alpha_t) = D_t \cos[C_t \arctan\{B_t \alpha_t - E_t(B_t \alpha_t - \arctan(B_t \alpha_t))\}].\cos(\alpha)$

$\alpha_t = \alpha + S_{Ht}$

and the residual moment M_{Zr}:

$M_{Zr}(\alpha_r) = D_r \cos[C_r \arctan(B_r \alpha_r)].\cos(\alpha)$

$\alpha_r = \alpha + S_{Hf}$

$S_{Hf} = S_{Hy} + S_{Vy}/K_y$

The scaled inclination angle is:

$\gamma_z = \gamma \cdot \lambda_{\gamma z}$

With coefficients

$B_t = (q_{Bz1} + q_{Bz2}\, df_z + q_{Bz3}\, df_z^2) \cdot (1 + q_{Bz4}\, \gamma_z + q_{Dz5}\, |\gamma_z|).\, \lambda_{Ky} / \lambda_{\mu y}$

$C_t = q_{Cz1}$

$D_t = F_z \cdot (q_{Dz1} + q_{Dz2}\, df_z) \cdot (1 + q_{Dz3}\, \gamma_z + q_{Dz4}\, \gamma^2_z) \cdot \frac{R_0}{F_{z0}} \cdot \lambda_t \cdot \zeta_5$

$E_t = (q_{Ez1} + q_{Ez2}\, df_z + q_{Ez3}\, df_z^2) \cdot \{1 + (q_{Ez4} + q_{Ez5}\, \gamma_z) \cdot \frac{2}{\Pi} \cdot \arctan(B_t.C_t.\alpha_t)\}$ with $E_t \leq 1$

$S_{Ht} = (q_{Hz1} + q_{Hz2}\, df_z) + (q_{Hz3} + q_{Hz4}\, df_z).\lambda_z$

$B_r = q_{Bz9} \cdot \lambda_{Ky} / \lambda_{\mu y} + q_{Bz10} \cdot B_y.C_y.\zeta_6$

$C_y = \zeta_7$

$D_r = F_z \cdot [(q_{Dz6} + q_{Dz7}\, df_z) \cdot \lambda_r + (q_{Dz8} + q_{Dz9}\, df_z) \cdot \gamma_z] \cdot R_0 \cdot \lambda_{\mu y} + \zeta_8 - 1$

An approximation for the aligning moment stiffness reads:

$K_z = -t \cdot K_y$

$(\approx -\frac{\partial M_z}{\partial \alpha}$ *at* $\alpha = 0)$

Aligning Torque coefficients in pure Side Slip

Following table shows the parameters for Aligning Torque coefficients in pure Side Slip which are used in the Adams Tire Property file for CAE purposes.

Table 6 Aligning Torque coefficients in pure Side Slip

Name	Name used in the tire property file	Explanation
Q_{bz1}	QBZ1	Trail slope factor for trail Bpt at Fznom
Q_{bz2}	QBZ2	Variation of slope Bpt with load
Q_{bz3}	QBZ3	Variation of slope Bpt with load squared
Q_{bz4}	QBZ4	Variation of slope Bpt with inclination
Q_{bz5}	QBZ5	Variation of slope Bpt with absolute inclination
Q_{bz9}	QBZ9	Slope factor Br of residual moment Mzr
Q_{bz10}	QBZ10	Slope factor Br of residual moment Mzr
Q_{cz1}	QCZ1	Shape factor Cpt for pneumatic trail
Q_{dz1}	QDZ1	Peak trail Dpt = Dpt*(Fz/Fznom*R0)
Q_{dz2}	QDZ2	Variation of peak Dpt with load
Q_{dz3}	QDZ3	Variation of peak Dpt with inclination
Q_{dz4}	QDZ4	Variation of peak Dpt with inclination squared
Q_{dz6}	QDZ6	Peak residual moment Dmr = Dmr/(Fz*R0)
Q_{dz7}	QDZ7	Variation of peak factor Dmr with load
Q_{dz8}	QDZ8	Variation of peak factor Dmr with inclination
Q_{dz9}	QDZ9	Variation of Dmr with inclination and load
Q_{ez1}	QEZ1	Trail curvature Ept at Fznom
Q_{ez2}	QEZ2	Variation of curvature Ept with load
Q_{ez3}	QEZ3	Variation of curvature Ept with load squared
Q_{ez4}	QEZ4	Variation of curvature Ept with sign of Alpha-t
Q_{ez5}	QEZ5	Variation of Ept with inclination and sign Alpha-t
Q_{hz1}	QHZ1	Trail horizontal shift Sht at Fznom
Q_{hz2}	QHZ2	Variation of shift Sht with load
Q_{hz3}	QHZ3	Variation of shift Sht with inclination
Q_{hz4}	QHZ4	Variation of shift Sht with inclination and load

Transient parameters

Relaxation behavior in the tire accounts for the fact that the lateral forces in the tire do not build up instantaneously, and the steady state levels are only attained once the tire travels a certain distance.

Both the longitudinal and the lateral relaxation lengths are defined as per the vertical load as:

$$\sigma_\kappa = F_z \,.\, (p_{Tx1} + p_{Tx2}\, df_z)\, .exp\, (\, p_{TX3}\, df_z\,) \,.\, \frac{R_0}{F_{z0}} \,.\, \lambda_{\sigma\kappa}$$

$$\sigma_\alpha = P_{Ty1}\ sin\ (2\ arctan \left\{\frac{F_z}{P_{Ty2} F_0 \lambda_{Fz0}}\right\} (1 - p_{Ky3}|\gamma_y|)\ R_o\ \lambda_{Fz0}\ \lambda_{\sigma\alpha}$$

Coefficients for transient response

Table 7 Transient parameters in the tire file

Name	Name used in the tire property file	Explanation
P_{Tx1}	PTX1	Longitudinal relaxation length at Fznom
P_{Tx2}	PTX2	Variation of longitudinal relaxation length with a load
P_{Tx3}	PTX3	Variation of longitudinal relaxation length with exponent of load
P_{Ty1}	PTY1	Peak value of relaxation length for lateral direction
P_{Ty5}	PTY2	Shape factor for lateral relaxation length
Q_{tz1}	QTZ1	Gyroscopic moment constant
M_{belt}	MBELT	Belt mass of the wheel

APPENDIX C – Optimization of Cornering Stiffness

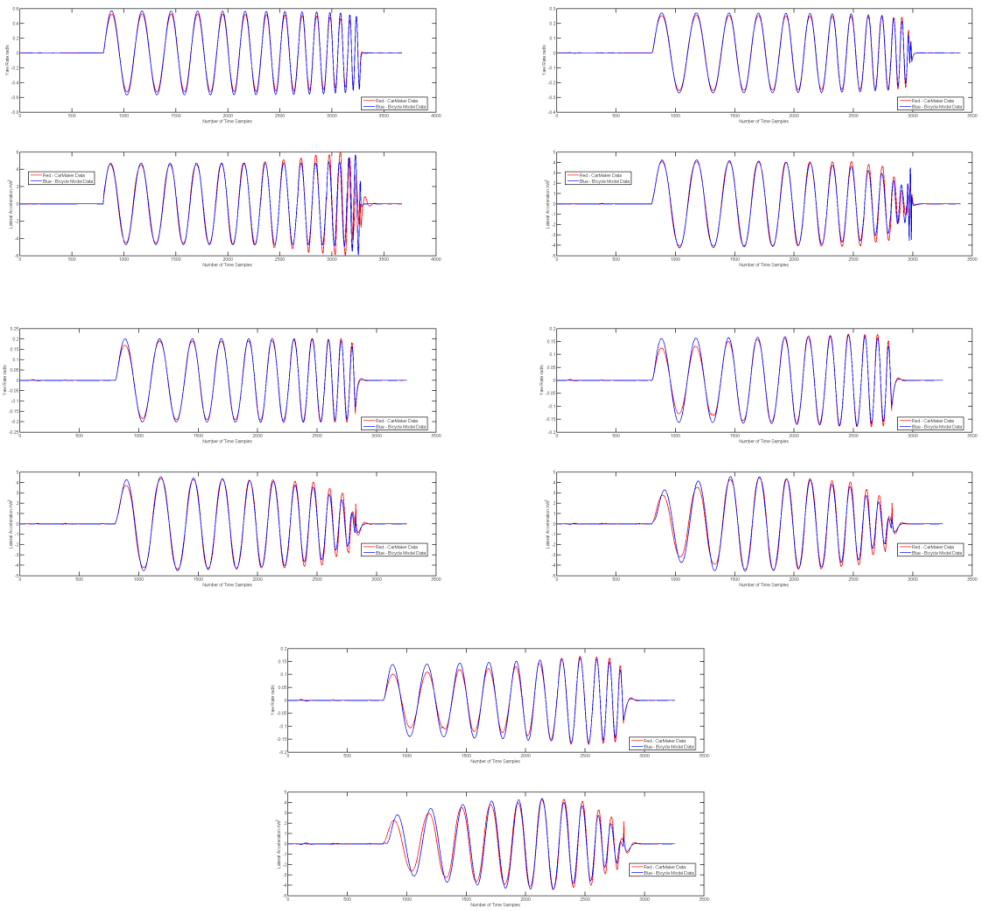

Figure 60 Preliminary Optimization task – Frequency sweep at various speeds

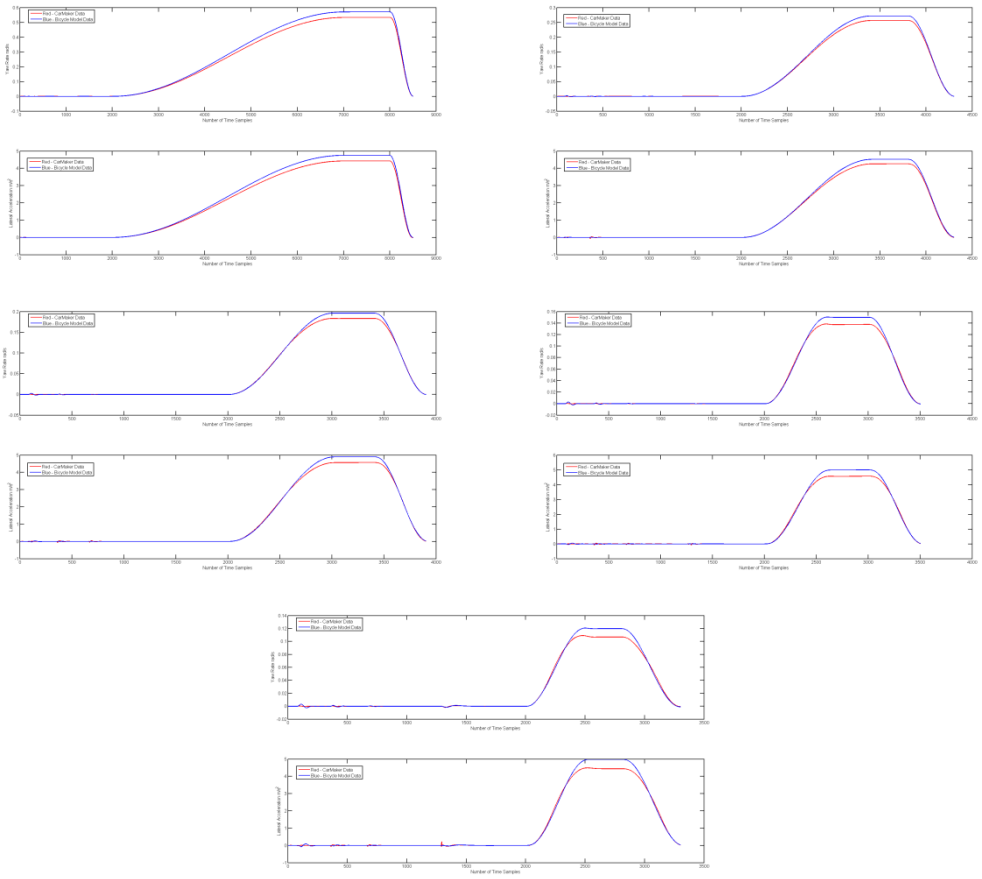

Figure 61 Preliminary Optimization task – Ramp Steer at various speeds

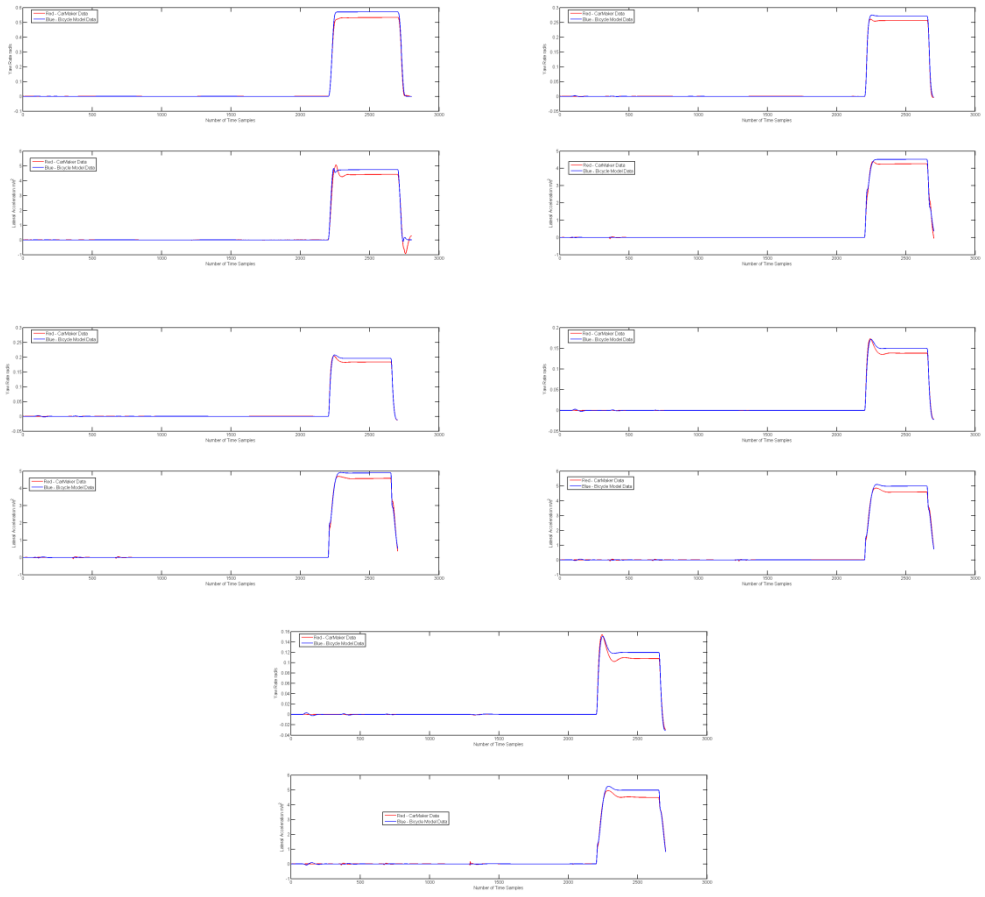

Figure 62 Preliminary Optimization task – Step Steer at various speeds

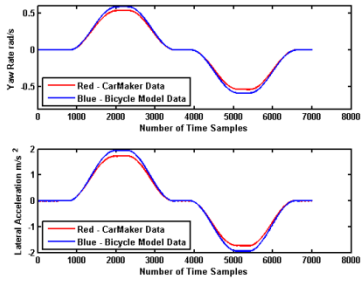

Figure 63 Preliminary Optimization task - Clothoid

APPENDIX D – Example of PAC2002 Tire Property File

```
[MDI_HEADER]
FILE_TYPE ='tir'
FILE_VERSION =3.0
FILE_FORMAT ='ASCII'
! : TIRE_VERSION : PAC2002
! : COMMENT : Tire 235/60R16
! : COMMENT : Manufacturer
! : COMMENT : Nom. section with (m) 0.235
! : COMMENT : Nom. aspect ratio (-) 60
! : COMMENT : Infl. pressure (Pa) 200000
! : COMMENT : Rim radius (m) 0.19
! : COMMENT : Measurement ID
! : COMMENT : Test speed (m/s) 16.6
! : COMMENT : Road surface
! : COMMENT : Road condition Dry
! : FILE_FORMAT : ASCII
! : Copyright MSC. Software, Fri Jan 23 14:30:06 2004
!
! USE_MODE specifies the type of calculation performed:
! 0: Fz only, no Magic Formula evaluation
! 1: Fx,My only
! 2: Fy,Mx,Mz only
! 3: Fx,Fy,Mx,My,Mz uncombined force/moment calculation
! 4: Fx,Fy,Mx,My,Mz combined force/moment calculation
! +10: including relaxation behaviour
! *-1: mirroring of tyre characteristics
!
! example: USE_MODE = -12 implies:
! -calculation of Fy,Mx,Mz only
! -including relaxation effects
! -mirrored tyre characteristics
$----------------------------------------------------------------
units
[UNITS]
LENGTH ='meter'
FORCE ='Newton'
ANGLE ='radians'
MASS ='kg'
TIME ='second'
$----------------------------------------------------------------
model
[MODEL]
PROPERTY_FILE_FORMAT='PAC2002'
USE_MODE = 14 $Tyre use switch (IUSED)
VXLOW = 1
LONGVL = 16.6
TYRESIDE = 'LEFT'
$-------------------------------------------------------------
dimensions
[DIMENSION]
UNLOADED_RADIUS = 0.344       $Free tyre radius
WIDTH = 0.235                 $Nominal section width of the
tyreASPECT_RATIO = 0.6        $Nominal aspect ratio
RIM_RADIUS = 0.19             $Nominal rim radius
RIM_WIDTH = 0.16              $Rim width
$----------------------------------------------------------------
shape
```

```
[SHAPE]
{radial width}
1.0 0.0
1.0 0.4
1.0 0.9
0.9 1.0
$-----------------------------------------------------------
parameter
[VERTICAL]
VERTICAL_STIFFNESS = 2.1e+005             $Tyre vertical stiffness
VERTICAL_DAMPING = 50                     $Tyre vertical damping
BREFF = 8.4                               $Low load stiffness e.r.r.
DREFF = 0.27                              $Peak value of e.r.r.
FREFF = 0.07                              $High load stiffness e.r.r.
FNOMIN = 4850                             $Nominal wheel load
$-----------------------------------------------------------
load_curve
$ For a non-linear tire vertical stiffness (optional)
$ Maximum of 100 points
[DEFLECTION_LOAD_CURVE]
{pen fz}
0.000 0.0
0.001 212.0
0.002 428.0
0.003 648.0
0.005 1100.0
0.010 2300.0
0.020 5000.0
0.030 8100.0
$-----------------------------------------------------
long_slip_range
[LONG_SLIP_RANGE]
KPUMIN = -1.5                             $Minimum valid wheel slip
KPUMAX = 1.5                              $Maximum valid wheel slip
$-----------------------------------------------------
slip_angle_range
[SLIP_ANGLE_RANGE]
ALPMIN = -1.5708                          $Minimum valid slip angle
ALPMAX = 1.5708                           $Maximum valid slip angle
$-----------------------------------------------
inclination_slip_range
[INCLINATION_ANGLE_RANGE]
CAMMIN = -0.26181                         $Minimum valid camber angle
CAMMAX = 0.26181                          $Maximum valid camber angle
$-----------------------------------------------
vertical_force_range
[VERTICAL_FORCE_RANGE]
FZMIN = 225                               $Minimum allowed wheel load
FZMAX = 10125                             $Maximum allowed wheel load
$-------------------------------------------------------------
scaling
[SCALING_COEFFICIENTS]
LFZO = 1               $Scale factor of nominal (rated) load
LCX  = 1               $Scale factor of Fx shape factor
LMUX = 1               $Scale factor of Fx peak friction coefficient
LEX  = 1               $Scale factor of Fx curvature factor
LKX  = 1               $Scale factor of Fx slip stiffness
LHX  = 1               $Scale factor of Fx horizontal shift
LVX  = 1               $Scale factor of Fx vertical shift
LGAX = 1               $Scale factor of camber for Fx
LCY  = 1               $Scale factor of Fy shape factor
```

```
PEY2 = -0.0063208 $Variation of curvature Efy with load
PEY3 = -9.9935    $Zero order camber dependency of curvature Efy
PEY4 = -760.14    $Variation of curvature Efy with camber
PKY1 = -21.92     $Maximum value of stiffness Kfy/Fznom
PKY2 = 2.0012     $Load at which Kfy reaches maximum value
PKY3 = -0.024778  $Variation of Kfy/Fznom with camber
PHY1 = 0.0026747  $Horizontal shift Shy at Fznom
PHY2 = 8.91e-005  $Variation of shift Shy with load
PHY3 = 0.031415   $Variation of shift Shy with camber
PVY1 = 0.037318   $Vertical shift in Svy/Fz at Fznom
PVY2 = -0.010049  $Variation of shift Svy/Fz with load
PVY3 = -0.32931   $Variation of shift Svy/Fz with camber
PVY4 = -0.69553   $Variation of shift Svy/Fz with camber and load
RBY1 = 7.1433     $Slope factor for combined Fy reduction
RBY2 = 9.1916     $Variation of slope Fy reduction with alpha
RBY3 = -0.027856  $Shift term for alpha in slope Fy reduction
RCY1 = 1.0719     $Shape factor for combined Fy reduction
REY1 = -0.27572   $Curvature factor of combined Fy
REY2 = 0.32802    $Curvature factor of combined Fy with load
RHY1 = 5.78e-006  $Shift factor for combined Fy reduction
RHY2 = -3.13e-005 $Shift factor for combined Fy reduction
RVY1 = -0.027825  $Kappa induced side force Svyk/Muy*Fz at Fznom
RVY2 = 0.053604   $Variation of Svyk/Muy*Fz with load
RVY3 = -0.27568   $Variation of Svyk/Muy*Fz with camber
RVY4 = 12.12      $Variation of Svyk/Muy*Fz with alpha
RVY5 = 1.9        $Variation of Svyk/Muy*Fz with kappa
RVY6 = -10.704    $Variation of Svyk/Muy*Fz with atan(kappa)
PTY1 = 2.1439     $Peak value of relaxation length SigAlp0/R0
PTY2 = 1.9829     $Value of Fz/Fznom where SigAlp0 is extreme
$----------------------------------------------------rolling
resistance
[ROLLING_COEFFICIENTS]
QSY1 = 0.01       $Rolling resistance torque coefficient
QSY2 = 0          $Rolling resistance torque depending on Fx
QSY3 = 0          $Rolling resistance torque depending on speed
QSY4 = 0          $Rolling resistance torque depending on speed ^4
$-------------------------------------------------------------
aligning
[ALIGNING_COEFFICIENTS]
QBZ1 = 10.904     $Trail slope factor for trail Bpt at Fznom
QBZ2 = -1.8412    $Variation of slope Bpt with load
QBZ3 = -0.52041   $Variation of slope Bpt with load squared
QBZ4 = 0.039211   $Variation of slope Bpt with camber
QBZ5 = 0.41511    $Variation of slope Bpt with absolute camber
QBZ9 = 8.9846     $Slope factor Br of residual torque Mzr
QBZ10 = 0         $Slope factor Br of residual torque Mzr
QCZ1 = 1.2136     $Shape factor Cpt for pneumatic trail
QDZ1 = 0.093509   $Peak trail Dpt" = Dpt*(Fz/Fznom*R0)
QDZ2 = -0.0092183 $Variation of peak Dpt" with load
QDZ3 = -0.057061  $Variation of peak Dpt" with camber
QDZ4 = 0.73954    $Variation of peak Dpt" with camber squared
QDZ6 = -0.0067783 $Peak residual torque Dmr" = Dmr/(Fz*R0)
QDZ7 = 0.0052254  $Variation of peak factor Dmr" with load
QDZ8 = -0.18175   $Variation of peak factor Dmr" with camber
QDZ9 = 0.029952   $Var. of peak factor Dmr" with camber and load
QEZ1 = -1.5697    $Trail curvature Ept at Fznom
QEZ2 = 0.33394    $Variation of curvature Ept with load
QEZ3 = 0          $Variation of curvature Ept with load squared
QEZ4 = 0.26711    $Variation of curvature Ept with sign of Alpha-t
```